Investigation of Deformation Behavior for Commercially Pure Titanium Grade 2 Through Continuous Forming Process

Mulualem Hailu Besha

PGR/18341/11

A thesis submitted to

The Department of Mechanical Design and Manufacturing Engineering
School of Mechanical, Chemical and Materials Engineering

Presented in Partial Fulfillment of the Requirement for the Degree of Master's in Manufacturing Engineering

Office of Graduate Studies
Adama Science and Technology University

Adama
June, 2021

Investigation of Deformation Behavior for Commercially Pure Titanium Grade 2 Through Continuous Forming Process

Mulualem Hailu Besha

PGR/18341/11

A thesis submitted in Partial Fulfillment of the Requirement for the Degree of Master's in Manufacturing Engineering

Main Advisor: Dr. Devendra kumar Sinha

Program of Mechanical Design and Manufacturing Engineering, School of Mechanical, Chemical and Materials Engineering (SoMCME), ASTU, ADAMA, ETHIOPIA.

Co-Advisor: Dr. C. Venkatesh

Program of Mechanical Design and Manufacturing Engineering, School of Mechanical, Chemical and Materials Engineering (SoMCME), ASTU, ADAMA, ETHIOPIA.

The Department of Mechanical Design and Manufacturing Engineering

School of Mechanical Chemical and Materials Engineering

Office of Graduate Studies

Adama Science and Technology University

Adama

June, 2021

APPROVAL OF BOARD OF EXAMINERS

We, the undersigned, members of the Board of Examiners of the final open defense by **Mulualem Hailu Besha** have read and evaluated his thesis entitled **“Investigation of Deformation Behavior for Commercially Pure Titanium Grade 2 through Continuous Forming Process”** and examined the candidate. This is therefore, to certify that the thesis has been accepted in partial fulfillment of the requirement of the Degree of Master’s in Manufacturing Engineering.

______________________	____________	______________
Name of student	Signature	Date
______________________	____________	______________
Advisor	Signature	Date
______________________	____________	______________
Internal Examiner	Signature	Date
______________________	____________	______________
External Examiner	Signature	Date
______________________	____________	______________
Chairperson	Signature	Date
______________________	____________	______________
Head of department	Signature	Date
______________________	____________	______________
School dean	Signature	Date
______________________	____________	______________
Post graduate dean	Signature	Date

DECLARATION

I hereby declare that this MSc Thesis is my original work and has not been presented for a degree in any other university, and all sources of material used for this thesis have been duly acknowledged.

Name: Mulualem Hailu Besha

Signature: ______________

This MSc Thesis has been submitted for examination with my approval as thesis advisor.

Name: Dr. Devendra kumar Sinha (Ph. D)

Signature: _______________

Date of submission: ______________

ADVISOR'S APPROVAL SHEET

To: Mechanical Design and Manufacturing Engineering Department.

Subject: Thesis Submission

This is to certify that the thesis entitled "**Investigation of Deformation Behavior for Commercially Pure Titanium Grade 2 through Continuous Forming Process"** submitted in partial fulfillment of the requirements for the degree of Master's in Manufacturing Engineering, the Graduate program of the department of Mechanical Design and Manufacturing Engineering, and has been carried out by **Mulualem Hailu Besha**, Id. No PGR/18341/11, under our supervision. Therefore, we recommend that the student has fulfilled the requirements and hence, hereby he can submit the thesis to the department.

______________________	______________________	______________________
Name of main Advisor	Signature	Date
______________________	______________________	______________________
Name of Co- Advisor	Signature	Date

ACKNOWLEDGEMENT

First of all, I would like to express my deepest gratitude to the almighty "**ALLAH**" for helping me to succeed in academic life and for being with me all to bless my efforts. Also, I would like to express my deepest appreciation and heart full gratitude to my major advisor **Dr. Devendra kumar Sinha** (Program of Mechanical Design and Manufacturing Engineering, Adama Science and Technology University) for his genius professional assistance, constructive comments with full knowledge, dedication to work and day to day guidance. And also, I would like to thanks my Co- Advisor **Dr. C. Venkatesh** (Program of Mechanical Design and Manufacturing Engineering, Adama Science and Technology University) for his constructive guidance and dedication to work. And also, I would like to thanks **Mr. Mengistu Gelaw** (Program chair of Mechanical Design and Manufacturing Engineering, Adama Science and Technology University) for helping us in all our needs beside the department, giving us information positively from time to time, and appreciation as a program chairs. And also I would like to thanks **Mr. Kamil** (Program of Material Science and Engineering, Adama Science and Technology University) for his positive guidance and full help during mechanical and metallurgical tests.

Finally, I would like to thanks all my family members specially my mother **Ms. Kedija Abdella** and my wife **Mrs. Asmanur Abadir** for their appreciation and support during my research work.

Table of Contents **Page no**

LIST OF TABLES

LIST OF FIGURES AND ILLUSTRATIONS

LIST OF ACRONYMS AND ABBREVIATIONS

$\Delta_{\sigma'}$	Quality Loss of Effective Stress
Δ_P	Quality Loss of Power Consumption
ACEF	Accumulative Continuous Extrusion Forming
Al	Aluminum
CONFORM	Continuous Forming
CP	Commercially pure.
Cr	Chromium
CRE	Continuous Rotary Extrusion.
Cu	Copper
DEFORM	Deformation of Forming
DOE	Design of Experiments
EBSD	Electron-Backscattered Diffraction.
F	Degree Fahrenheit
FB	Fields- Backofen
Fe	Iron
FEM	Finite Element Method
$GC_{\sigma'}$	Grey Relational Coefficient of Effective Stress
GC_P	Grey Relational Coefficient of Power Consumption
G_i	Grey Relational Grade
HB	Brinel Hardness.
HSS	High Speed Steel
Mg	Magnesium
MPa	Mega Pascal
MRPI	Multi-Response Performance Index
NACE	National Association of Corrosion Engineers.
^{O}C	Degree Celsius
OM	Optical Microscopy
P	Power Consumption
R-conform	Repetitive continuous forming
RSM	Response Surface Methodology
S/N	Signal-to-Noise Ratio
Si	Silicon
TEM	Transmission Electron Microscopy.

Ti	Titanium
V	Vanadium
Wt.	Weight
Zr	Zirconium
σ'	Effective Stress

ABSTRACT

In this study, the investigation of deformation behavior for CP-Titanium grade 2 feedstock materials through Continuous Forming process was carried out. The theoretical analysis, numerical simulation and experimental validation, including testing and characterization of the feedstock before and after deformation were carried out. The theoretical analysis was carried out through Upper Bound Method. The numerical simulation was carried out through the three-dimensional finite element tool DEFORM-3D. The experimental plan and design was carried out using Taguchi (2^3) array methods in MINTAB platform by considering extrusion wheel velocity and feedstock temperature as chief extrusion parameters. The experimental analysis and validation of numerical results were carried out by extrusion forming of 12.5 mm CP- Titanium grade 2 feedstock materials using TBJ350 CONFORM machine setup. The optimization process of parameters for optimum value of response variables were carried out through Grey Relational Analysis. The special case study for optimization of effective stress for Titanium grade 5 feedstock materials was also carried out using Response Surface Methodology. The 12.5 mm diameter feedstock rod was extruded to 10 mm, 8 mm and 6 mm rod. It was observed that the power consumption for 6 mm extruded rod through Upper Bound technology, DEFORM-3D and experimentation was 45.48 kW, 47.75 kW and 50.13 kW respectively. Therefore, the numerical results were found to be in full agreement with the theoretical and experimental results, thereby maintaining the error up to 5 %. The numerical results reveals that the effective-stress of feedstock material was high in the biting-deformation region and then gradually decreases towards the flowing direction of the material. It was found that the optimum values of extrusion wheel velocity and feedstock temperature during continuous forming process for target value of 500 MPa were 16 RPM and 398.5 ^{0}C. It was observed that as the feedstock temperature increases, the value of effective stresses which occur in other region decreases to some extent. So, the results declared that increasing extrusion wheel velocity and feedstock temperature of material will reduce the shear strength of feedstock material during the continuous forming process. Therefore, the load requirement for deformation can be reduced. Moreover, the wear of extrusion shoe which is one of the most important elements can also be minimized thereby the life of extrusion shoe material can be enhanced. From the hardness test, it was observed that the hardness of the extruded feedstock of 6 mm diameter was 242.8 VHN which was improved by 67.45 % when compared with the raw feedstock material. The increment in the tensile strength was observed after deformation of the feedstock material (83.14% for 6 mm rod, 71.51 % for 8 mm rod and 40.98 % for 10 mm rod). The optical microscopy reveals that the grain refinement was achieved after deformation of the feedstock material. The Grey Relational Analysis reveals that the optimum values of effective stresses and power consumption was found to be at 8 RPM as the wheel velocity and 200 ^{0}C as the feedstock temperature. The proposed thesis will be helpful for the metal forming industries working in this area where titanium products strength can be enhanced.

***Keywords**: Continuous Extrusion; CP- Titanium grade 2; Feedstock temperature; DEFORM-3D; Extrusion wheel velocity; FEM, Extrusion ratio.*

CHAPTER ONE

INTRODUCTION

1.1 Background of the study

Metal forming is a large set and very important manufacturing operation. It enjoys industrial importance among various production operations due to its advantages such as cost effectiveness, enhanced mechanical properties, flexible operations, higher productivity, considerable material saving.

The objects and articles that we use in our daily life are man-made, engineering parts, which are obtained from some raw material through some manufacturing process. All these objects are made of a number of small components assembled into finished product. For instance, an automobile is supposed to be an assembly of more than 15000 parts, produced through various manufacturing operations. Manufacturing of finished parts and components from raw materials is one of the most important steps in production.

Production incorporates all kind of manufacturing processes. Manufacturing refers to the conversion of raw materials into finished products employing suitable techniques. There are several methods of manufacturing such as metal casting, metal forming, metal machining, metal joining and finishing. Some of the modern manufacturing processes includes micro-machining, Nano- fabrication, ultra-precision manufacturing etc.

In order to fulfill the requirements of the ever-increasing demands of various types of industries, the manufacturing engineer has to choose the right type of material and the right type of equipment for manufacture so that, the cost of production and the energy consumption are minimum. The selection of suitable manufacturing process should also include concerns for environmental impacts such as air pollution, waste disposal etc.

The present study is concentrated on one of the important manufacturing processes called, metal forming.

1.2 Classification of Metal Forming Processes

Classically, metal forming processes can be classified into two major categories: the first one is bulk forming and the second is sheet metal forming.

Bulk forming: It is a severe deformation process resulting in massive shape change. The surface area-to-volume of the work is relatively small. The nature of force applied may be compressive, compressive and tensile, shear or a combination of these forces. Mostly done in hot working conditions. Examples of bulk forming products are gear, bushed, valves, engine parts such as valves, connecting rods, hydraulic valves, etc.

Sheet metal forming: Sheet metal forming involves forming and cutting operations performed on metal sheets, strips, and coils. The surface area-to-volume ratio of the starting metal is relatively high. Tools include punch, die that are used to deform the sheets.

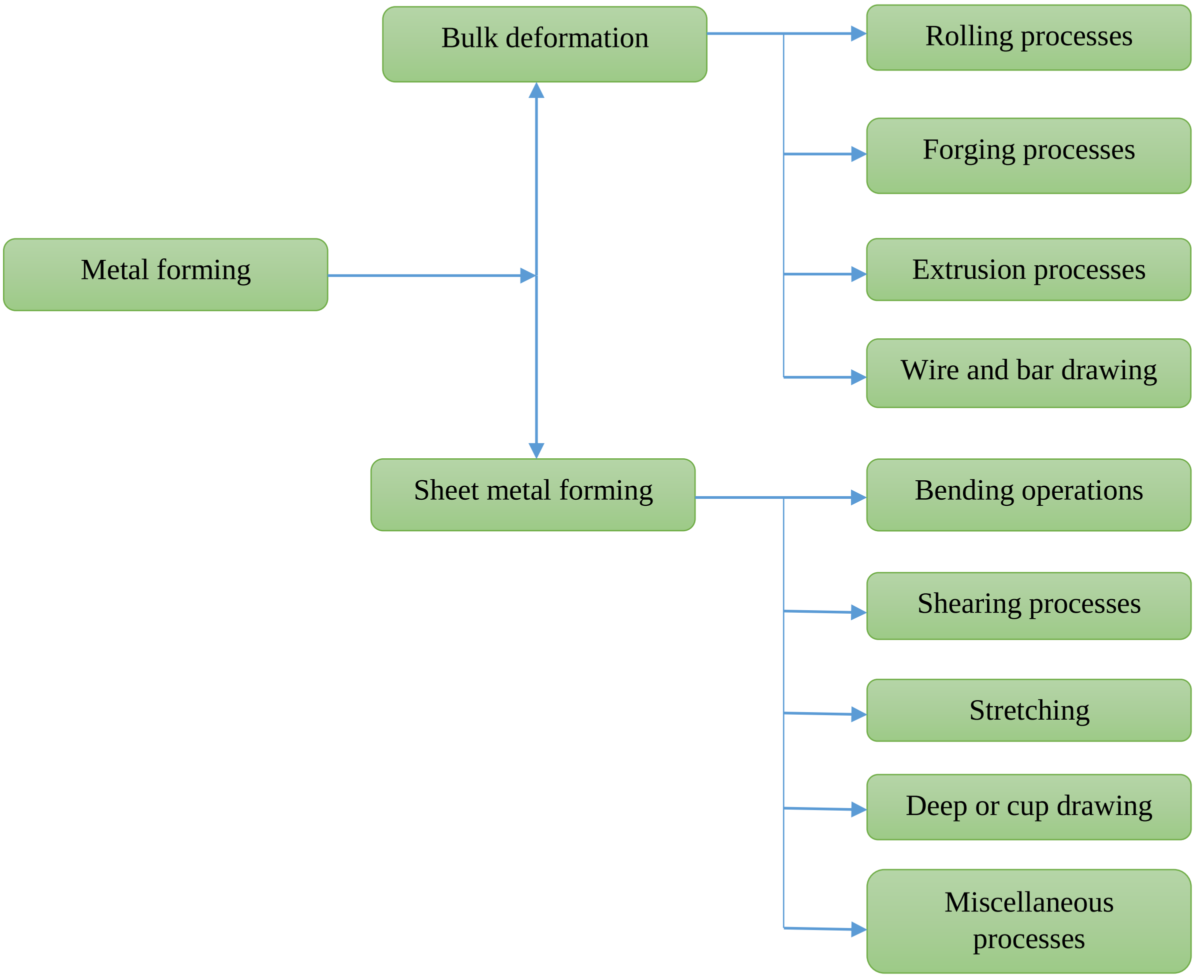

Figure 1. 1 General classification of metal forming processes.

1.3 Short Description On Some of Metal Forming Operations

1.3.1 Bulk Forming Processes:

Rolling is a compressive deformation process, which is used for producing semi-finished products such as bars, sheets, plates and finished products such as angles, channels, sections. Rolling can be carried out in both hot and cold working conditions.

Forging is a bulk metal forming process in which the billet material is shaped into finished part by the application of compressive and tensile forces with the help of a pair of tools called die and punch. Forging can be done in open dies or closed dies. Open die forging is usually used for preliminary shaping of raw materials into a form suitable for subsequent forming or machining Open die forming is done using a pair of flat faced dies for operations such as drawing out, thinning, etc. Closed die forming is performed by squeezing the raw material called billet inside the cavity formed between a pair of shaped dies. Such as pump parts, valve parts, connecting rods, small gear, spanner etc.

1.3.2 Sheet Metal Forming Process:

Deep drawing is a sheet metal forming process in which a sheet metal is forced into cup of hollow shape without altering its thickness-using tensile and compressive forces. Complex shapes can be produced by deep drawing of blanks in stages- redrawing, multiple draw deep drawing etc.

1.4 Extrusion Processes

Extrusion processes is a bulk metal forming process in which the feedstock material is compressed to flow through a narrow opening of constant cross-section or varying cross-section in order to reduce the diameter and increase the length. It can be done hot or cold. Extruded products include shafts, tubes, cans, cups, gears etc.

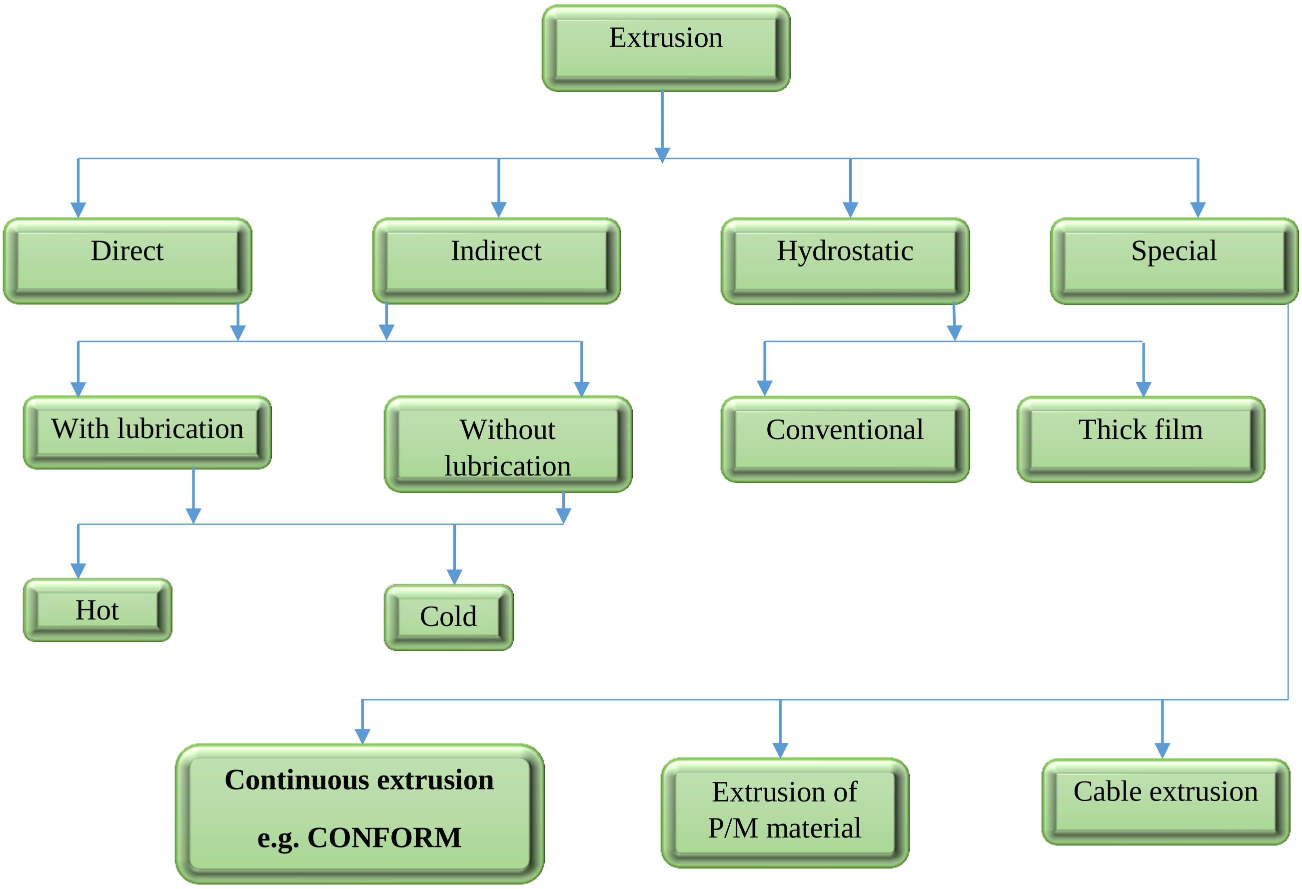

Figure 1. 2 Classification of extrusion process; *Bauser.M et al.* (2006)

1.5 Continuous Extrusion Process

The continuous extrusion process was discovered by Derek GREEN in 1970s *Green (1972), Etherington (1974).* Continuous extrusion is particularly beneficial for processing non-ferrous metals such as, (Al and Cu), which require breakdown processing of the coarse grain structure. A coarse grain structure can be transformed into uniform fine-grained metal (10-20 μm) in a single pass. In the continuous extrusion process, the friction force between the extrusion wheel and the feedstock material is used for the deformation and finally, products of various shapes are formed which is not possible by other methods *Etherington (1974).* As the feedstock is moved along with the extrusion wheel, its temperature keeps on increasing and also the microstructure of the feedstock material changes due to the severe plastic deformation phenomenon *Bing et al. (2017).* The continuous extrusion process consumes less energy input as compared to the conventional extrusion process and also produces products of infinite length besides the better mechanical and metallurgical properties of products *Nijenthan Rajendran et.al (2018), Monika Mitka et.al (2018).* The optimal design of the continuous forming process was carried out through numerical simulation. It was found that extrusion wheel velocity does not have too much influence on the flow of materials unless it is too high *Kim et.al (1998).* The gap between the extrusion wheel and shoe which is known as the flash gap should be minimum and the bottom portion of the die should be longer relative to the upper part for uniform flow of material. The effect of heating the feedstock material before feeding into the grooved portion of the wheel was carried out for aluminum-strontium alloys *Xinbing et.al (2017).* It was found that the temperature of feedstock material kept on increasing in the grooved portion of the wheel as well as in the die chamber and maximum temperature was observed at the exit portion of the die. Furthermore, the maximum stress was observed near the abutment where the material turns into the die chamber. The mathematical modeling optimization of process parameters in continuous extrusion process was carried out to predict the best value of mechanical properties of extruded feedstock material in the continuous extrusion process *Sinha et.al (2018).* Figure 1.3 represents the schematic diagram, principle and details of tooling in continuous extrusion process.

a *b*

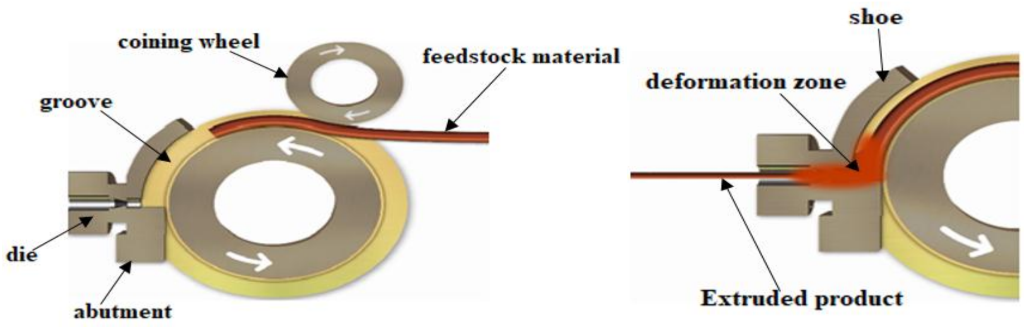

Figure 1. 3 Schematic diagram of CONFORM; (a) General view; (b) Deformation zone. *(Mulualem et al. 2021)*

Kim et.al (1998) studied optimal design of continuous forming process and performed set of simulation, analyzed the process parameters and proposed an optimal design. They found out that rotating wheel velocity does not have remarkable influence on material flow unless it is extremely high. The flash gap should be minimum and increasing the lower straight part of the die should be longer relative to the upper part to result in uniform flow. *Xinbing et.al (2017)* studied Effect of Billet Preheating Temperature on Continuous extrusion forming of Aluminum-strontium alloys. DEFORM-3D and finite element method model was used to studied numerical simulation and experimental analysis of microstructure and mechanical properties of preheated Aluminum-strontium alloys. The numerical simulation results shown that the temperature starts to increase once the billet enters into the cavity during the process of aluminum-strontium alloys, and the extreme temperature appears at the die exit. And moreover, the extreme equivalent stress appears in the right-angle bending zone. *Nijenthan Rajendran et.al (2018)* studied Effect of tool geometry on velocity and strain rate field in continuous rotary extrusion of magnesium AZ91 alloy. Finite element method analysis has been done to study the consequence of different draft angle and feeder plate geometry in the exit die on the metal flow in the continuous rotary extrusion of AZ91 magnesium alloy and also, in the nonexistence of draft angle the deformation chamber of metal in the middle travel faster. For bigger feeder plates in continuous rotary extrusion, process deformation zone occupied when rotation of wheel has been higher.

1.5.1 Advantages of Continuous Extrusion Process.

Continuous forming process has several advantages, when compared with conventional forming processes. Such as, High dimensional accuracy, Excellent surface finish, Bright annealed material, No degradation of conductivity, Infinite length, Minimum scrap generation, Material as per exact packing requirements of the customer, Instant production of finished material in a single operation and Consistent mechanical properties.

Several investigations have been carried out on the deformation behavior of Aluminum and Copper feedstock material in the continuous forming process, but very few investigations have been carried out on the deformation behavior of CP-Titanium grade 2. In the present study, the deformation behavior of CP-Titanium grade 2 feedstock material has been investigated by through theoretical analysis, numerical analysis and experimental analysis in the continuous forming process. The DEFORM-3D tool has been implemented for numerical analysis to examine the deformation behavior of CP-Titanium grade 2 at different combinations of extrusion wheel angular velocities and heat treatment conditions of feedstock material and experimental using TJ350 continuous forming machine. The distributions of velocity field, stress field, strain field, temperature field and damage field were investigated under different extrusion wheel angular velocities and preheating condition. It could provide the theoretical, numerical and experimental guide for actual production of CP-Titanium grade 2 product. At the same time, it is important to improve the quality of product and select tools and dies materials. Non-Ferrous metals (Al, Cu, etc.) were chosen due the following attractive reasons, like high strength, low weight ratio and outstanding corrosion resistance which are natural. Non-Ferrous metals and their alloys have brought about a wide range of successful applications requiring high levels of reliable performance in surgery and medicine as well as in aerospace, automotive, chemical plants and other major industries. In many of the engineering applications, Non-Ferrous metals takes over heavier, less serviceable or less cost-effective materials. Designs created with the properties provided by Non-Ferrous metals often produce dependable, economic and more durable systems and components. Non-Ferrous metals components often substantially surpass the performance and service life expectations at a lower overall cost. Non-Ferrous metals (Al, Cu, etc.) are the one that are most extensively used. They have a credible machinability and excellent mechanical properties. For various weight reduction applications in aerospace, automotive and marine equipment, their alloys have the best overall performance. From non-ferrous material specially titanium alloy is also known to have wide range of applications in medicine. The biocompatibility of Titanium alloy is exceptional, especially when the requirement is to have a direct contact with tissue or bone.

1.6 Problem Statement

In the modern industries, there is a high demand of materials which has an excellent upgraded mechanical, metallurgical and material property that are capable of high strength, low weight ratio, outstanding corrosion resistance, and resistance to high-elevated temperature and also, it had been founded that the power consumption, effective stresses, other mechanical and metallurgical properties are lower bounded with traditional forming processes. As a result, the tooling and operation costs also increase. Meeting the requirement of modern industries will be researcher's goal.

It is a fact, that out of all manufacturing processes, metal-forming processes provides the product of highest strength. Among all metal forming processes, the continuous forming process provides product of infinite length, complex profile with better quality. Because of its superiority and impact on the current forming technology, demand of products produced by continuous extrusion from industry has been growing rapidly. This can ensure high surface quality, reduced effective stresses and minimum power consumption, besides better mechanical and metallurgical properties in comparison to conventional extrusion process. The materials like titanium alloys are can replace the existing material used in automobile and aerospace applications, if processed through Continuous forming process.

1.7 Scope of the Study

This study focuses on the deformation behaviour investigation of commercially pure titanium grade 2 feedstock material in continuous forming process. The study also explores the theoretically, numerically and experimentally. In this process, feedstock temperature and extrusion wheel velocity as wheel as extrusion ratio are considered as chief process parameters. This study is limited only to three types of die diameters, which are 6 mm, 8 mm and 10 mm.

1.8 Objectives

1.8.1 General objectives

- The general objective is to investigate deformation behavior of CP- Titanium grade 2 through continuous forming process.

1.8.2 Specific objectives

- To determine the total load required for the deformation of CP- Titanium grade 2 during continuous forming process.

- To carry out Numerical simulations of CP- Titanium grade 2 in continuous forming process through DEFORM-3D.
- To carry out experiments at different extrusion ratios and feedstock temperatures.
- To investigate the mechanical and metallurgical properties of feedstock material before and after deformation.
- To optimize the process parameters using Grey Relational Analysis.

1.9 Thesis Organization

This thesis paper consists five chapters. Chapter one briefly explains the background study of metal forming process as well as specifically about continuous forming process. This chapter includes problem statements, scope of the study, general and specific objectives of the study along with thesis structures. Chapter two presents the efforts of researchers from old to recent ones which are related to this study. Chapter three explains about varieties of materials, which are used in the study and methods that are applied during the analysis to achieve the goal of the study. This chapter includes material used, model approach, experimental plan and design, finite element formulation, numerical simulation data, theoretical analysis formulation, experimental analysis, material characterization and analysis of optimization process. Chapter four explains results and discussions from theoretical analysis part, numerical analysis part, experimental analysis parts and optimization process. Chapter five highlights conclusion and recommendations. In this chapter, the output /final results of the study are elaborated and also, future works on the study are suggested.

CHAPTER TWO

LITERATURE REVIEW

In the past decades, several researches have been done on continuous metal forming processes by using different kinds of feedstock materials, to fulfill the need of industries sectors from time to time. In this section, based on the past work of researchers, which are related to the present study have been categorized and reviewed accordingly, from the past to recent ones.

2.1. Analysis of optimization process parameters

2.2. Analysis of metallurgical properties

2.3. Analysis of mechanical strength/properties

2.1 Analysis of Optimization Process Parameters

Kim et al. (1998) studied optimal design of continuous forming process. performed set of simulation, analyzed the process parameters and proposed an optimal design. They found out that rotating wheel velocity does not have remarkable influence on material flow unless it is extremely high. The flash gap should be minimum and increasing the lower straight part of the die should be longer relative to the upper part to result in uniform flow.

Kim et al. (2000) studied the application of upper bound method to the continuous forming process. To verify the aim, similarity equations which is upper bound method used for calculating the power. And also finite element method simulation was carried out to verify theoretical results. In addition, the theoretical result approved by numerical simulations. Depending on numerical result the complicated calculation of conform process can be demonstrated by equivalent side extrusion. And also the comparison was made with respect to extrusion ration, the extrusion ratio increase as power decrease.

Cho and Jeong (2000) investigated the parametric surface defect occurrence in continuous forming process by the finite element method. Several parameters considered to examine their effects on surface defects occurrence such as, the wheel velocity, the extrusion ratio, the flash-gap size, the friction coefficient and the abutment height their effects which have on the surface defects. On continuous forming process both theoretical analysis and finite element method formulations applied to examine the parametric effect phenomena.

Cho and Jeong (2001) adopted the parametric curling phenomenon in continuous forming process by three-dimensional finite element analysis. Numerical analysis was carried out in order to investigate the significant effects of process parameter. The curling phenomenon influenced by flash gap size and abutment height but does not by wheel velocity. The numerical results, indicated that curling phenomenon minimized by reducing flash gap size and abutment height.

Katajarinne et al. (2006) studied the Numerical simulation of flash formation in continuous rotary extrusion of copper. In the process 5–25% material losses due to flash formation. Flash formations was investigated under different kinds of frictional conditions by using finite element simulations, and Numerical simulation argued that flash formed highly dependent on friction conditions. Especially secondary grip zone area was extremely friction dependent.

Manninen et al (2006) analyzed flash formation in continuous rotary extrusion of copper. Flash shape and scrap produced were estimated by using analytical model. The model indicated that the correlation between flash gap size, friction, geometric factor and extrusion pressure and flash formation. Experimental and numerical results verified by justifying with theoretical results.

Peng-yue et al (2007) investigated the effect of extrusion wheel angular velocity on continuous extrusion forming process of copper concave bus bar. DEFORM-3D software was used to investigate different effects of extrusion process such as stress, temperature, damage, strain, and distribution of velocity field under angular velocity of the driving wheel. So the result indicated that each and every effect of extrusion process highly influenced by the amount of wheel angular velocity.

Ying et al. (2012) investigated the effect of process parameters on sheath forming of continuous extrusion sheathing of aluminum. DEFORM-3D software was used to analyze the effect of wheel velocity and material flow passage length during extrusion sheathing process and also experimentally validated. Process parameter effects such as, temperature, bending phenomena, extrusion velocity and cross-section feature of materials were estimated and experimentally verified.

Xin et al. (2017) Studied the effect of Billet Preheating Temperature on Continuous extrusion forming of aluminum-strontium alloys. DEFORM-3D and finite element method model was used to studied numerical simulation and experimental analysis of microstructure and mechanical properties of preheated aluminum-strontium alloys. The numerical simulation results shown that the temperature starts to rise after the billet enters into the cavity during the process of aluminum-strontium alloys, and the maximum temperature appears at the die exit. And moreover, the maximum equivalent stress appears in the right-angle bending zone.

Thomas et al. (2017) investigated Continuous extrusion of a commercially pure titanium powder via the continuous forming process. DEFORM-3D was used to study the numerical simulation of commercially pure titanium powder. The grain size has been shown to decrease with increasing wheel speed with an associated increase in tensile strength. Finite-element modelling of the process shows the formation of the characteristic macrostructure from powder fed continuous forming. The process was continuous, utilizes, standard equipment and does not require powder preheating or inert gas shrouding providing a footing for a true cost reduction in long section titanium mill product.

Rajendran et al. (2018) studied the effect of tool geometry on velocity and strain rate field in continuous rotary extrusion of magnesium AZ91 alloy. Finite element method analysis has been done to study the effect of different draft angle and feeder plate geometry in the exit die on the metal flow in the continuous rotary extrusion of AZ91 magnesium alloy. And the results indicated that due to plugging in absence of inlet draft the deformation zone filled faster. and also, in the absence of draft angle the deformation chamber of metal in the middle move faster. For bigger feeder plates in continuous rotary extrusion process deformation zone filled when rotation of wheel has been higher.

Mitka et al. (2018) studied the continuous rotary extrusion of AZ81 magnesium alloy. to optimize the parameters of continuous rotary extrusion for magnesium alloys. During continuous rotary extrusion process the speed of rotating wheel was controlled and the die temperature was enumerated. The testing of mechanical properties and microstructure examination had been taken to select effective parameters to obtained rods from AZ81 magnesium alloys in the continuous rotary extrusion process.

2.2 Analysis of Metallurgical Properties

Zhao et al. (2013) analyzed the effect of deformation speed on the microstructure and mechanical properties of AA6063 aluminum alloy during continuous extrusion process. Under different extrusion wheel angular velocity experimental and numerical simulations undertaken to analyze the process of AA6063 aluminum alloy material. And after aging treatment, finally argued that the mechanical properties of the AA6063 aluminum alloy highly influenced by induced temperature which occurs due to deformation velocity. Also, temperature increment has slight grain size increment during the process.

Bing et al. (2014) studied the flow characteristics of brass rod during continuous extrusion. The uniformity of flowing material is the main influencing parameter product quality of the material (brass alloy rod). To studied the flow characteristics of the material they take two different samples which are on two different channel round-table and table-cone. Finally, they understand that from two samples during the table-cone have uniform and fine grain size, which will make a sample with excellent properties during continuous extrusions.

Ying et al. (2016) studied the microstructure and properties of Al−0.70Fe−0.24Cu alloy conductor prepared by horizontal continuous casting and subsequent continuous extrusion forming. They studied the mechanical and material properties of the Al−0.70Fe−0.24Cu alloy at 90 °C and 76 MPa for one hundred hours. Strain-induced precipitation, transformation of crystal orientation and grain refinement of the Al-7Cu-2Fe phase induced by conform process which improved comprehensive properties of alloys.

Shen et al. (2015) obtained the ultrafine-grained of Al–0.2Sc–0.1Zr alloy: The mechanistic contribution of Nano-sized precipitates on grain refinement during the novel process of accumulative continuous extrusion. Electron-backscattered diffraction (EBSD) and transmission electron microscopy (TEM) used to investigate the impact of Al_3 (Sc, Zr) on the grain refinement of Al–0.2Sc–0.1Zr (wt. %) Alloys and pure Al processed in the same manner was compared with the results by using accumulative continuous extrusion forming (ACEF). The Obtained result was successful which is refined from 100 µm to 0.8 µm.

Su et al. (2016) studied the grain refinement in an Aluminum-Erbium alloy during accumulative continuous extrusion forming. Accumulative continuous extrusion forming was used to refined the grain of Aluminum-Erbium alloy. On the grain refinement the effect of dispersed particles was also investigated. Four passes of accumulative continuous extrusion forming (ACEF) exposed extraordinary efficiency in minimizing grain sizes of Aluminum-Erbium (wt. %) alloy from 26.01 µm to 1.3 µm. In addition, fine grains are acquired because grain growth is clogged as a result of embarrass boundary flows.

Ji et al. (2016) investigated the microstructures and properties of Aluminum–Magnesium–Silicon alloy overhead conductor by horizontal continuous casting and continuous extrusion forming process. To investigate the possibility of achievement for Aluminum–Magnesium–Silicon alloy overhead conductor with continuous in-line solution treatment, and amend its properties based on horizontal continuous casting and sub- sequence continuous extrusion forming. Generally, elongation of 6.0%, electrical Conductivity of 55.7% IACS (Indian association for the cultivation of science) and tensile strength of 334.7 MPa were captured after drawing and aging at 155 °C for three hour. And they concluded that conform process can appropriately refine grains and amend mechanical properties of High speed steel alloy, which can contribute to the posterior processes.

Xin et al. (2017) investigated the microstructure evolution of aluminum-strontium master alloy during continuous forming processes. microstructure evolution of aluminum-strontium master alloy examined by using X-ray diffractometer, scanning electron microscope and transmission electron microscope. Result indicate that the continuous extrusion process could change the alloy particles significantly in size and morphology. The as-cast needle-like Al_4Sr (Aluminum-Strontium) particles are broken into small blocks in upsetting zone and crushed heavily in adhesion zone. Plenty of dislocations get tangled up in right-angle bending zone. Al_4Sr (Aluminum-Strontium) particles grow in the extending zone. Finally, Al_4Sr (Aluminum-Strontium) particles in products are approximately 28 μm in length. Al_2Sr (Aluminum-Strontium) particles precipitate during the process. Compared with products by horizontal extrusion, Al_4Sr (Aluminum-Strontium) particles by continuous extrusion are finer and distribute more evenly.

Yuan et al. (2017) studied the microstructure evolution and properties of Copper-Chromium alloy during continuous extrusion process. optical microscopy, transmission electron, microscopy, hardness and conductivity measurement was used to investigate microstructure evolution and properties of Copper-Chromium alloys. The results showed that hardness increased firstly until reaching the maximum value of 148 HB in right-angle bending, and then decreased in the extending extrusion zone. And also, in adhesion zone sub are grains formed.

Li et al. (2017) studied characteristics of microstructure evolution of two-phase H62 brass alloy during continuous extrusion. The optical microscope and transmission electron microscope were used to observe the whole regions of H62 brass. After continuous extrusion the grain of H62 brass alloy refined. The result indicated that the microstructure in groove rolling region was flatter than that in raw material.

2.3 Analysis of Mechanical Properties

Hu et al. (2017) investigated the enhanced mechanical properties of an Aluminum-Magnesium-Silicon alloy by repetitive continuous extrusion forming process and subsequent aging treatment. The result indicated that as the number of conform passes increase ductility and tensile strength of Aluminum-Magnesium-Silicon alloy increased. supersaturated solid solution of Continuous formation was obtained with structural homogeneity. And also, at the same time gradual increase of dislocation density obtained.

Hu et al. (2019) investigated the improvement of the mechanical properties of aluminum-magnesium-silicon alloys with Nano-scale precipitates after repetitive continuous extrusion forming and T8tempering. repetitive continuous extrusion forming (R-Conform) followed by T8 tempering treatment was found to be a practical approach for earning superior strength with high ductility in an aluminum-magnesium-silicon alloy. The evolution of mechanical properties and microstructure of the aluminum-magnesium-silicon alloy, and its mutual relationship during this novel approach were investigated. The result revealed that a homogeneous and sophisticated microstructure was formed during the repetitive continuous extrusion forming process, which improved the mechanical properties of the Aluminum-Magnesium-Silicon alloy.

Fu-rong et al. (2013) carried out the force analysis and experimental study of pure aluminum and Aluminum-Titanium-Boron alloy continuous expansion extrusion forming process. Slab method was used to establish force equilibrium equations of different deformation zones which is available during the process such as primary gripping zone, gripping zone, conical expansion chamber zone, cylindrical zone and sizing zone of die. They were obtained any wrapping angle of continuous forming machine to an expansion chamber. Finally, they proved that the experimental results of radial forces matched with theoretical formula. *Xin-bing et al. (2013)* proposed Continuous extrusion and rolling forming velocity of copper strip. They determined the bite condition and established compatibility equation of the process by means of DEFORM-3D software to perform and identify the relation between the roll-forming and continuous extrusion velocity of the material. Numerical simulation outcome verified the compatibility equation of roll-forming and continuous extrusion velocity.

2.4 LITERATURE GAP

Over the past decades several researches have been done on different material through continuous forming process, but almost none was found on Commercially Pure Titanium grade 2 material through continuous forming process. So this study aims on the investigation of deformation behavior of commercially pure titanium grade 2 metal in continuous forming process to improve the mechanical and metallurgical capability of material to make Commercially Pure Titanium grade 2 material highly needed in the Industrial, Medical, Automobile, Aerospace and Marine sector.

CHAPTER THREE

MATERIALS AND METHODS

3.1 Introduction

This Chapter highlights the materials used and methodology followed to investigate the deformation behaviour of commercially pure titanium grade 2 material through continuous forming process.

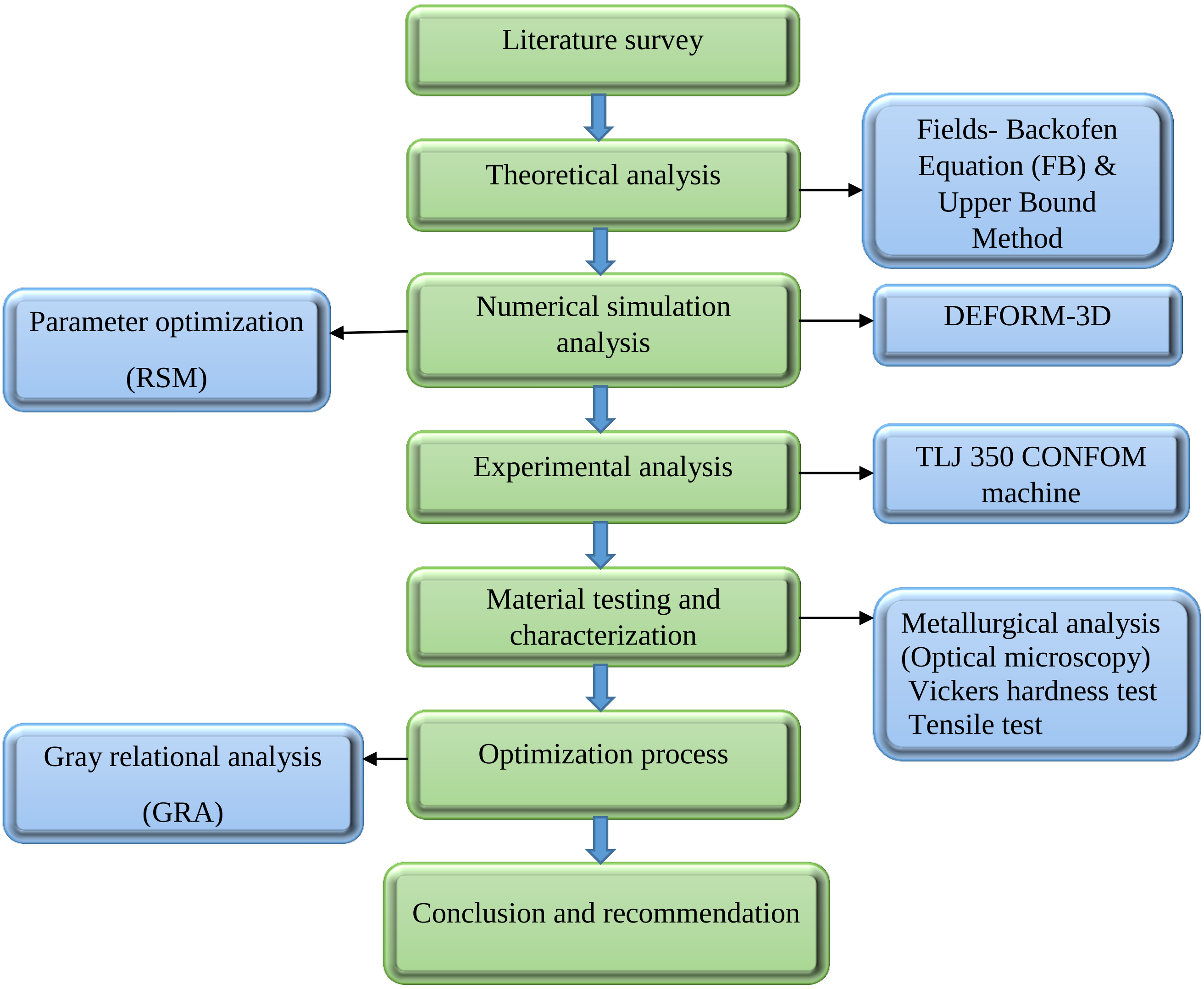

Figure 3. 1 Flow chart of methodology

3.2 Material and Methods

The complete approach that used for theoretical, numerical and experimental analysis of deformation behavior of CP- Titanium grade 2 material during continuous forming process have been explained concisely in this section. The continuous forming processes of raw material has been conducted in Banira Industrial Estate, Jalan Complex, Jungalpur, Howrah, India. CP-Titanium grade 2 material has been served as a feedstock material in the continuous forming process study. Theoretical, Numerical and Experimental analysis techniques were implemented for better understanding of feedstock material during the process. CP-Titanium grade 2 has capable of high strength, low weight ratio, outstanding corrosion resistance, and resistance to high-elevated temperature and also Titanium grade 2 has excellent weldability, cold formability and fabricability for industrial uses with excellent resistance to highly oxidizing media with or without chlorides. This is approved under the national association of corrosion engineers for sour service use.

Generally, commercially pure Titanium can exist in two crystalline structures, namely Hexagonal closed-packed (HCP) and Body centered cubic (BCC) structures *Gilbert and Shannon (1991), Lonardelli et.al (2007).* However, at room temperature, commercially pure Titanium has poor formability and limited ductility due to the intrinsic characteristics of the HCP structure *Chen and Chiu (2005),* in which few slip systems are activated. Twin systems are necessary in order to maintain the deformation compatibility *Chun et.al (2005).* In order to obtain large deformations, it is necessary to deform commercially pure Titanium at higher temperatures, where non-basal slip systems can be activated for improved ductility *Boyer et.al 1994, Huang et.al 2007.* However, excessively high temperatures or low strain rates lead to increased recovery, reducing the hardness. Although, the formability can be improved at elevated temperatures, a manufacturing process at warm temperatures is more economical and more desirable. The details of elemental composition of Titanium grade 2 feedstock material has been shown below in table 3.1.

Table 3. 1 Elemental composition of CP-Titanium grade 2 feedstock material

Content	**Nitrogen**	**Carbon**	**Hydrogen**	**Iron**	**Oxygen**	**Titanium**
in wt.%	0.03	0.08	0.015	0.30	0.25	99.325

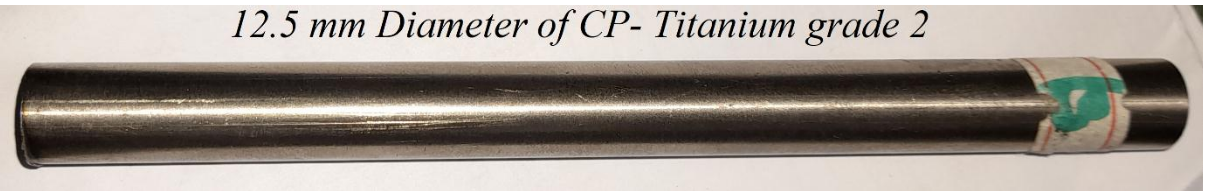

Figure 3. 2 Feedstock material

Table 3. 2 Physical properties of CP-Titanium grade 2 *[31] [32]*

Physical properties	**Metric**
Density	4.51 g/cc

Table 3. 3 Mechanical properties of CP-Titanium grade 2 *[31] [32]*

Mechanical properties	**Metric**
Hardness, Vickers	145
Tensile strength, ultimate	344 MPa
Tensile strength, yield	275-410 MPa
Elongation at break	20 %
Modulus of elasticity	105 GPa
Poisons ratio	0.37
Shear modulus	45 GPa

Table 3. 4 Thermal properties of CP-Titanium grade 2 *[31] [32]*

Thermal properties	**Metric**
Specific heat capacity	0.523 J/g-^{0}C
Thermal conductivity	16.4 W/m-K
Melting point	Max 1665 ^{0}C
Heat of fusion	325 J/g

3.3 Model Approach

Stress as a result of deformation is dependent on strain rate ($\dot{\boldsymbol{\epsilon}}$), strain ($\boldsymbol{\epsilon}$), and temprature ($\boldsymbol{T}$), which can be described by the following function: *Henry S. Valberg (2010)*

$$\boldsymbol{\sigma} = f\,(\dot{\boldsymbol{\epsilon}}, \boldsymbol{\epsilon}, \boldsymbol{T})$$

The plastic deformation behavior of commercially pure Titanium depends strongly on strain rate and temperature. The plastic flow response of this material is described by a deformation constitutive equation incorporating the effects of temperature, strain rate, strain and work hardening rate *Tsao et.al (2012).*

3.4 Flow Stress Behavior

To meditate through hot working process, it is critical to have understanding on the flow stress behaviour of material at elevated temperatures. Flow stress behaviour can be determined by two types of factors such as material factors and process factors. flow stress *(σ)*,work-hardening exponent *(n)* and strain rate sensitivity *(m)* are material factors and deformation temperature *(T)*, true strain *(ε)*,and strain rate *(ε̇)* are processes factors , this study investigates the flow stress behaviour of CP-Titanium grade 2 during hot working condition at several deformation temperature, strain rates and strains. A formulation called Fields–Backofen (FB) has been implemented to investigate the flow stresses behaviour of commercially pure Titanium grade 2 feedstock material at numerous preheating temperature condition under designed reference strain rate and strain values and recommended in a simple form below.

Case studies are designed to calculate the flow stress feedstock material required for deformation of CP-Titanium grade 2 under the given different conditions. Strain rates s^{-1} (8.3 x 10^{-4}, 2.5 x 10^{-3}, 1.6 x 10^{-2}, 5.0 x 10^{-2}), strain (0.03 - 0.34) and deformation temperature (200 - 600 ^{0}C). The flow stress formulation of commercially pure titanium material can be obtained through Fields- Backofen equations *Tsao et.al (2012).*

$$\sigma = K \,.\, \varepsilon^{n} \,.\, \dot{\varepsilon}^{\,m} \tag{3.1}$$

$$n = 0.02045 + 0.04652 \log \dot{\varepsilon} + 190.34785/T \tag{3.2}$$

$$m = 0.370407 - 148.44644/T \tag{3.3}$$

$$K = -658.94329 + 5.08403 \log \dot{\varepsilon} + 991426.1572/T \tag{3.4}$$

The above formulation should be applied for the following conditions,

$$0.03 \leq \varepsilon \leq 0.34 \,,\, 5.0 \text{ x } 10^{-2} \leq \dot{\varepsilon} \leq 8.3 \text{ x } 10^{-4} \,,\, 473 \leq T \leq 873\ (K)$$

where σ is the flow stress, K is the strength coefficient, ε is the strain, n is the work hardening exponent, $\dot{\varepsilon}$ is the strain rate , and m is the strain rate sensitivity exponent.

3.5 Theoretical Analysis

Continuous forming processes can be classified into five sub-regions such as biting, upsetting, filling, extruding and flashing for the analysis of power, that is required during deformation processes. Nevertheless, the power that required for the sub-regions of biting and upsetting are very small than other sub-regions in steady-state processes *Cho et.al (2001)*, so the effects can be neglected without a significant loss of accuracy. Hence, for continuous forming processes similarity for it can be made to the side extrusion without a flash gap as illustrated below in figure 3.3 where extrusion wheel (driving wheel) is assumed as a rigid and non-friction side plate.

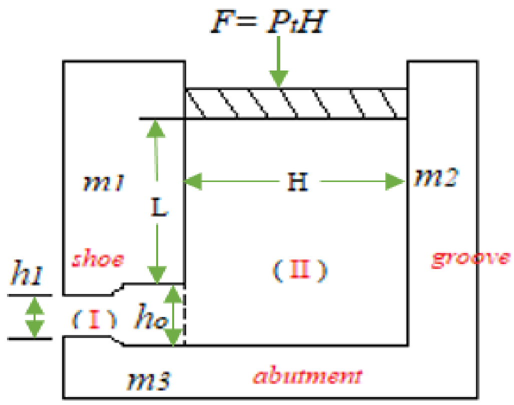

Figure 3. 3 Similarity of the 2D plane continuous forming process to the side extrusion process (a unit depth-of-plane problem).

3.5.1 In the die region

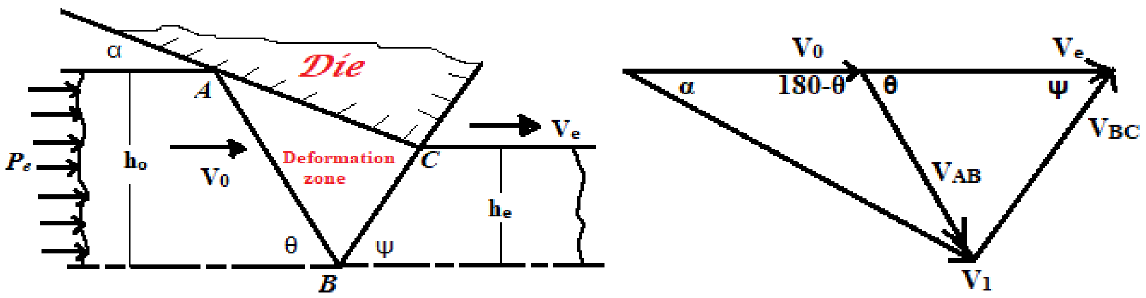

Figure 3. 4 a) Description of die region. b) Hodograph representation.

In the die region (I), there exist two planes of tangential velocity discontinuity which are AB and BC, while it cross plane AB, the tangential velocity discontinuity is V_{AB}. Similarly, while it crosses plane BC, the tangential velocity discontinuity is $V_{BC,}$ as shown on the hodograph representation.

Rate of external work , $\frac{dw_e}{dt} = p_{e_d}\, h_o\, v_o$ (3.5)

Rate of internal work , $\frac{dw_i}{dt} = k(v^*_{AB}\,.\overline{AB} + v^*_{BC}\,.\overline{BC})$ (3.6)

By equating Equations (3.5) and (3.6) , Average extrusion pressure in the die region (p_{e_d}) can be calculated as , $\frac{dw_i}{dt} = \frac{dw_e}{dt}$

$$\frac{p_{e_d}}{2k} = \frac{1}{2h_o v_o}\left[\frac{v_0 \sin\alpha}{\sin(\theta-\alpha)}\,.\overline{AB} + \frac{v_0 \sin\alpha}{\sin(\theta-\alpha)}\,.\frac{sin\theta}{sin\varphi} * \overline{BC}\,\right]$$

$$p_{e_d} = \frac{k \sin\alpha}{h_0 \sin(\theta-\alpha)}\left[\frac{h_0}{sin\theta} + \frac{h_e sin\theta}{sin^2\varphi}\right] \quad (3.7)$$

3.5.2 In the groove region

The average extrusion pressure is obtained by considering the velocity discontinuity, friction forces at the side and abutment surfaces. The total rate of energy consumption in this region is expressed by the following equations.

$$\frac{dw_e}{dt} = p_{e_d}\, h_o\, v_o \tag{3.8}$$

$$\frac{dw_i}{dt} = m_2\text{k}\,(\,L + h_0\,)\, v_0 + \; m_1 kLv_0 + m_3 k\,\frac{H^2}{h_0}\; v_0 + k\,\frac{h_0^2+H^2}{h_0}\; v_0 \tag{3.9}$$

By equating Equations (3.8) and (3.9) , Average extrusion pressure in the groove region (p_{e_G}) can be calculated as , $\frac{dw_i}{dt} = \frac{dw_e}{dt}$

$$[m_2\text{k}\,(\,L + h_0\,)\, v_0 + \; m_1 kLv_0 + m_3 k\,\frac{H^2}{h_0}\; v_0 + \; k\,\frac{h_0^2+H^2}{h_0}\; v_0\,] = p_{e_G}\, H\, v_0$$

$$p_{e_G} \;=\; \frac{k}{H}\,[\,m_2(\,L + h_0\,) + m_1 L + m_3\frac{H^2}{h_0} \;+\; \frac{h_0^2+H^2}{h_0}] \tag{3.10}$$

Where m_1 *is* friction coefficient on the shoe, m_2 is friction coefficient inside the groove, m_3 is friction coefficient on the abutment. Then, the total extrusion pressure is the sum of average extrusion pressure in the die and average extrusion pressure in groove.

$$p_{e_T} \;=\; p_{e_d} + p_{e_G} \tag{3.11}$$

The force required to carry out extrusion process can be calculated as,

$$F = p_{e_T} * H \qquad \text{(N)} \tag{3.12}$$

Then, the power required during the continuous forming process can be calculated as,

$$P = \frac{F*H*2\pi*N}{60} \qquad \text{(W)} \tag{3.13}$$

3.6 Finite Element Formulation

The deformation behaviors of the material in the metal forming process are generally explained through rigid viscoplastic formulation *[Shiro Kobayashi et.al (1989)]*. Differential and integral equations can be resolved by a numerical method called the finite element method. The commercial finite element method code was applied through DEFORM-3D *[Tung-Sheng Yang et.al, (2008)]* for carrying out numerical simulation analysis of deformation behaviour. The basic equations of the rigid-plastic element are as follows:

$$\text{Equilibrium equation:} \quad \sigma_{ij,j} = 0 \tag{3.14}$$

Velocity strain-rate relations and incompressibility equations:

$$\dot{\varepsilon}_{ij} = \frac{1}{2}(u_{ij} + u_{ji}) \tag{3.15}$$

$$\dot{\varepsilon}_v = u_{ij} = 0 \tag{3.16}$$

Constitutive equations: $\sigma'_{ij} = \frac{2\bar{\sigma}}{2\dot{\bar{\varepsilon}}}\dot{\varepsilon}_{ij}$, $\bar{\sigma} = \sqrt{\frac{3}{2}\acute{\sigma}_{ij}\acute{\sigma}_{ij}}$, $\dot{\bar{\varepsilon}} = \sqrt{\frac{3}{2}(\dot{\varepsilon}_{ij}\dot{\varepsilon}_{ij})}$ (3.17)

Yield criterion: $\bar{\sigma}(\dot{\varepsilon}, \dot{\bar{\varepsilon}}, T) = \sqrt{3/2}\,(\sigma' ij\sigma' ij)$ ^1/2 (3.18)

Boundary conditions: $\sigma_{ij}n_i = F_j \text{ on } S_F$, $u_i = U_i \text{ on } S_U$ (3.19)

Where σ_{ij} and $\dot{\varepsilon}_{ij}$ are the stress and the strain rate, respectively, $\bar{\sigma}$ and $\dot{\bar{\varepsilon}}$ are the effective stress and the effective strain rate, respectively, F_j is the force on the boundary surface of S_F, and U_i is the deformation velocity on the boundary surface of S_U. The weak form of rigid-plastic FEM can be determined by applying the variation method to Eqs. (3.14) – (3.18), i.e.

$$\int_V \bar{\sigma}\delta\bar{\varepsilon}dv + K\int \varepsilon_V \,\delta\varepsilon_V dV - \int_{S_F} F_i\,\delta u_i dS = 0 \quad (3.20)$$

Where *V* and *S* are the volume and the surface area of the material, respectively, and *K* is the penalty constant. The most important and crucial part of simulation in software is the selection of appropriate material model. DEFORM-3D contains various material models (for elastic-plastic, rigid-plastic and porous material), and each model has different suitability, so selection of correct material model as per the requirement is the prime necessity to get the accurate results. Most of the material models require detailed material properties such as young’s modulus of elasticity, strain hardening exponent, and strength coefficient, etc., as input to preprocessor before running the solver. In addition to material properties, preprocessor also requires input of detailed process parameters such as friction coefficient, extrusion wheel velocity, heat transfer coefficients etc. Yielding criteria which is used for solving of problem is Von Mises (in the Deform3-D). Equation (3.21) and (3.22) shows the effective strain and effective stress respectively.

$$\bar{\varepsilon} = \frac{\sqrt{2}}{3}\sqrt{(\varepsilon_1 - \varepsilon_2)^2 + (\varepsilon_2 - \varepsilon_3)^2 + (\varepsilon_3 - \varepsilon_1)^2} \quad (3.21)$$

$$\bar{\sigma} = \frac{1}{\sqrt{2}}\sqrt{(\sigma_1 - \sigma_2)^2 + (\sigma_2 - \sigma_3)^2 + (\sigma_3 - \sigma_1)^2} \quad (3.22)$$

Where ε_i and σ_i are principle strain and principle stress in direction i respectively.

3.7. Numerical Simulation

DEFORM-3D is a tool that based on a three-dimensional finite element simulation system to explore numerous forming and heat treatment conditions in the metal forming industries sectors. Designers and engineers are allowed to reduce material costs during production, shop floor costs, redesign of tooling, and improve tool life and also production time of new product. Mainly there are three major components in the Deform-3D tool system, the preprocessor, simulation engine, and the postprocessor as shown in Fig. 3.5.

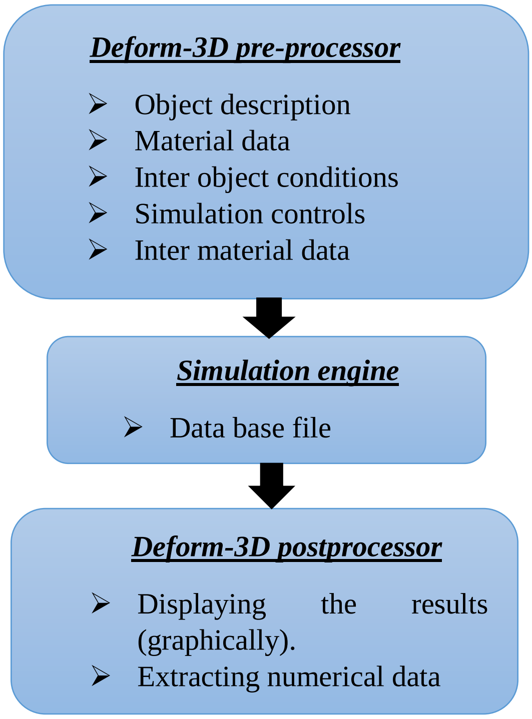

Figure 3. 5 The flow processes of Deform-3D tool system.

DEFORM-3D is custom-made for deformation modeling affords easy data preparation and exploration so engineers can focus on forming, not on learning a cumbersome computer system. A key component of this is a fully automatic, optimized remeshing system, tailored for large deformation problems.

Deform-3D preprocessor, for creating, assembling, or modifying the data required to analyze the simulation, and for generating the required database file. In this step CAD model of the work piece, extrusion wheel, coining wheel, extrusion shoe, abutment and die as. stl file is imported into the pre-processor of the simulation package (DEFORM-3D). Then the following characteristics of the objects need to be defined in detail.

The DEFORM preprocessor uses a graphical user interface to assemble the data required to run the simulation. Input data includes

- ✓ **Object description:** Includes all data associated with an object, including geometry, mesh, temperature, material, etc.
- ✓ **Material data:** Includes data describing the behavior of the material under the conditions which it will reasonably experience during deformation.
- ✓ **Inter object conditions:** Describes how the objects interact with each other, including contact, friction, and heat transfer between objects.

- ✓ **Simulation controls:** Includes instructions on the methods DEFORM should use to solve the problem, including the conditions of the processing environment, what physical processes should be modeled, how many discrete time steps should be used to model the process, etc.
- ✓ **Inter material data:** Describes the physical process of one phase of a material transforming into other phases of the same material in a heat treatment process. For example, the transformation of austenite into pearlite, banite, and martensite.

Simulation engine, for performing the numerical calculations required to analyze the process, and writing the results to the database file. The simulation engine reads the database file, performs the actual solution calculation, and appends the appropriate solution data to the database file. The simulation engine also works seamlessly with the Automatic Mesh Generation (AMG) system to generate a new FEM mesh on the work piece whenever necessary. While the simulation engine is running, it writes status information, including any error messages, to the message (.MSG) and log (.LOG) files.

Deform-3D postprocessor, for reading the database file from the simulation engine and displaying the results graphically and for extracting numerical data. In this step different types of defects, load requirement and torque required for extrusion are studied. Temperature, Effective stress, effective strain, velocity distribution and damage distribution are also found. This step gives the modifications required in geometry or boundary conditions to obtain the optimum result.

Assumptions made during simulations of Continuous Extrusion process are as follows:

- ✓ Work piece material is assumed to be Rigid Visco-Plastic materials
- ✓ The material is homogeneous and isotropic
- ✓ There is no strain hardening
- ✓ Interfaces are either frictionless or sticking friction prevails.
- ✓ Due to the nature of work piece to be Rigid Visco-Plastic materials coulomb friction coefficient has been used.
- ✓ Deformation occurring by shear on a few discrete planes. (Everywhere else the material is rigid).

By simulating manufacturing processes on a computer, this advanced tool allows designers and engineers to:

- ✓ Reduce the need for costly shop floor trials and redesign of tooling and processes
- ✓ Improve tool and die design to reduce production and material costs

- ✓ Shorten lead time in bringing a new product to market

Among the vast range of capabilities some capabilities of the DEFORM tool are as follows:

- ✓ Coupled modeling of deformation and heat transfer for simulation of Cold, Warm and hot forming processes.
- ✓ Extensive material database for many common alloys
- ✓ Contour plots of temperature, strain, stress, damage etc.
- ✓ Self-contact boundary condition with robust remeshing allows a simulation to continue to completion even after a lap or fold is formed.

3.6 Design of experiments (DOE)

Design of experiment (DOE) is a method of defining and investigating all possible conditions involving multiple factors, parameter and variables in the experimental analysis. Taguchi method is a commonly used problem-solving tool which can improve the performance of the product, process design and system. And also is a process optimization method that is based on 8-steps of planning, conducting and evaluating results of matrix experiments to determine the best levels of control factors. The primary goal is to keep the variance in the output very low even in the presence of noise inputs. As shown below in Experimental plan and Design table of Taguchi L9 (2^3) array two variables considered as a factor with three levels.

Table 3. 5 Experimental plan and Design table of Taguchi L9 (2^3) array.

Run Order	Extrusion wheel Velocity (RPM)	Feedstock Temperature (^{0}C)
1	4	200
2	4	400
3	4	600
4	8	200
5	8	400
6	8	600
7	12	200
8	12	400
9	12	600

Table 3. 6 Numerical Simulation data of CP -Titanium Grade 2.

Geometry data	
Wheel diameter, *D* (mm)	350
Die diameter, *d,* (mm)	6
Material width, *H* (mm)	9
Die length, *L*(mm)	10
Simulation data	
Wheel velocity,(RPM)	4/8/12
Environment temperature(^{0}C)	25
Time steps(s)	5
Feedstock Temperature(^{0}C)	200/400/600
Feedstock Material data	
Yield stress(MPa)	375
Strain rate sensitivity	0.22
Heat capacity(N/mm^2/^{0}C)	526.3
Conductivity (N/s/^{0}C)	6.7
Convective heat transfer coefficient(N/s/^{0}C/mm)	0.02
Emissivity coefficient	0.3
Heat transfer Coefficient (N/s/^{0}C/mm)	30
Friction coefficient (Interface)	0.3 (Feedstock and Wheel groove), 0.3 (Abutment and Feedstock), 0.1 (Die and Feedstock)

3.7 Experimental Procedures

The experiments analysis was executed on the commercial pure Titanium Grade 2 rods of 12.5 mm diameter, which were prepared by continuous casting and rolling. During the continuous forming process, the feedstock material was firstly cleaned and extruded to coiled materials with diameter of 10 mm, 8 mm and 6 mm, on a TBJ 350 continuous forming machine at an Extrusion Wheel Velocity of 4 rpm and feedstock temperatures (1000) ^{0}C.

3.9 Material Characterizations

In the present study, material characterization analysis has been conducted after commercially pure titanium grade 2 feedstock material deformed through continuous forming machine at 1000 ^{O}C preheating temperature and different extrusion ratio. To understand the improvement that appears on the feedstock materials after deformation process conducted.

Table 3. 7 Resources required during material characterization

s.no	Resources
1	Abrasive cutting machine
2	Sand papers
3	Polishing machine
4	Diamond suspension liquid
5	Water
6	Dryer (air compressor)
7	Etchants
8	Optical microscopy

3.9.1 Microstructure analysis

Microstructural examination is generally performed using optical microscopes (OM) to magnify features of the material under analysis. Metallurgical examinations may evaluate:

- ✓ Intergranular Attack or Corrosion,
- ✓ Grain Size,
- ✓ Extent of Decarburization and Carburization
- ✓ Inclusion Rating
- ✓ Percent Spheroidization

Sample Preparation

In order to identify and evaluate the microstructure of material, it is very important to prepare the sample carefully and properly. The following steps have been carried out to analyze the microstructural examination of the deformed specimens.

1. *Sectioning:* specimens are carefully sectioned to avoid altering or destroying the structure of the materials. Abrasive cutting wheel has been used, it’s important to keep the specimens cool with coolant to avoid overheat.
2. *Mounting:* after the specimen is sectioned to a convenient size, it is mounted in a plastic or epoxy material to facilitate handling and the grinding and polishing steps. Mounting media ensured to be compatible with the specimen with respect to hardness and abrasion resistance. Typical mounting materials are thermosetting phenolic such as Bakelite, and thermoplastic materials such as methyl methacrylate (Lucite).

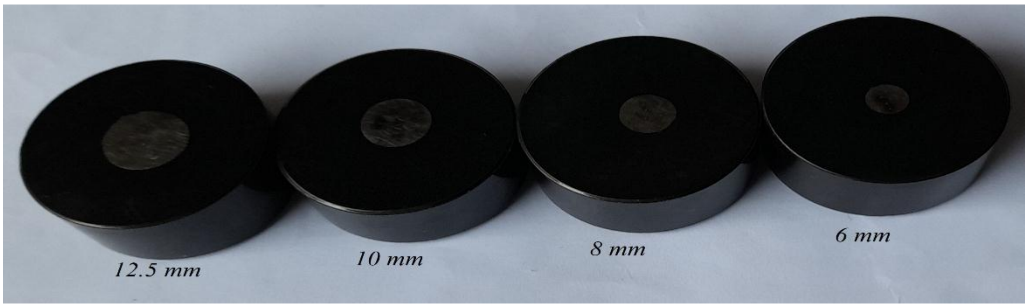

Figure 3. 6 Mounted Process of 12.5 mm raw material and 10 mm, 8 mm, 6 mm of deformed products.

3. *Grinding:* grinding follows mounting to remove the surface damage that occurred during the sectioning step and to provide a flat surface. grinding involves the use of a series of progressively finer abrasive grits (sand paper). Four types of grits size abrasives have been used for grinding processes (coarse grinding (240 µm), fine grinding (320 µm), super fine grinding (400µm), ultrafine grinding (600µm)). This procedure provides a flat surface of the specimens which has been deformed in the previous sectioning steps.
4. *Polishing:* the polishing step removes the last thin layer of the deformed metal.it provides a mirror like surface. Diamond suspension has been used for lubrication during the process
5. *Etching:* the final step that might be used is etching to show the microstructure of the test specimens. This step reveals features such as grain boundaries, twins and second phase particles not seen in the unetched sample. In this step 50ml ethanol and 0.5 ml Nitric acid (HNO_3) have been used as etching chemicals.

Finally, optical microscopy has been used to see the microstructural surface of the specimens by 200µm.

3.9.2 Hardness Test

Hardness test has been conducted to know the resistance of CP-Titanium Grade-2 feedstock material to plastic deformation which induced by applied force, by using Vickers hardness test (HVS- 50) methods consisting of a diamond indenter in the form of right pyramids with a square base and an angle of 136 degrees between opposite faces subjected to a load of 10 kgf and the full load is applied for average time of 10 to 15 seconds.

$$HV = \frac{Constant\ x\ Test\ Force}{surface\ area\ of\ indentation}$$

$$= 0.102\ x\ 2F(sin\frac{136}{2})/d^2$$

Where F- is test force, d- surface area indentation and 136^0 is the angle between the opposite faces subjected to a load of 10 kgf.

3.9.3 Tensile Test

Tensile testing is a fundamental material science and engineering test in which a sample is subjected to a controlled tension until its failure. And also, Tensile testing performed to find how strong a material is and also how much it can be stretched before its failure. This test technique is used to determine yield strength,ultimate tensile strength, ductility and so on. In this study the Tensile test has been conducted on raw material and deformed product of CP-Titanium grade 2 material by using tensile test machine with a maximum force 50 KN.

3.8 Analysis Grey Relation and Taguchi Methods

Grey relational analysis is one of multiple responses optimization techniques that used for solving interrelationships among the multiple responses. In this approach a grey relational grade is obtained for analyzing the relational degree of the multiple responses. *Lin et al. (2002)* have attempted grey relational based approach to solve multi-response problems in the Taguchi methods.

3.8.1 Signal to noise (S/N) ratio

Transform the original response data into S/N ratio (η) using the appropriate formulae depending on the type of quality characteristic. Equation 3.23 express the smaller-the better quality characteristics. The S/N ratio (η) is given by

$$\eta = -10 \log \left[\frac{1}{n} \Sigma (Yij)^2 \right] \qquad 3.23$$

where n- is the number of replications

3.8.2 Normalizing

Normalize Y_{ij} as Z_{ij} ($0 \leq Z_{ij} \leq 1$) by the following formula to avoid the effect of using different units and to reduce variability. Normalization is a transformation performed on a single input to distribute the data evenly and scale it into acceptable range for further analysis.

$$Z_{ij} = \frac{maxYij - Yij}{maxYij - minYij} \qquad 3.24$$

3.8.3 Computation of grey relational coefficient (GC)

Grey relational coefficient is used for determining how close Y_{oj} and Y_{ij}.

$$GC_{ij} = \frac{\Delta \min + \lambda \Delta max}{\Delta ij + \lambda \Delta max} \qquad 3.25$$

where $i = 1, 2 \ldots n$ - experiments *and* $j = 1, 2 \ldots, m$ – responses

GCij = grey relational coefficient for the *i*th experiment/trial and *j*th dependent variable/ response

Δ= absolute difference between Y_{oj} and Y_{ij} which is a deviation from target value and can be treated as quality loss.

Y_{oj} = optimum performance value or the ideal normalized value of j_{th} response

Y_{ij} = the i_{th} normalized value of the j_{th} response/dependent variable

Δmin = minimum value of Δ

Δmax = maximum value of Δ

λ - is the distinguishing coefficient which is defined in the range $0 \leq \lambda \leq 1$ (the value may be adjusted on the practical needs of the system)

3.8.4 Computation of grey relational grade (G_i).

Grey relational grade determines the optimum points of multi response by calculating the average values of grey relational coefficient of responses at each experiment trials. So, the optimum value of each response is considered at the highest value of grey relational grade.

$$G_i = \frac{1}{m} \Sigma GC_{ij} \qquad 3.26$$

where *m* is the number of responses

CHAPTER FOUR

RESULTS AND DISCUSSION

4.1 Introduction

In this Chapter, the overall findings in the investigation of deformation behaviour of CP – Titanium grade 2 material during continuous forming process through theoretical, Numerical and experimental analysis have been elaborated in the below sections and subsections.

4.2 Flow Stress Analysis

Case studies are designed to calculate the flow stress of commercially pure titanium feedstock material required for deformation under the given different conditions. $\dot{\varepsilon}_{ref}$ (reference strain rate) = 8.3 x 10^{-4} s^{-1} , $\dot{\varepsilon}$ (strain rate) = (8.3 x 10^{-4} – 5.0 x 10^{-2}) s^{-1} , strain = (0.03 – 0.34), reference strain = 0.03.

Table 4. 1 Flow stress and shear stress analysis results of CP- Titanium grade 2 feedstock material under different preheating temperature through Fields- Backofen equations. .

S.no	Temperature (^{0}C)	Flow stress (MPa)	Shear stress of the Material (MPa) [$K= \boldsymbol{\sigma_y}/\sqrt{3}$]
1	200	357.65	206
2	400	157.21	90.76
3	600	79.95	46.16

4.3 Theoretical Analysis

Here , According to the minimization of total rate of energy consumption *($\frac{dw_T}{dt}$)*, the value of θ_{min} = 90 and corresponding value of α = 30.

Case study 1: In the die region

Die diameter d, (h_e) = 6 mm, Extrusion wheel velocity = 4 rpm, Initial temperature of feedstock material =200 ^{0}C, Chamber height (h_0) = 10 mm, Shear stress of the feedstock Material (K) at Initial temperature =206 (MPa), α = 30

Average extrusion pressure in the die region (p_{e_d}) can be calculated as ,

$$p_{e_d} = = \frac{k \sin\alpha}{h_0 \sin(\theta-\alpha)} \left[\frac{h_0}{sin\theta} + \frac{h_e sin\theta}{sin^2\varphi}\right]$$

$$p_{e_d} = = \frac{345.7 \sin 30^0}{10\sin(90^0 - 30^0)} \left[\frac{10}{sin90^0} + \frac{6sin90^0}{(sin30)^2}\right]$$

$$p_{e_d} = 1113.79 \quad \text{MPa}$$

Case study 1: In the groove region

Material width, *H = 12.5 mm*, Die length, *L =10mm*, Friction coefficient on the shoe, m_1= 0.3,

Friction coefficient inside the groove, m_2= 0, Friction coefficient on the abutment, m_3 = 0.3.

$$p_{e_G} = \frac{k}{H} [m_2(L + h_0) + m_1 L + m_3 \frac{H^2}{h_0} + \frac{h_0^2+H^2}{h_0}]$$

$$p_{e_G} = 548.99 \quad \text{MPa}$$

Then, the total extrusion pressure is the sum of average extrusion pressure in the die and average extrusion pressure in groove.

$$p_{e_T} = p_{e_d} + p_{e_G}$$

$$p_{e_T} = 1662.78 \quad \text{MPa}$$

The force required to carry out extrusion process can be calculated as (unit depth of the material)

$$F = p_{e_T} * H \qquad \text{(N)}$$

$$F = 1662.78 * 12.5 * 1$$

$$F = 20.78 \quad KN$$

Then, the power required during the CONFORM process can be calculated as,

$$P = \frac{F*H*2\pi*N}{60} \qquad \text{(W)}$$

$$P = \frac{20.78 *12.5*2\pi*4}{60}$$

$$P = 108.83 \qquad KW$$

Case study 2: In the die region

Die diameter d, (h_e) = 6 mm, Extrusion wheel velocity = 4 rpm, Initial temperature of feedstock material = 400^{0}C, Chamber height (h_0) = 10 mm, Shear stress of the feedstock Material (K) at Initial temperature =90.76 (MPa), α = 30

Average extrusion pressure in the die region (p_{e_d}) can be calculated as ,

$$p_{e_d} = = \frac{k \sin\alpha}{h_0 \sin(\theta - \alpha)} [\frac{h_0}{sin\theta} + \frac{h_e sin\theta}{sin^2\varphi}]$$

$$p_{e_d} = = \frac{90.76 \sin 30^0}{10\sin(90^0 - 30^0)} [\frac{10}{sin90^0} + \frac{6sin90^0}{(sin30)^2}]$$

$$p_{e_d} = 490.7 \qquad \text{MPa}$$

Case study 2: In the groove region

Material width, H = *12.5 mm*, Die length, L =*10mm*, Friction coefficient on the shoe, m_1= 0.3, Friction coefficient inside the groove, m_2= 0, Friction coefficient on the abutment, m_3 = 0.3.

$$p_{e_G} = \frac{k}{H}\left[m_2(L + h_0) + m_1 L + m_3 \frac{H^2}{h_0} + \frac{h_0^2 + H^2}{h_0}\right]$$

$$p_{e_G} = 241.78 \quad \text{MPa}$$

Then, the total extrusion pressure is the sum of average extrusion pressure in the die and average extrusion pressure in groove.

$$p_{e_T} = p_{e_d} + p_{e_G}$$

$$p_{e_T} = 732.49 \quad \text{MPa}$$

The force required to carry out extrusion process can be calculated as (unit depth of the material)

$$F = p_{e_T} * H \qquad \text{(N)}$$

$$F = 732.49 * 12.5 * 1$$

$$F = 9.16 \quad KN$$

Then, the power required during the CONFORM process can be calculated as,

$$P = \frac{F * H * 2\pi * N}{60} \qquad \text{(W)}$$

$$P = \frac{9.16 * 12.5 * 2\pi * 4}{60}$$

$$P = 47.96 \quad KW$$

Case study 3: In the die region

Die diameter d, (h_e) = 6 mm, Extrusion wheel velocity = 4 rpm, Initial temperature of feedstock material =600 ^{0}C, Chamber height (h_0) = 10 mm, Shear stress of the feedstock Material (K) at Initial temperature =46.16 (MPa), α = 30

Average extrusion pressure in the die region (p_{e_d}) can be calculated as ,

$$p_{e_d} = = \frac{k \sin\alpha}{h_0 \sin(\theta - \alpha)}\left[\frac{h_0}{sin\theta} + \frac{h_e sin\theta}{sin^2\varphi}\right]$$

$$p_{e_d} = = \frac{46.16 \sin 30^0}{10\sin(90^0 - 30^0)}\left[\frac{10}{sin 90^0} + \frac{6 sin 90^0}{(sin 30)^2}\right]$$

$$p_{e_d} = 249.58 \quad \text{MPa}$$

Case study 3: In the groove region

Material width, H = *12.5 mm*, Die length, L =*10mm*, Friction coefficient on the shoe, m_1= 0.3, Friction coefficient inside the groove, m_2= 0, Friction coefficient on the abutment, m_3 = 0.3.

$$p_{e_G} = \frac{k}{H} [m_2(L + h_0) + m_1 L + m_3 \frac{H^2}{h_0} + \frac{h_0^2 + H^2}{h_0}]$$

$$p_{e_G} = 122.97 \quad \text{MPa}$$

Then, the total extrusion pressure is the sum of average extrusion pressure in the die and average extrusion pressure in groove.

$$p_{e_T} = p_{e_d} + p_{e_G}$$

$$p_{e_T} = 372.55 \quad \text{MPa}$$

The force required to carry out extrusion process can be calculated as (unit depth of the material)

$$F = p_{e_T} * H \qquad \text{(N)}$$

$$F = 372.55 * 12.5 * 1$$

$$F = 4.66 \quad KN$$

Then, the power required during the CONFORM process can be calculated as,

$$P = \frac{F*H*2\pi*N}{60} \qquad \text{(W)}$$

$$P = \frac{4.66 *12.5*2\pi*4}{60}$$

$$P = 24.38 \quad KW$$

Case study 4: In the die region

Die diameter d, (h_e) = 6 mm, Extrusion wheel velocity = 8 rpm, Initial temperature of feedstock material =200 ^{0}C, Chamber height (h_0) = 10 mm, Shear stress of the feedstock Material (K) at Initial temperature =206 (MPa), α = 30

Average extrusion pressure in the die region (p_{e_d}) can be calculated as ,

$$p_{e_d} = = \frac{k \sin\alpha}{h_0 \sin(\theta - \alpha)} [\frac{h_0}{sin\theta} + \frac{h_e sin\theta}{sin^2\varphi}]$$

$$p_{e_d} = = \frac{345.7 \sin 30^0}{10\sin(90^0 - 30^0)} [\frac{10}{sin90^0} + \frac{6sin90^0}{(sin30)^2}]$$

$$p_{e_d} = 1113.79 \quad \text{MPa}$$

Case study 4: In the groove region

Material width, H = *12.5 mm*, Die length, L =*10mm*, Friction coefficient on the shoe, m_1= 0.3, Friction coefficient inside the groove, m_2= 0, Friction coefficient on the abutment, m_3 = 0.3.

$$p_{e_G} = \frac{k}{H}\ [m_2(L + h_0) + m_1 L + m_3 \frac{H^2}{h_0} + \frac{h_0^2+H^2}{h_0}]$$

$$p_{e_G} = 548.99 \quad \text{MPa}$$

Then, the total extrusion pressure is the sum of average extrusion pressure in the die and average extrusion pressure in groove.

$$p_{e_T} = p_{e_d} + p_{e_G}$$

$$p_{e_T} = 1662.78 \quad \text{MPa}$$

The force required to carry out extrusion process can be calculated as (unit depth of the material)

$$F = p_{e_T} * H \qquad \text{(N)}$$

$$F = 1662.78 * 12.5 * 1$$

$$F = 20.78 \quad KN$$

Then, the power required during the CONFORM process can be calculated as,

$$P = \frac{F*H*2\pi*N}{60} \qquad \text{(W)}$$

$$P = \frac{20.78 *12.5*2\pi*8}{60}$$

$$P = 217.61 \qquad KW$$

Case study 5: In the die region

Die diameter d, (h_e) = 6 mm, Extrusion wheel velocity = 8 rpm, Initial temperature of feedstock material = 400 ^{0}C, Chamber height (h_0) = 10 mm, Shear stress of the feedstock Material (K) at Initial temperature =90.76 (MPa), α = 30

Average extrusion pressure in the die region (p_{e_d}) can be calculated as ,

$$p_{e_d} == \frac{k \sin\alpha}{h_0 \sin(\theta-\alpha)}\ [\frac{h_0}{sin\theta} + \frac{h_e sin\theta}{sin^2\varphi}]$$

$$p_{e_d} == \frac{90.76 \sin 30^0}{10\sin(90^0 - 30^0)}\ [\frac{10}{sin90^0} + \frac{6sin90^0}{(sin30)^2}]$$

$$p_{e_d} = 490.7 \qquad \text{MPa}$$

Case study 5: In the groove region

Material width, H = *12.5 mm*, Die length, L =*10mm*, Friction coefficient on the shoe, m_1= 0.3, Friction coefficient inside the groove, m_2= 0, Friction coefficient on the abutment, m_3 = 0.3.

$$p_{e_G} = \frac{k}{H} [m_2(L + h_0) + m_1 L + m_3 \frac{H^2}{h_0} + \frac{h_0^2+H^2}{h_0}]$$

$$p_{e_G} = 241.78 \quad \text{MPa}$$

Then, the total extrusion pressure is the sum of average extrusion pressure in the die and average extrusion pressure in groove.

$$p_{e_T} = p_{e_d} + p_{e_G}$$

$$p_{e_T} = 732.49 \quad \text{MPa}$$

The force required to carry out extrusion process can be calculated as (unit depth of the material)

$$F = p_{e_T} * H \qquad \text{(N)}$$

$$F = 732.49 * 12.5 * 1$$

$$F = 9.16 \quad KN$$

Then, the power required during the CONFORM process can be calculated as,

$$P = \frac{F*H*2\pi*N}{60} \qquad \text{(W)}$$

$$P = \frac{9.16 *12.5*2\pi*8}{60}$$

$$P = 95.9 \quad KW$$

Case study 6: In the die region

Die diameter d, (h_e) = 6 mm, Extrusion wheel velocity = 8 rpm, Initial temperature of feedstock material =600 ^{0}C, Chamber height (h_0) = 10 mm, Shear stress of the feedstock Material (K) at Initial temperature =46.16 (MPa), α = 30

Average extrusion pressure in the die region (p_{e_d}) can be calculated as ,

$$p_{e_d} == \frac{k \sin\alpha}{h_0 \sin(\theta - \alpha)} [\frac{h_0}{sin\theta} + \frac{h_e sin\theta}{sin^2\varphi}]$$

$$p_{e_d} == \frac{46.16 \sin 30^0}{10\sin(90^0 - 30^0)} [\frac{10}{sin90^0} + \frac{6sin90^0}{(sin30)^2}]$$

$$p_{e_d} = 249.58 \quad \text{MPa}$$

Case study 6: In the groove region

Material width, H = *12.5 mm*, Die length, L =*10mm*, Friction coefficient on the shoe, m_1= 0.3, Friction coefficient inside the groove, m_2= 0, Friction coefficient on the abutment, m_3 = 0.3.

$$p_{e_G} = \frac{k}{H} [m_2(L + h_0) + m_1 L + m_3 \frac{H^2}{h_0} + \frac{h_0^2+H^2}{h_0}]$$

$$p_{e_G} = 122.97 \quad \text{MPa}$$

Then, the total extrusion pressure is the sum of average extrusion pressure in the die and average extrusion pressure in groove.

$$p_{e_T} = p_{e_d} + p_{e_G}$$

$$p_{e_T} = 372.55 \quad \text{MPa}$$

The force required to carry out extrusion process can be calculated as (unit depth of the material)

$$F = p_{e_T} * H \qquad \text{(N)}$$

$$F = 372.55 * 12.5 * 1$$

$$F = 4.66 \quad KN$$

Then, the power required during the CONFORM process can be calculated as,

$$P = \frac{F*H*2\pi*N}{60} \qquad \text{(W)}$$

$$P = \frac{4.66 *12.5*2\pi*8}{60}$$

$$P = 48.88 \quad KW$$

Case study 7: In the die region

Die diameter d, (h_e) = 6 mm, Extrusion wheel velocity = 12 rpm, Initial temperature of feedstock material =200 ^{0}C, Chamber height (h_0) = 10 mm, Shear stress of the feedstock Material (K) at Initial temperature =206 (MPa), α = 30

Average extrusion pressure in the die region (p_{e_d}) can be calculated as,

$$p_{e_d} = = \frac{k \sin\alpha}{h_0 \sin(\theta - \alpha)} [\frac{h_0}{sin\theta} + \frac{h_e sin\theta}{sin^2\varphi}]$$

$$p_{e_d} = = \frac{345.7 \sin 30^0}{10\sin(90^0 - 30^0)} [\frac{10}{sin90^0} + \frac{6sin90^0}{(sin30)^2}]$$

$$p_{e_d} = 1113.79 \quad \text{MPa}$$

Case study 7: In the groove region

Material width, H = *12.5 mm*, Die length, L =*10mm*, Friction coefficient on the shoe, m_1= 0.3, Friction coefficient inside the groove, m_2= 0, Friction coefficient on the abutment, m_3 = 0.3.

$$p_{e_G} = \frac{k}{H} [m_2(L + h_0) + m_1 L + m_3 \frac{H^2}{h_0} + \frac{h_0^2+H^2}{h_0}]$$

$$p_{e_G} = 548.99 \quad \text{MPa}$$

Then, the total extrusion pressure is the sum of average extrusion pressure in the die and average extrusion pressure in groove.

$$p_{e_T} = p_{e_d} + p_{e_G}$$

$$p_{e_T} = 1662.78 \quad \text{MPa}$$

The force required to carry out extrusion process can be calculated as (unit depth of the material)

$$F = p_{e_T} * H \qquad \text{(N)}$$

$$F = 1662.78 * 12.5 * 1$$

$$F = 20.78 \quad KN$$

Then, the power required during the CONFORM process can be calculated as,

$$P = \frac{F*H*2\pi*N}{60} \qquad \text{(W)}$$

$$P = \frac{20.78 *12.5*2\pi*12}{60}$$

$$P = 326.4 \qquad KW$$

Case study 8: In the die region

Die diameter d, (h_e) = 6 mm, Extrusion wheel velocity = 12 rpm, Initial temperature of feedstock material = 400 ^{0}C, Chamber height (h_0) = 10 mm, Shear stress of the feedstock Material (K) at Initial temperature =90.76 (MPa), α = 30

Average extrusion pressure in the die region (p_{e_d}) can be calculated as ,

$$p_{e_d} == \frac{k \sin\alpha}{h_0 \sin(\theta - \alpha)} [\frac{h_0}{sin\theta} + \frac{h_e sin\theta}{sin^2\varphi}]$$

$$p_{e_d} == \frac{90.76 \sin 30^0}{10\sin(90^0 - 30^0)} [\frac{10}{sin90^0} + \frac{6sin90^0}{(sin30)^2}]$$

$$p_{e_d} = 490.7 \qquad \text{MPa}$$

Case study 8: In the groove region

Material width, *H = 12.5 mm*, Die length, *L =10mm*, Friction coefficient on the shoe, m_1= 0.3, Friction coefficient inside the groove, m_2= 0, Friction coefficient on the abutment, m_3 = 0.3.

$$p_{e_G} = \frac{k}{H} [m_2(L + h_0) + m_1 L + m_3 \frac{H^2}{h_0} + \frac{h_0^2+H^2}{h_0}]$$

$$p_{e_G} = 241.78 \quad \text{MPa}$$

Then, the total extrusion pressure is the sum of average extrusion pressure in the die and average extrusion pressure in groove.

$$p_{e_T} = p_{e_d} + p_{e_G}$$

$$p_{e_T} = 732.49 \quad \text{MPa}$$

The force required to carry out extrusion process can be calculated as (unit depth of the material)

$$F = p_{e_T} * H \qquad \text{(N)}$$

$$F = 732.49 * 12.5 * 1$$

$$F = 9.16 \quad KN$$

Then, the power required during the CONFORM process can be calculated as,

$$P = \frac{F*H*2\pi*N}{60} \qquad \text{(W)}$$

$$P = \frac{9.16 *12.5*2\pi*12}{60}$$

$$P = 143.88 \quad KW$$

Case study 9: In the die region

Die diameter d, (h_e) = 6 mm, Extrusion wheel velocity = 12 rpm, Initial temperature of feedstock material = 600 ^{0}C, Chamber height (h_0) = 10 mm, Shear stress of the feedstock Material (K) at Initial temperature =46.16 (MPa), α = 30

Average extrusion pressure in the die region (p_{e_d}) can be calculated as ,

$$p_{e_d} = = \frac{k \sin\alpha}{h_0 \sin(\theta - \alpha)} [\frac{h_0}{sin\theta} + \frac{h_e sin\theta}{sin^2\varphi}]$$

$$p_{e_d} = = \frac{46.16 \sin 30^0}{10\sin(90^0 - 30^0)} [\frac{10}{sin90^0} + \frac{6sin90^0}{(sin30)^2}]$$

$$p_{e_d} = 249.58 \quad \text{MPa}$$

Case study 9: In the groove region

Material width, H = *12.5 mm*, Die length, L =*10mm*, Friction coefficient on the shoe, m_1= 0.3, Friction coefficient inside the groove, m_2= 0, Friction coefficient on the abutment, m_3 = 0.3.

$$p_{e_G} = \frac{k}{H}\left[m_2(L + h_0) + m_1 L + m_3 \frac{H^2}{h_0} + \frac{h_0^2 + H^2}{h_0}\right]$$

$$p_{e_G} = 122.97 \quad \text{MPa}$$

Then, the total extrusion pressure is the sum of average extrusion pressure in the die and average extrusion pressure in groove.

$$p_{e_T} = p_{e_d} + p_{e_G}$$

$$p_{e_T} = 372.55 \quad \text{MPa}$$

The force required to carry out extrusion process can be calculated as (unit depth of the material)

$$F = p_{e_T} * H \qquad \text{(N)}$$

$$F = 372.55 * 12.5 * 1$$

$$F = 4.66 \quad KN$$

Then, the power required during the CONFORM process can be calculated as,

$$P = \frac{F * H * 2\pi * N}{60} \qquad \text{(W)}$$

$$P = \frac{4.66 * 12.5 * 2\pi * 12}{60}$$

$$P = 73.28 \quad KW$$

Table 4. 2 Theoretical Analysis results of CP-Titanium grade 2 material.

Run Order	Extrusion wheel Velocity (RPM)	Feedstock Temperature (^{0}C)	Total required pressure (MPa)	Load required (KN)	Power required (KW)
1	4	200	1662.78	20.78	108.83
2	4	400	732.49	9.16	47.96
3	4	600	372.55	4.66	24.38
4	8	200	1662.78	20.78	217.61
5	8	400	732.49	9.16	95.9
6	8	600	372.55	4.66	48.88
7	12	200	1662.78	20.78	326.4
8	12	400	732.49	9.16	143.88
9	12	600	372.55	4.66	73.28

4.4 Numerical Simulations Analysis

For the analysis of numerical simulation results, the plastic deformation of the feedstock material in entire continuous extrusion process is divided into two basic stages. In the first stage of plastic deformation, deformation of the feedstock material takes place from the entry of feedstock material in the grooved portion of extrusion wheel until it hits the abutment. The second stage of plastic deformation consists of deformation of feedstock material after striking the abutment till the extrusion of feedstock material through the die orifice.

4.4.1 Establishment of finite element model.

The finite element model of the extrusion and roll with a diameter of 350 mm (Fig. 4.1) was established by a TBJ 350 continuous extrusion machine.

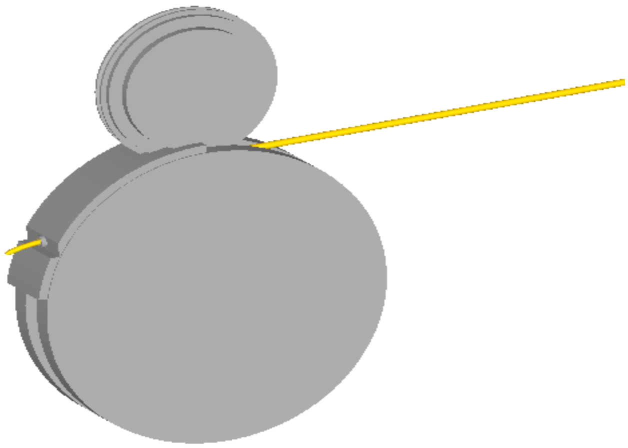

Figure 4. 1 The Finite Element Model of The CONFORM.

4.4.2 Simulation of 12.5 mm Titanium Grade 2 Feedstock Material

The finite element simulation of titanium grade 2 feedstock material for 12.5 mm diameter has been done at different extrusion wheel velocities, different preheating temperature and the table below shows the input parameters used in the simulations. The following parameters have been studied after successful run of the finite element simulations for 12.5 mm diameter titanium grade 2 feedstock material:

- ✓ The total load required for deformation of the CP-Titanium grade 2.
- ✓ The torque required for deformation of the CP-Titanium grade 2.
- ✓ The effective stress distribution.
- ✓ The effective strain distribution
- ✓ Damage distribution
- ✓ Temperature distribution
- ✓ Velocity distribution

The details of tetrahedron mesh elements for simulation of 12.5 mm diameter of CP-Titanium grade 2 feedstock material shown below in Table 4.3

Table 4. 3 Details of tetrahedron mesh elements for 12.5 mm diameter CP-Titanium grade 2 feedstock

S. No.	Objects	Mesh-Elements
1	Work piece	72055
2	Extrusion Wheel	148537
3	Extrusion shoe	24885
4	Coining Wheel	65307
5	Abutment	76391
6	Die	45589

As shown below from case study 1 to case study 3, the numerical simulation results of 12.5 mm CP-Titanium grade 2 displayed at 4 rpm extrusion wheel velocity and 200 ^{0}C, 400 ^{0}C, 600 ^{0}C feedstock temperature. In each case various results are displayed such as total load required for deformation, torque required for deformation. effective stress distribution, effective strain distribution, Damage distribution, Temperature distribution and Velocity distribution of CP-Titanium grade 2.

Case study 1: Simulation run at 4 rpm extrusion wheel velocity and 200 ^{0}C preheating temperature.

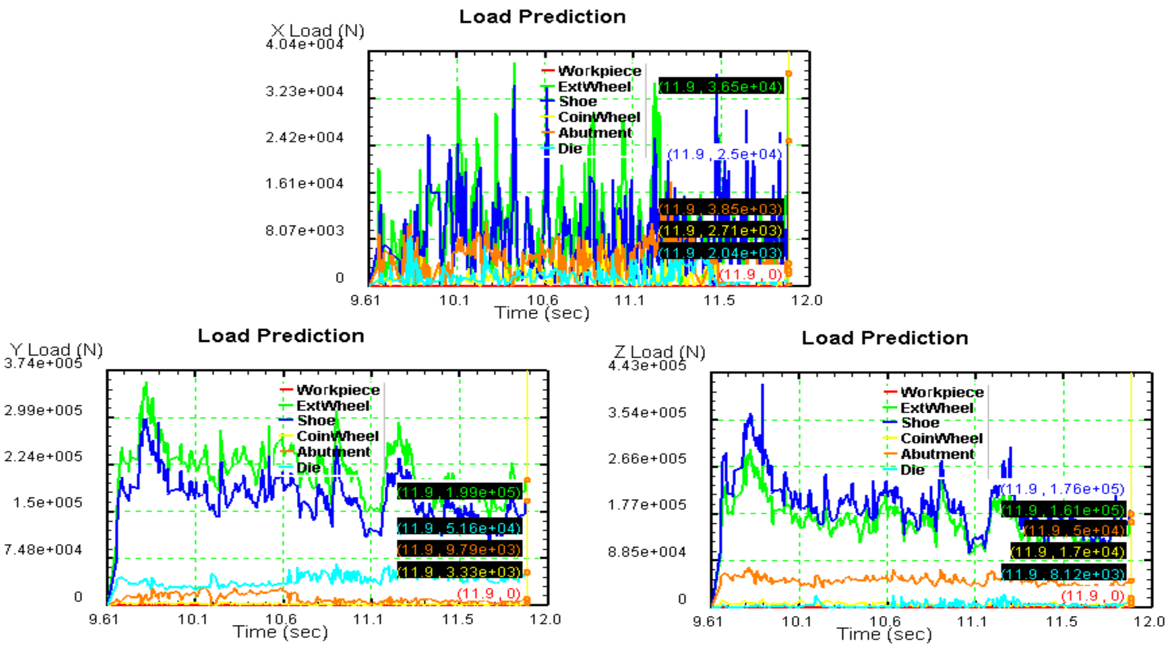

Figure 4. 2 The total load required for deformation of 12.5 mm CP-Titanium grade 2 under 4 rpm (extrusion wheel velocity) and 200 ^{0}C (feedstock temperature). (x, y and z loads).

Figure 4.2 demonstrates the total load required for deformation at 4 rpm and 200 ^{0}C. total load (x-load, y-load and z- load). At this condition the highest load applied in the x – axis direction is on extrusion wheel and shoe surface which is 3.65 x 10^4 and 2.5 x 10^4 respectively, in the y- axis direction is on extrusion wheel and shoe surface which is 1.99 x 10^5 and 1.43 x 10^5 respectively, in z- axis direction is on extrusion wheel and shoe surface which is 1.61 x 10^5 and 1.76 x 10^5 respectively. So, from all machine parts the highest load applied is on the extrusion wheel material from y-axis direction which is 1.99 x 10^5 N.

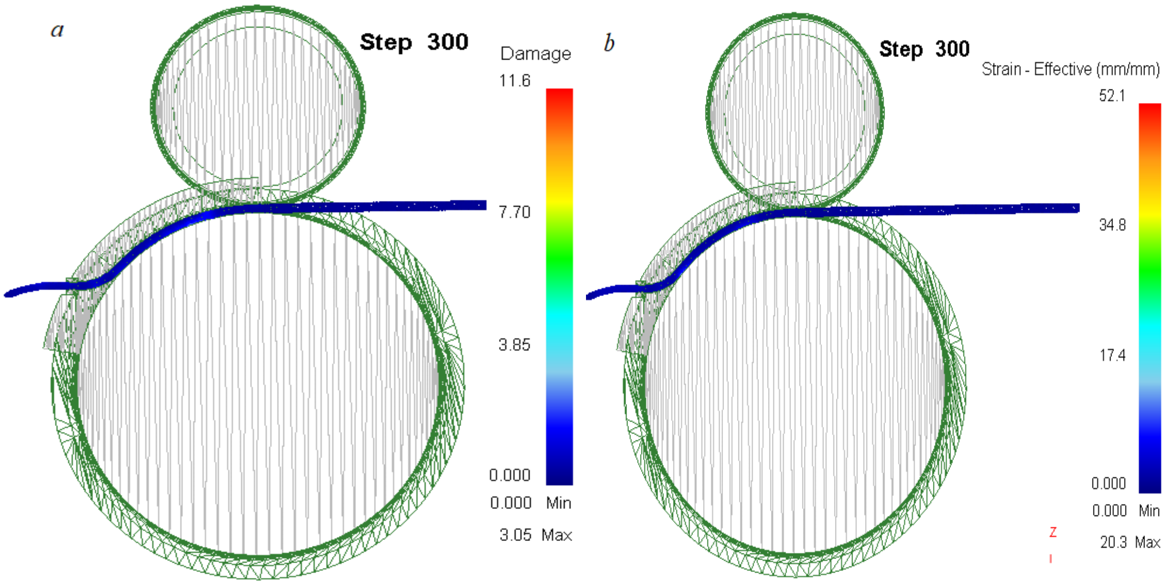

Figure 4. 3 (a) Damage distribution and (b) Effective-strain distribution of 12.5 mm CP-Titanium grade 2 under 4 rpm (extrusion wheel velocity) and 200 ^{0}C (feedstock temperature).

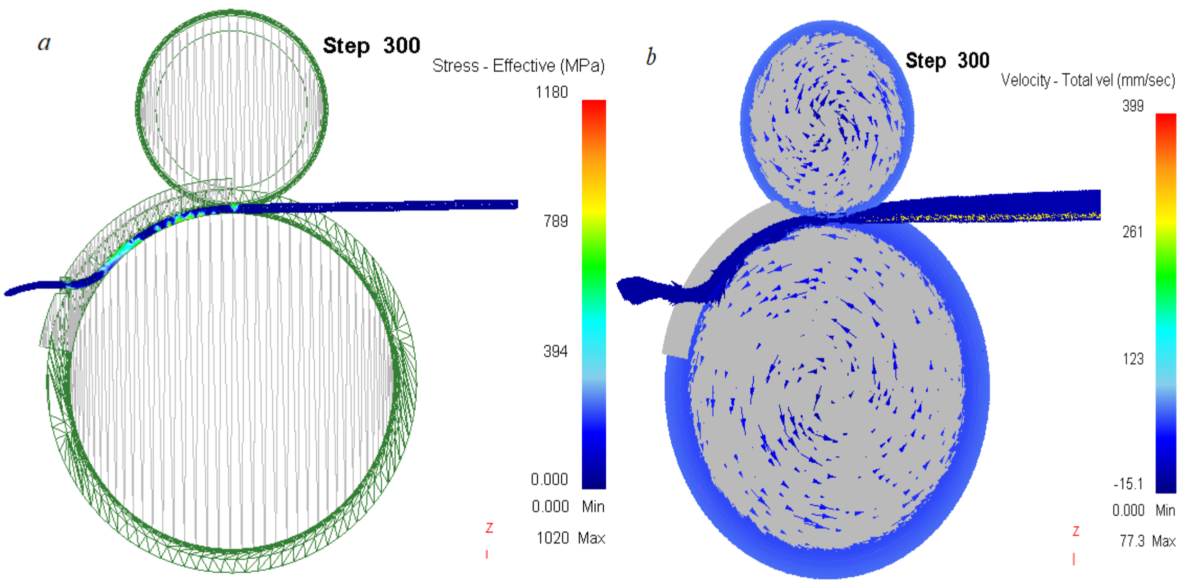

Figure 4. 4 (a) Effective-stress distribution and (b) Total velocity distribution of 12.5 mm CP-Titanium grade 2 under 4 rpm (extrusion wheel velocity) and 200 ^{0}C (feedstock temperature).

Figure 4.3 above elucidates the damage distribution and effective-strain distribution of 12.5 mm CP-Titanium grade 2 simulation results at 4 rpm extrusion wheel velocity and 200 ^{0}C feedstock temperature. As the simulation results displayes the effective strain distribution scored during the process is 20.3 mm/mm and the damage distribution value is 3.05. Figure 4.4 above portrays the effective-stress distribution and total velocity distribution of 12.5 mm CP-Titanium grade 2 simulation results at 4 rpm extrusion wheel velocity and 200 ^{0}C feedstock temperature. As the simulation results displayes the effective stress distribution scored during the process is 1020 MPa and the total velocity distribution value is 77.3 mm/sec.

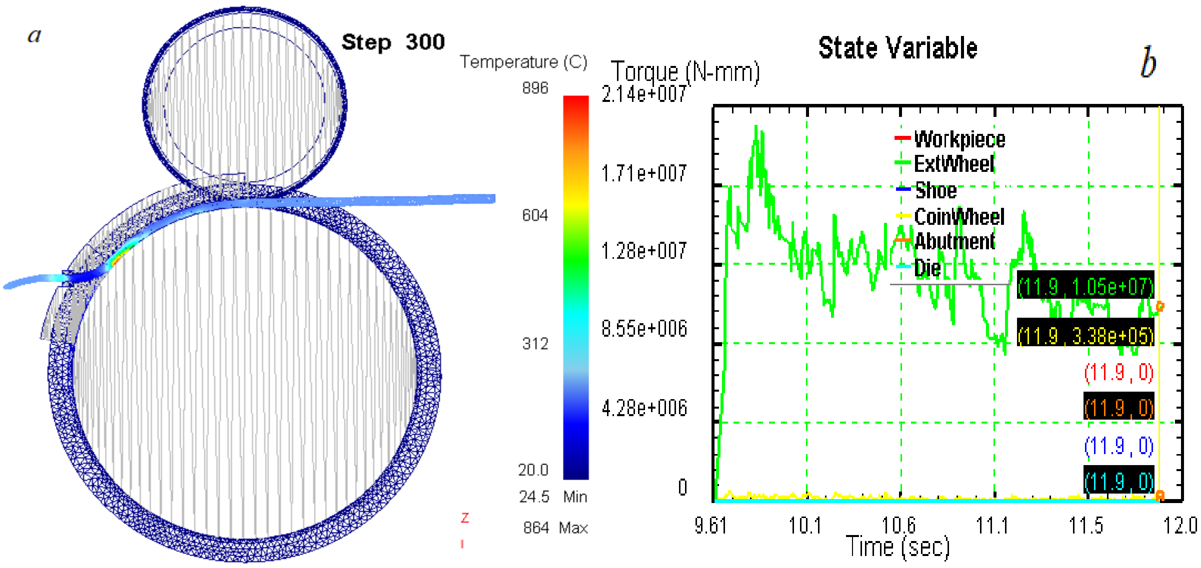

Figure 4. 5 (a) Temperature distribution and (b) Total torque required for deformation of 12.5 mm CP-Titanium grade 2 under 4 rpm (extrusion wheel velocity) and 200 ^{0}C (feedstock temperature).

Figure 4.5 above displayes the temperature distribution and total torque consumed during deformation. As its displayed, the temperature distribution recorded as 864 ^{0}C and total torque consumed by extrusion wheel recorded as 1.05 x 10^{7} and by coining wheel recorded as 3.38 x 10^{5}. Figure 4.6 demonstrates the total load required for deformation at 4 rpm and 400 ^{0}C. total load (x-load, y-load and z- load). At this condition the highest load applied in the x – axis direction is on shoe surface and abutment part which is 4.98 x 10^{3} and 4.77 x 10^{3} respectively, in the y- axis direction is on extrusion wheel and shoe surface which is 2.24 x 10^{5} and 1.81 x 10^{5} respectively, in z- axis direction is on extrusion wheel and shoe surface which is 1.58 x 10^{5} and 1.92 x 10^{5} respectively. So, from all machine parts the highest load applied is on the extrusion wheel material from y-axis direction which is 2.24 x 10^{5} N.

In numerical experiment one, high amount of power consumed because the preheating temperature of feedstock material is low and rpm amount the extrusion wheel velocity is also in slow motion due to those reasons plastic deformation process is become tough So, in this condition the effective stress of CP-Titanium grade 2 is high.

Case study 2. Simulation run at 4 rpm extrusion wheel velocity and 400 ^{0}C preheating temperature.

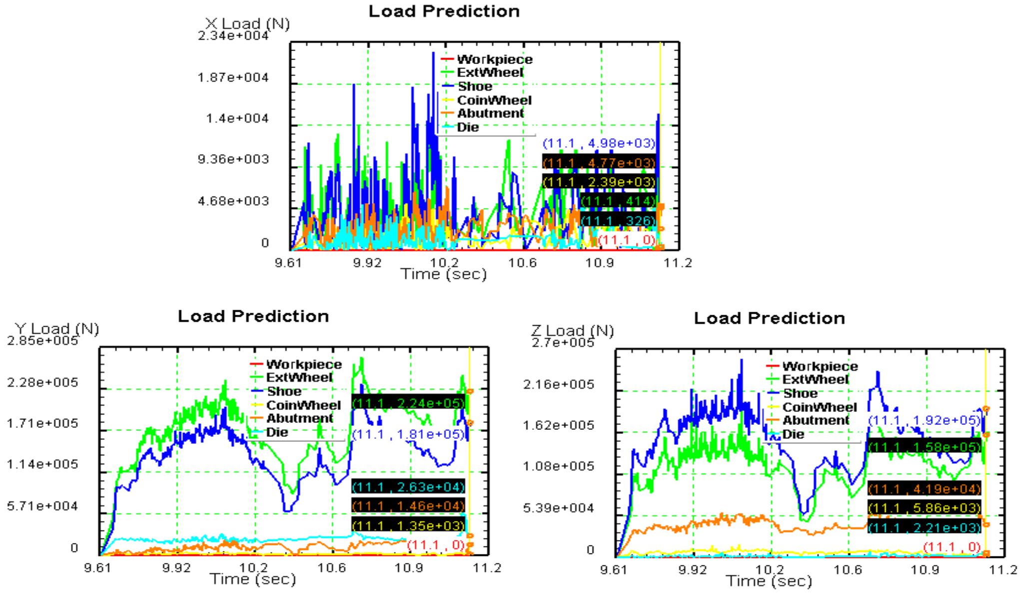

Figure 4. 6 The total load required for deformation of the 12.5 mm CP-Titanium grade 2 under 4 rpm extrusion wheel velocity and 400 ^{0}C feedstock temperature.

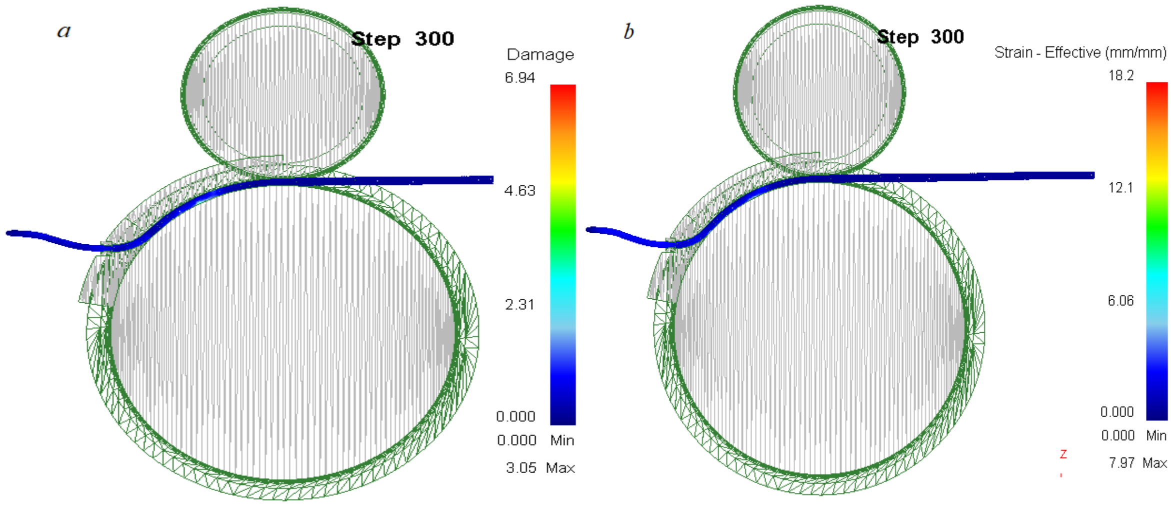

Figure 4. 7 (a) Damage distrubution and (b) Effective-strain distribution of 12.5 mm CP-Titanium grade 2 under 4 rpm (extrusion wheel velocity) and 400 ^{0}C (feedstock temperature).

Figure 4.7 above illustrates the damage distribution and effective-strain distribution of 12.5 mm CP-Titanium grade 2 simulation results at 4 rpm extrusion wheel velocity and 400 ^{0}C feedstock temperature. As the simulation results displayes the effective strain distribution scored during the process is 7.97 mm/mm and the damage distribution value is 3.05

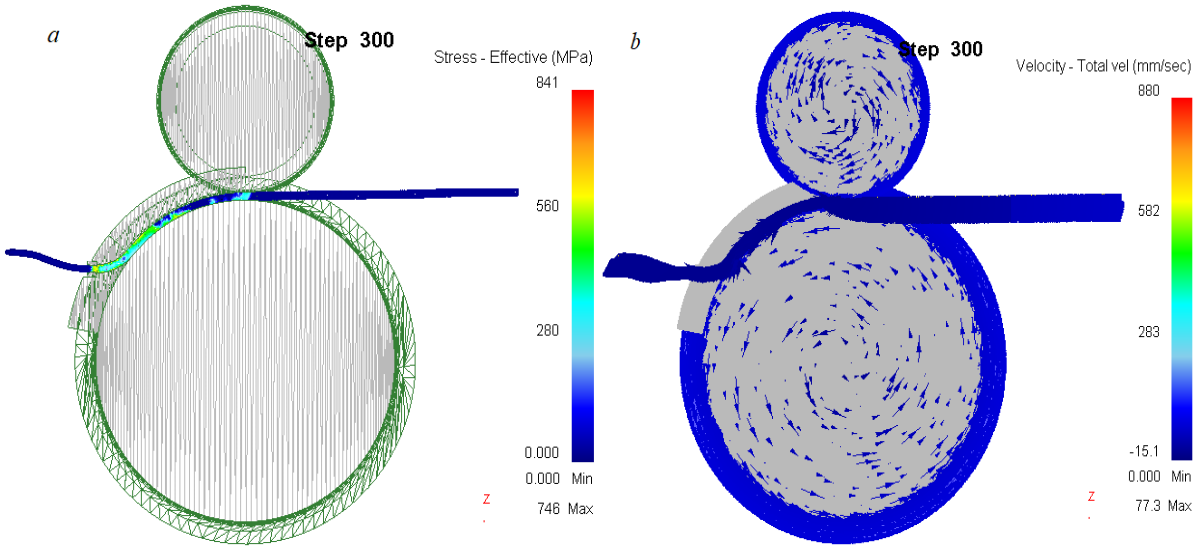

Figure 4. 8 (a) Effective-stress distribution and (b) Total velocity distribution of 12.5 mm CP-Titanium grade 2 under 4 rpm (extrusion wheel velocity) and 400 ^{0}C (feedstock temperature).

Figure 4.8 above depicts the effective-stress distribution and total velocity distribution of 12.5 mm CP-Titanium grade 2 simulation results at 4 rpm extrusion wheel velocity and 400 ^{0}C feedstock temperature. As the simulation results displayes the effective stress distribution scored during the process is 746 MPa and the total velocity distribution value is 77.3 mm/sec.

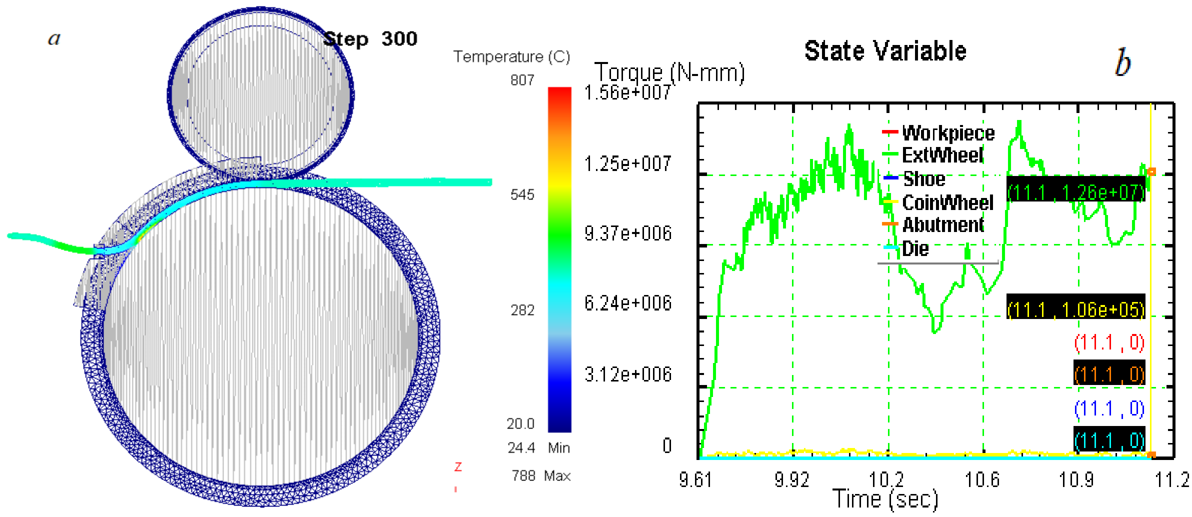

Figure 4. 9 (a) Temperature distribution and (b) Total torque required for deformation of 12.5 mm CP-Titanium grade 2 under 4 rpm extrusion wheel velocity and 400 ^{0}C feedstock temperature.

Case study 3. Simulation run at 4 rpm extrusion wheel velocity and 600 ^{0}C preheating temperature

Figure 4.10 below demonstrates the total load required for deformation at 4 rpm and 600 ^{0}C. total load (x-load, y-load and z- load). At this condition the highest load applied in the x –

axis direction is on die and abutment material which is 1.85 x 10^3 and 6.97 x 10^3 respectively, in the y- axis direction is on extrusion wheel and shoe surface which is 1.23 x 10^5 and 8.91 x 10^4 respectively, in z- axis direction is on extrusion wheel and shoe surface which is 7.23 x 10^4 and 8.73 x 10^4 respectively. So, from all machine parts the highest load applied is on the extrusion wheel material from y-axis direction which is 1.23 x 10^5 N.

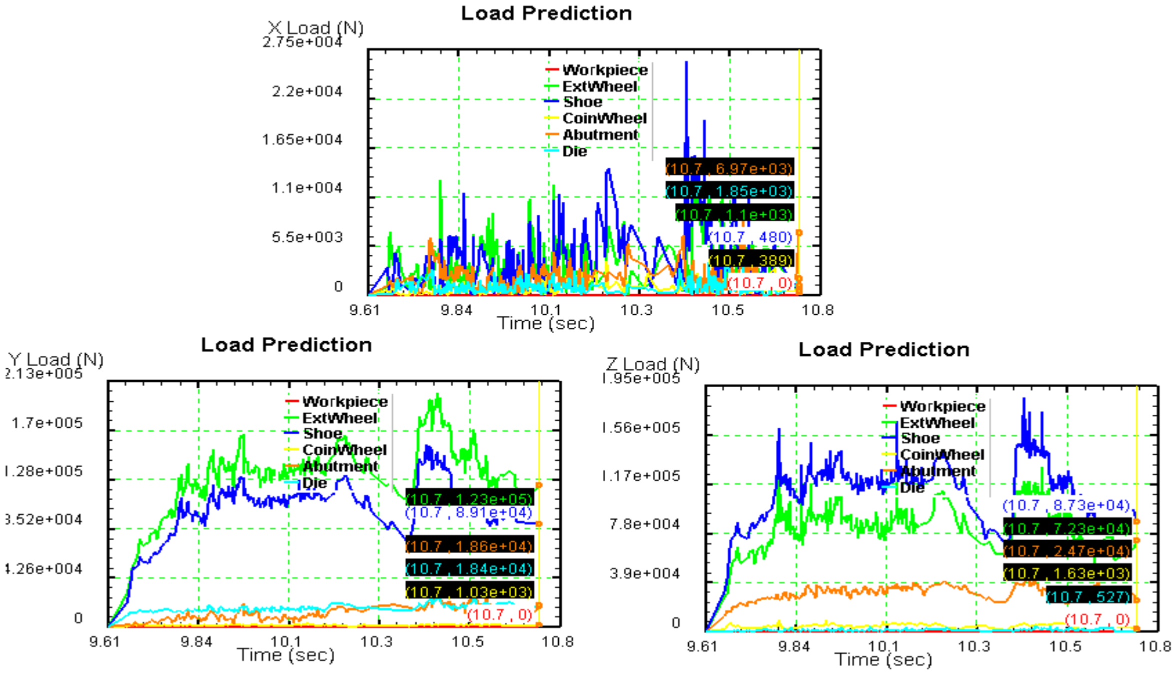

Figure 4. 10 The total load required for deformation of the 12.5 mm CP-Titanium grade 2 under 4 rpm extrusion wheel velocity and 600 ^{0}C feedstock temperature.

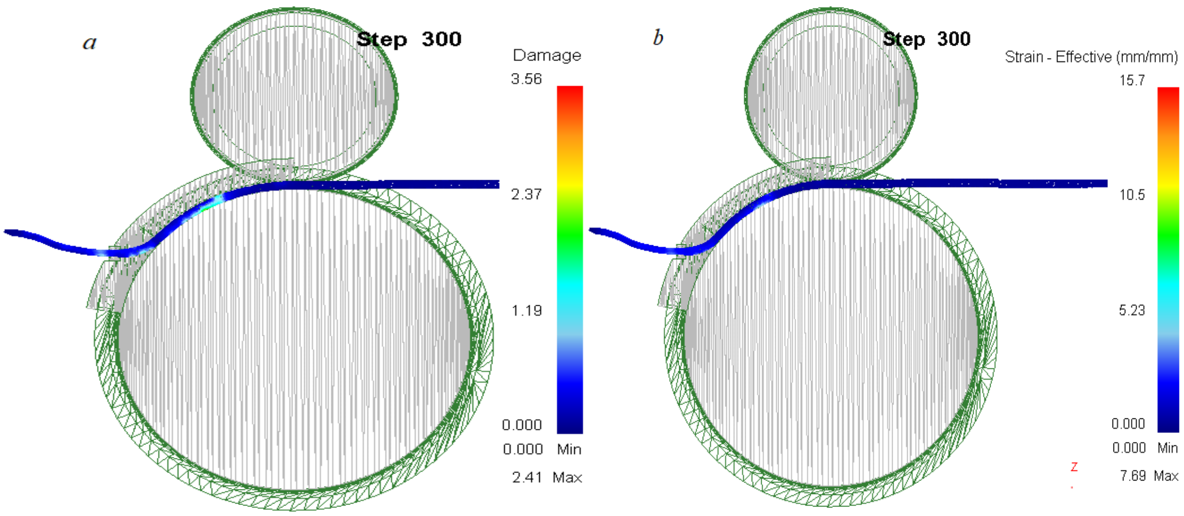

Figure 4. 11 (a) Damage distrubution and (b) Effective-strain distribution of 12.5 mm CP-Titanium grade 2 under 4 rpm extrusion wheel velocity and 600 ^{0}C feedstock temperature.

Figure 4.11 shown above illustrates the damage distribution and effective-strain distribution of 12.5 mm CP-Titanium grade 2 simulation results at 4 rpm extrusion wheel velocity and

600 0C feedstock temperature. As the simulation results displayes the effective strain distribution scored during the process is 7.69 mm/mm and the damage distribution value is 2.41.

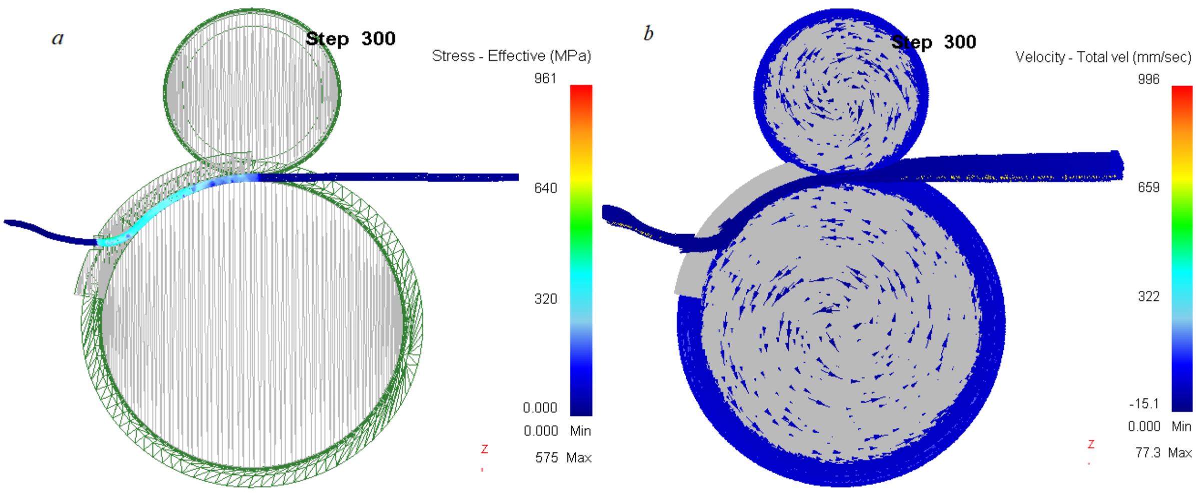

Figure 4. 12 (a) Effective-stress distribution and (b) Total velocity distribution of 12.5 mm CP-Titanium grade 2 under 4 rpm extrusion wheel velocity and 600 ^{0}C feedstock temperature.

Figure 4.12 shown above depicts the effective-stress distribution and total velocity distribution of 12.5 mm CP-Titanium grade 2 simulation results at 4 rpm extrusion wheel velocity and 600 0C feedstock temperature. As the simulation results displayes the effective stress distribution scored during the process is 575 MPa and the total velocity distribution value is 77.3 mm/sec.

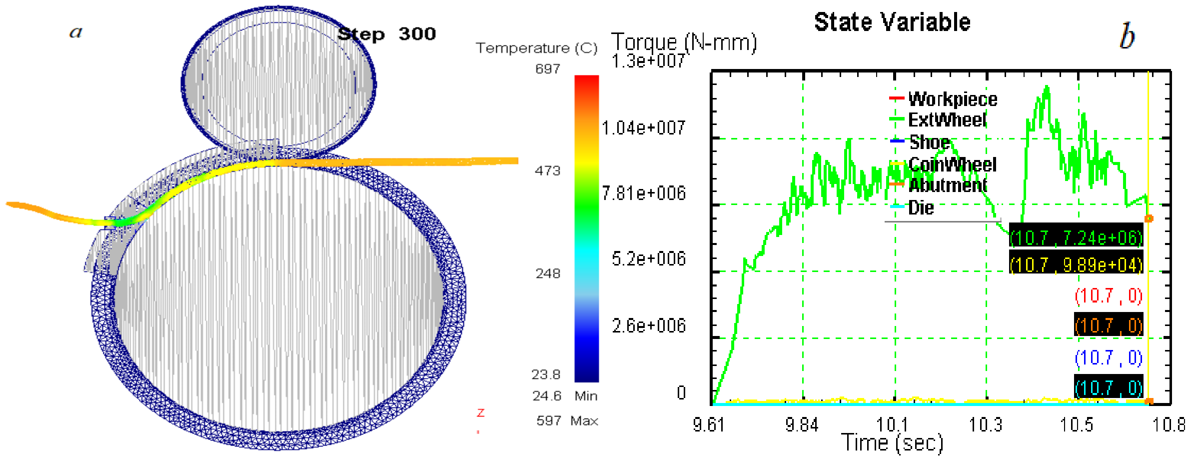

Figure 4. 13 (a) Temperature distribution and (b) Total torque required for deformation of 12.5 mm CP-Titanium grade 2 under 4 rpm extrusion wheel velocity and 600 ^{0}C feedstock temperature.

Figure 4.13 shown above depicts the temperature distribution and total torque required for deformation of work material at 4 rpm and 600 ^{0}C preheating temperature. As its displayed the temperature and total torque highly minimized during the process due to high preheating conditions. As shown below from case study 4 to case study 6, the numerical simulation results of 12.5 mm CP-Titanium grade 2 displayed at 8 rpm extrusion wheel velocity and 200 ^{0}C, 400 ^{0}C, 600 ^{0}C feedstock temperature. In each case various results are displayed such as total load required for deformation, torque required for deformation. effective stress distribution, effective strain distribution, Damage distribution, Temperature distribution and Velocity distribution of CP-Titanium grade 2.

Case study 4. Simulation run at 8 rpm extrusion wheel velocity and 200 ^{0}C preheating temperature.

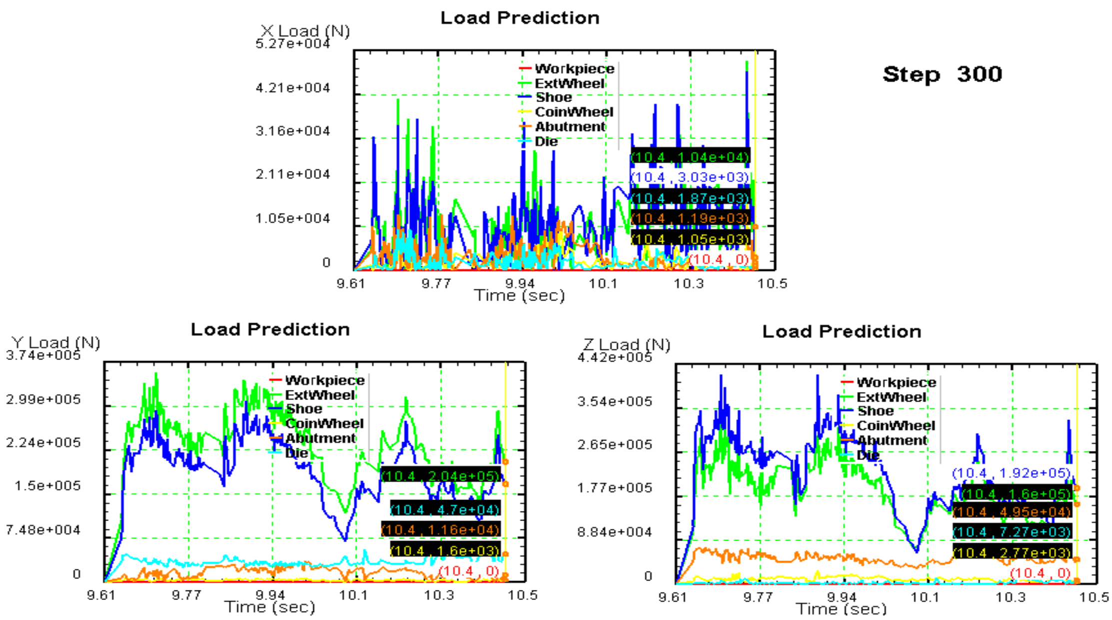

Figure 4. 14 The total load required for deformation of the 12.5 mm CP-Titanium grade 2 under 8 rpm (extrusion wheel velocity) and 200 ^{0}C (feedstock temperature).

Figure 4.14 demonstrates the total load required for deformation at 8 rpm and 200 ^{0}C. total load x-load, y-load and z- load. At this condition the highest load applied in the x – axis direction is on extrusion wheel and shoe surface which is 1.04 x 10^4 and 3.03 x 10^3 respectively, in the y- axis direction is on extrusion wheel and shoe surface which is 2.04 x 10^5 and 4.7 x 10^4 respectively, in z- axis direction is on extrusion wheel and shoe surface which is 1.6 x 10^5 and 1.92 x 10^5 respectively. So, from all machine parts the highest load applied is on the extrusion wheel material from y-axis direction which is 2.04 x 10^5 N. Figure 4.15 shown below illustrates the damage distribution and effective-strain distribution of 12.5 mm CP-Titanium grade 2 simulation results at 8 rpm extrusion wheel velocity and 200 ^{0}C feedstock temperature. As the simulation results displayes the effective strain distribution scored during the process is 12.9 mm/mm and the damage distribution value is 2.82.

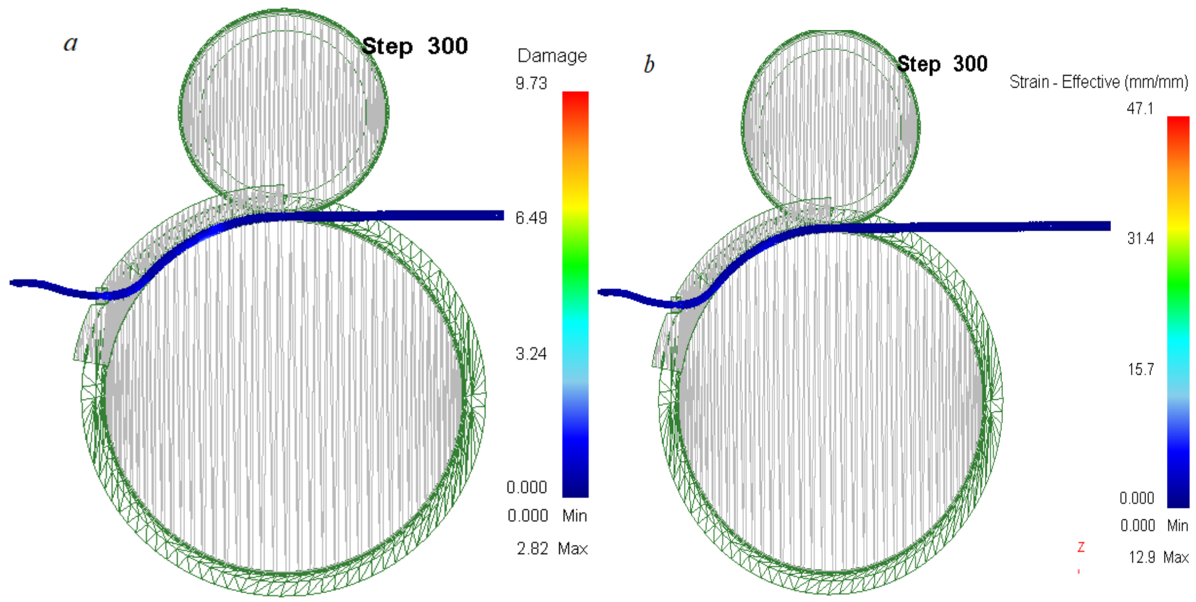

Figure 4. 15 (a) Damage distrubution and (b) Effective-strain distribution of 12.5 mm CP-Titanium grade 2 under 8 rpm extrusion wheel velocity and 200 ^{0}C feedstock temperature.

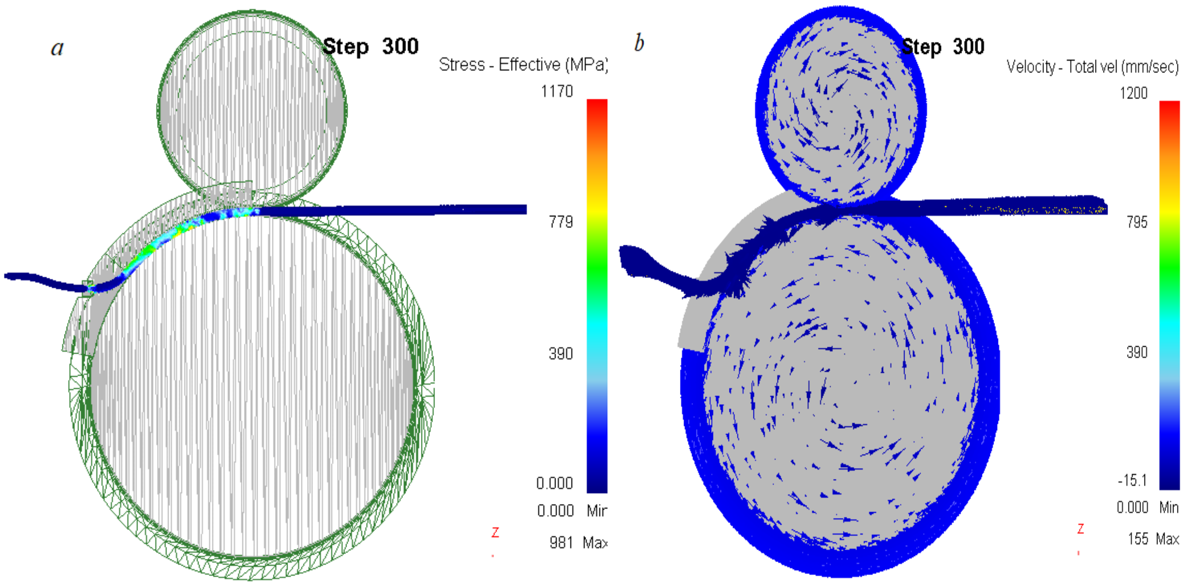

Figure 4. 16 (a) Effective-stress distribution and (b) Total velocity distribution of 12.5 mm CP-Titanium grade 2 under 8 rpm extrusion wheel velocity and 200 ^{0}C feedstock temperature.

Figure 4.16 above depicts the effective-stress distribution and total velocity distribution of 12.5 mm CP-Titanium grade 2 simulation results at 8 rpm extrusion wheel velocity and 200 ^{0}C feedstock temperature. As the simulation results displayes the effective stress distribution scored during the process is 981 MPa and the total velocity distribution value is 155 mm/sec.

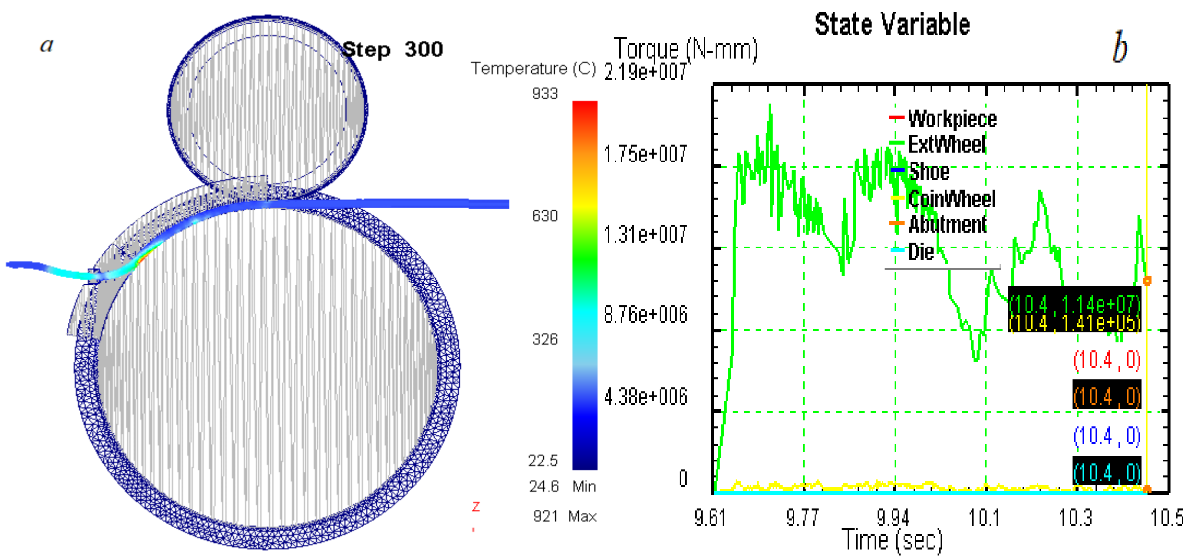

Figure 4. 17 (a) Temperature distribution and (b) Total torque required for deformation of 12.5 mm CP-Titanium grade 2 under 8 rpm extrusion wheel velocity and 200 ^{0}C feedstock temperature.

Figure 4.17 shown above depicts, the temperature distribution and total torque required for deformation of work material at 8 rpm and 200 ^{0}C preheating temperature. As its displayed the temperature and total torque scored maximum during the process due to low preheating condition of feedstock material.

Case study 5. Simulation run at 8 rpm extrusion wheel velocity and 400 ^{0}C preheating temperature.

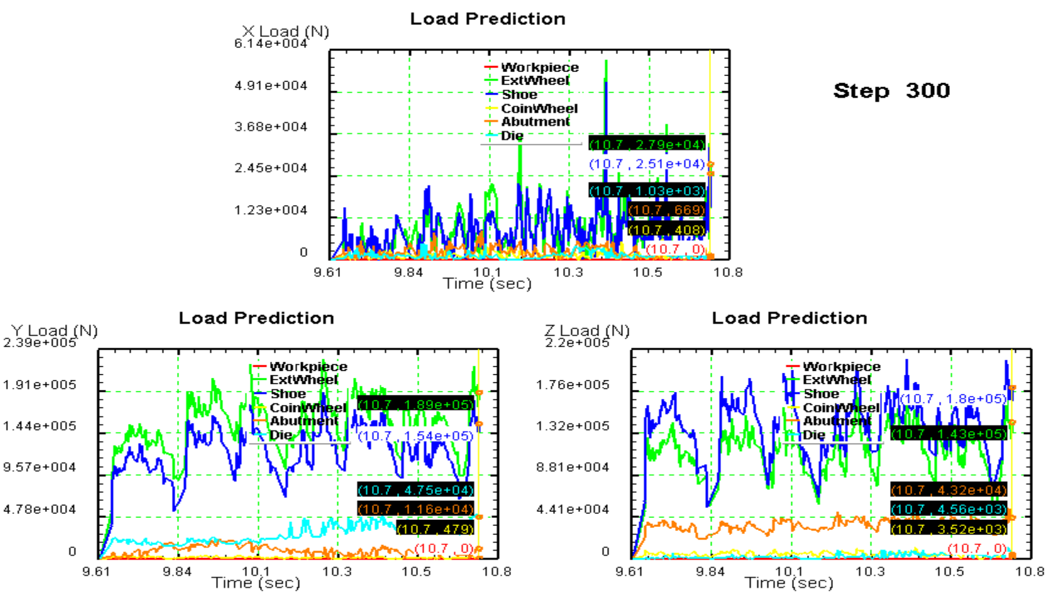

Figure 4. 18 The total load required for deformation of the 12.5 mm CP-Titanium grade 2 under 8 rpm extrusion wheel velocity and 400 ^{0}C feedstock temperature.

Figure 4.18 demonstrates the total load required for deformation at 8 rpm and 400 ^{0}C. total load x-load, y-load and z- load. At this condition the highest load applied in the x – axis direction is on extrusion wheel and shoe surface which is 2.79 x 10^4 and 2.51 x 10^4 respectively, in the y- axis direction is on extrusion wheel and shoe surface which is 1.89 x 10^5 and 1.54 x 10^5 respectively, in z- axis direction is on extrusion wheel and shoe surface which is 1.43 x 10^5 and 1.8 x 10^5 respectively. So, from all machine parts the highest load applied is on the extrusion wheel material from y-axis direction which is 1.89 x 10^5 N.

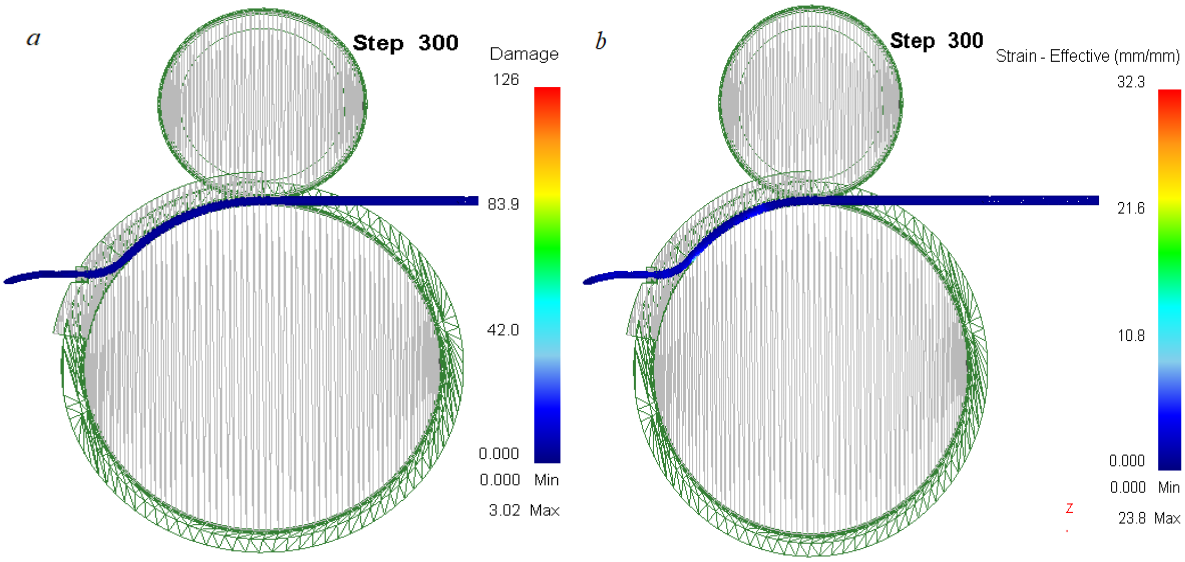

Figure 4. 19 (a) Damage distrubution and (b) Effective-strain distribution of 12.5 mm CP-Titanium grade 2 under 8 rpm extrusion wheel velocity and 400 ^{0}C feedstock temperature.

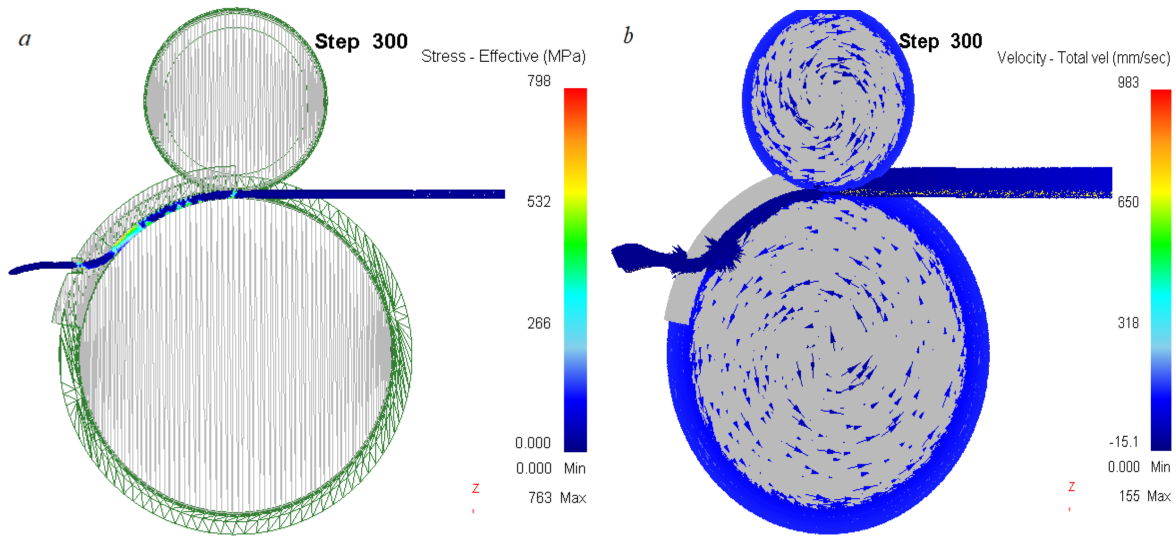

Figure 4. 20 (a) Effective-stress distribution and (b) Total velocity distribution of 12.5 mm CP-Titanium grade 2 under 8 rpm extrusion wheel velocity and 400 ^{0}C feedstock temperature.

Figure 4.19 shown above illustrates, the damage distribution and effective-strain distribution of 12.5 mm CP-Titanium grade 2 simulation results at 8 rpm extrusion wheel velocity and 400 ^{0}C feedstock temperature. As the simulation result displayes, the effective strain distribution scored during the process is 23.8 mm/mm and the damage distribution value is 3.02. Figure 4.20 shown above depicts, the effective-stress distribution and total velocity distribution of 12.5 mm CP-Titanium grade 2 simulation results at 8 rpm extrusion wheel velocity and 400 ^{0}C feedstock temperature. As the simulation results displayes the effective stress distribution scored during the process is 15.3 mm/mm and the total velocity distribution value is 155 mm/sec.

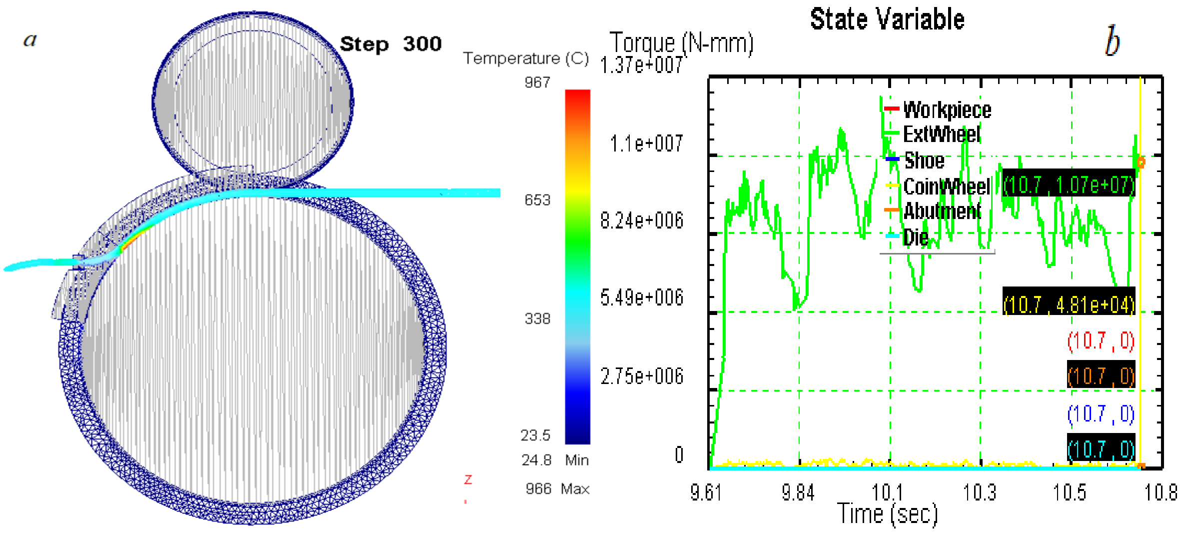

Figure 4. 21 (a) Temperature distribution and (b) Total torque required for deformation of 12.5 mm CP-Titanium grade 2 under 8 rpm extrusion wheel velocity and 400 ^{0}C feedstock temperature.

Figure 4.21 shown above depicts, the temperature distribution and total torque required for deformation of work material at 8 rpm and 400 ^{0}C preheating temperature. As its displayed the temperature appears maximum in the deformation regions due to physical shearing of work material and high heat has been generated and total torque required scored maximum on extrusion wheel material during the process.

Case study 6. Simulation run at 8 rpm extrusion wheel velocity and 600 ^{0}C preheating temperature.

Figure 4.22 below demonstrates the total load required for deformation at 8 rpm and 600 ^{0}C. total load (x-load, y-load and z- load). At this condition the highest load applied in the x – axis direction is on extrusion wheel and abutment material which is 4.68 x 10^{3} and 2.87 x 10^{3} respectively, in the y- axis direction is on extrusion wheel and shoe surface which is 1.39 x 10^{5} and 1.18 x 10^{5} respectively, in z- axis direction is on extrusion wheel and shoe surface which is 8.43 x 10^5 and 1.2 x 10^5 respectively. So, from all machine parts the highest load applied is on the extrusion wheel material from y-axis direction which is 1.39 x 10^5 N.

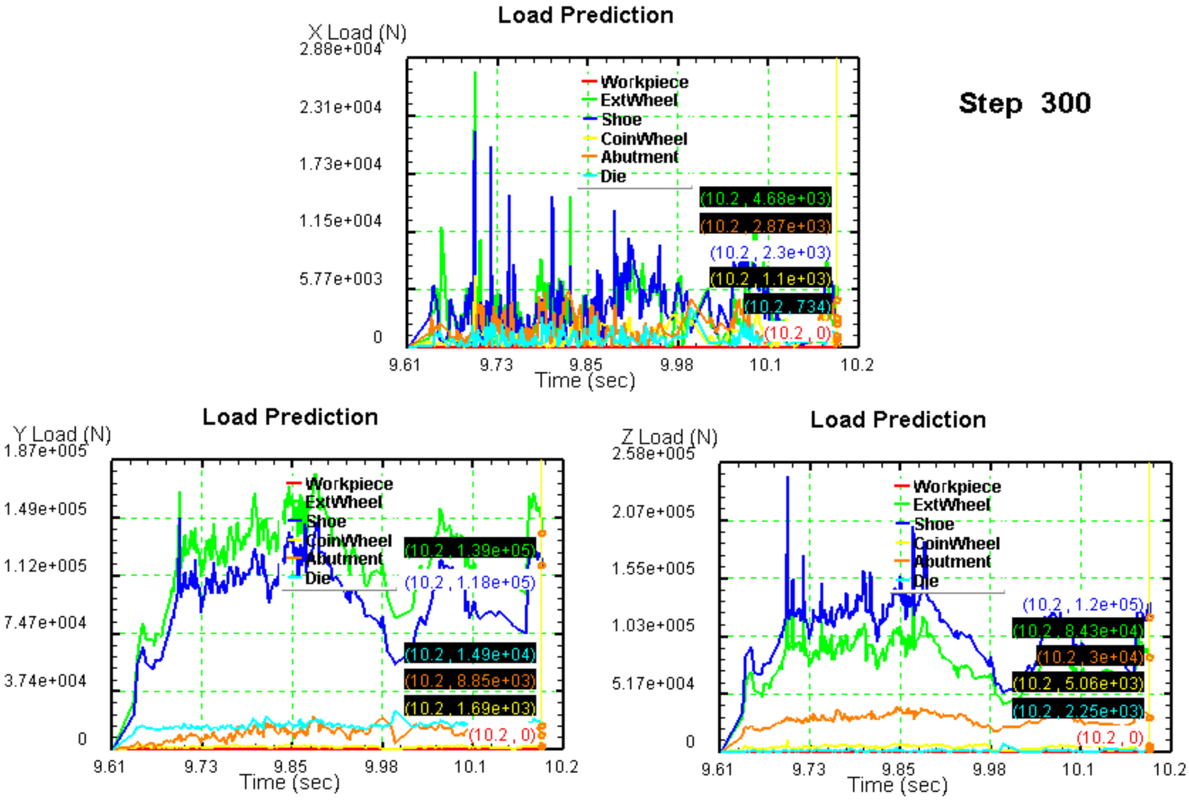

Figure 4. 22 The total load required for deformation of the 12.5 mm CP-Titanium grade 2 under 8 rpm extrusion wheel velocity and 600 ^{0}C feedstock temperature.

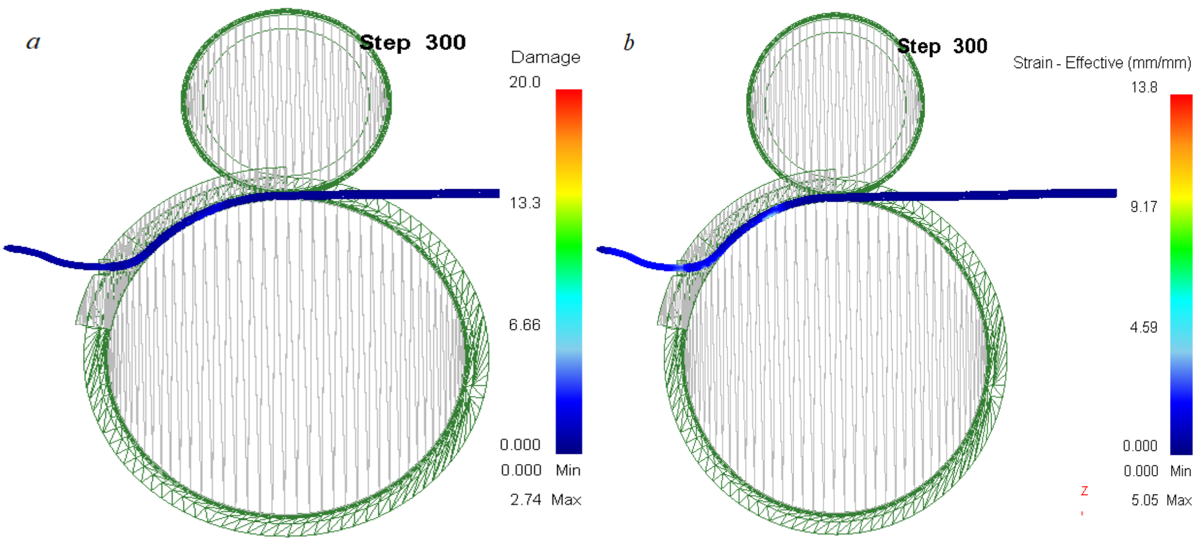

Figure 4. 23 (a) Damage distrubution and (b) Effective-strain distribution of 12.5 mm CP-Titanium grade 2 under 8 rpm extrusion wheel velocity and 600 ^{0}C feedstock temperature.

Figure 4.23 above illustrates the damage distribution and effective-strain distribution of 12.5 mm CP-Titanium grade 2 simulation results at 8 rpm extrusion wheel velocity and 600 ^{0}C feedstock temperature. As the simulation results displayes the effective strain distribution scored during the process is 5.05 mm/mm and the damage distribution value is 2.74. Figure 4.24 shown below depicts the effective-stress distribution and total velocity distribution of 12.5 mm CP-Titanium grade 2 simulation results at 8 rpm extrusion wheel velocity and 600 ^{0}C feedstock temperature. As the simulation results displayes the effective stress distribution scored during the process is 479 MPa and the total velocity distribution value is 557 mm/sec.

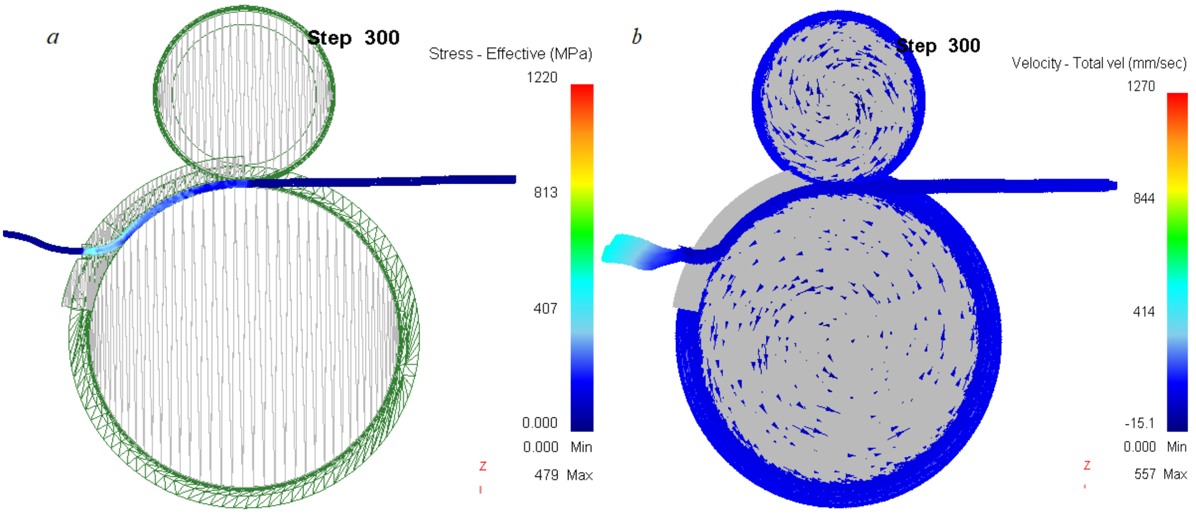

Figure 4. 24 (a) Effective-stress distribution and (b) Total velocity distribution of 12.5 mm CP-Titanium grade 2 under 8 rpm extrusion wheel velocity and 600 ^{0}C feedstock temperature.

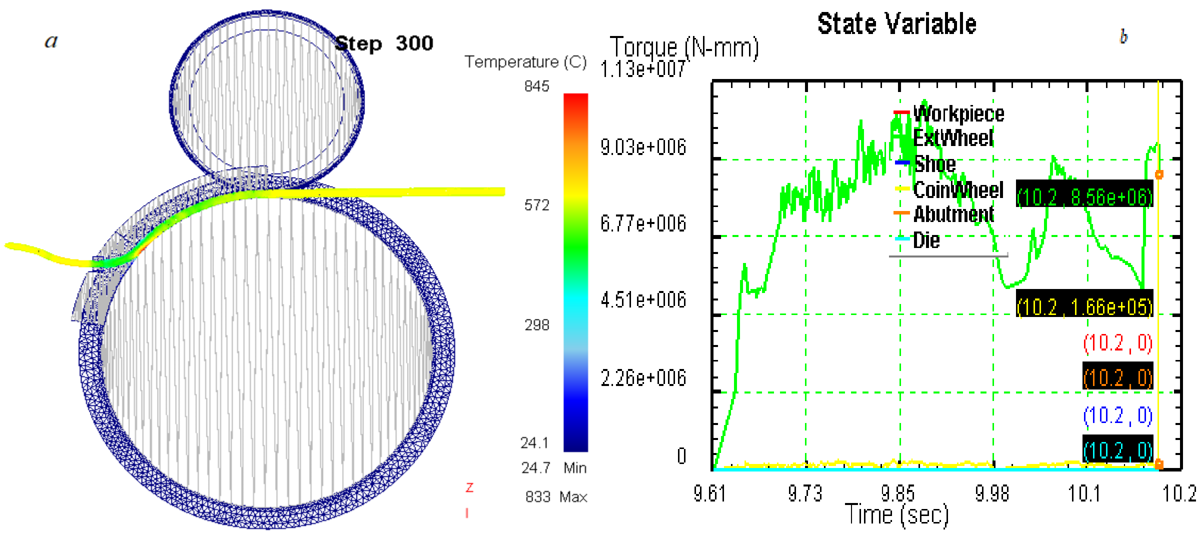

Figure 4. 25 (a) Temperature distribution and (b) Total torque required for deformation of 12.5 mm CP-Titanium grade 2 under 8 rpm extrusion wheel velocity and 600 ^{0}C feedstock temperature.

Figure 4.25 above depicts, the temperature distribution and total torque required for deformation of work material at 8 rpm and 600 ^{0}C preheating temperature. As its displayed the temperature appears 833 ^{0}C in the deformation regions due to physical shearing of work material and total torque required scored maximum on extrusion wheel material during the process. As shown below from case study 7 to case study 9, the numerical simulation results of 12.5 mm CP-Titanium grade 2 displayed at 12 rpm extrusion wheel velocity and 200 ^{0}C, 400 ^{0}C, 600 ^{0}C feedstock temperature. In each case various results are displayed such as total load required for deformation, torque required for deformation, effective stress distribution, effective strain distribution, Damage distribution, Temperature distribution and Velocity distribution of CP-Titanium grade 2.

Case study 7. Simulation run at 12 rpm extrusion wheel velocity and 200 ^{0}C preheating temperature. Figure 4.26 demonstrates the total load required for deformation at 12 rpm and 200 ^{0}C. total load x-load, y-load and z- load. At this condition the highest load applied in the x – axis direction is on extrusion wheel and shoe surface which is 1.83 x 10^4 and 1.74 x 10^4 respectively, in the y- axis direction is on extrusion wheel and shoe surface which is 1.36 x 10^5 and 1.13 x 10^5 respectively, in z- axis direction is on extrusion wheel and shoe surface which is 1.32 x 10^5 and 1.48 x 10^5 respectively. So, from all machine parts the highest load applied is on the shoe material from z-axis direction which is 1.48 x 10^5 N.

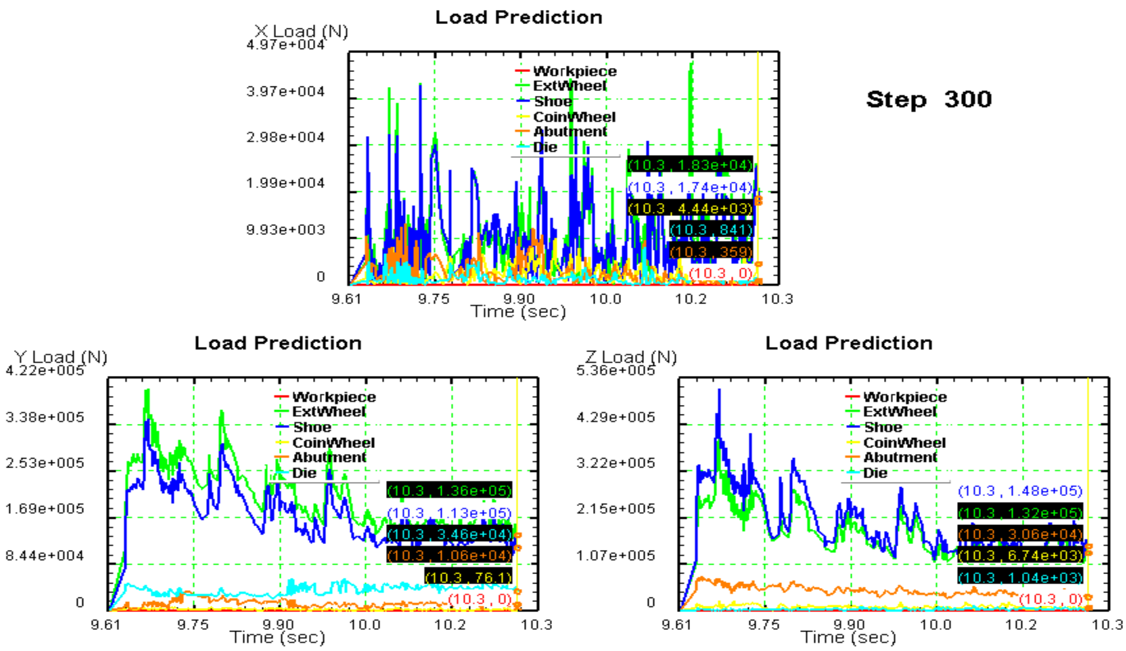

Figure 4. 26 The total load required for deformation of the 12.5 mm CP-Titanium grade 2 under 12 rpm extrusion wheel velocity and 200 ^{0}C feedstock temperature.

Figure 4.27 shown below illustrates the damage distribution and effective-strain distribution of 12.5 mm CP-Titanium grade 2 simulation results at 12 rpm extrusion wheel velocity and 200 ^{0}C feedstock temperature. As the simulation results displayes the effective strain distribution scored during the process is 26.3 mm/mm and the damage distribution value is 3.21.

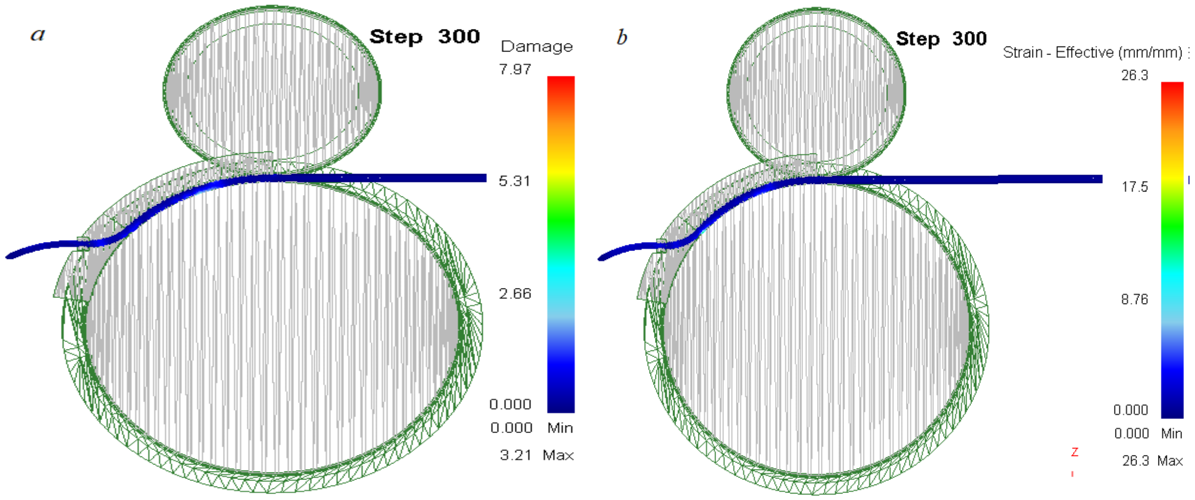

Figure 4. 27 (a) Damage distrubution and (b) Effective-strain distribution of 12.5 mm CP-Titanium grade 2 under 12 rpm extrusion wheel velocity and 200 ^{0}C feedstock temperature.

Figure 4.28 shown below depicts the effective-stress distribution and total velocity distribution of 12.5 mm CP-Titanium grade 2 simulation results at 12 rpm extrusion wheel velocity and 200 ^{0}C feedstock temperature. As the simulation results displayes the effective stress distribution scored during the process is 935 MPa and the total velocity distribution value is 235 mm/sec.

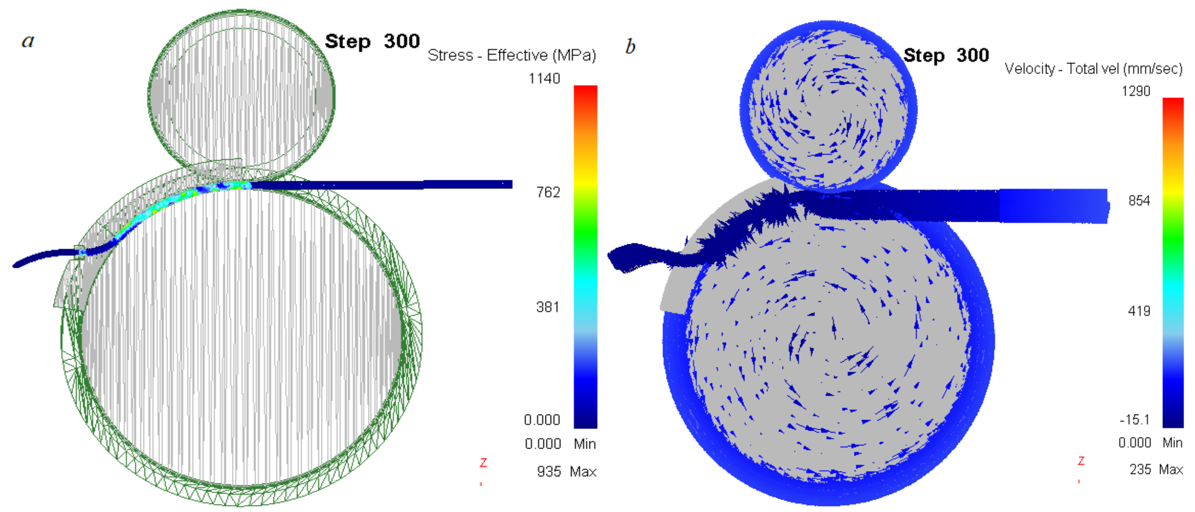

Figure 4. 28 (a) Effective-stress distribution and (b) Total velocity distribution of 12.5 mm CP-Titanium grade 2 under 12 rpm extrusion wheel velocity and 200 ^{0}C feedstock temperature.

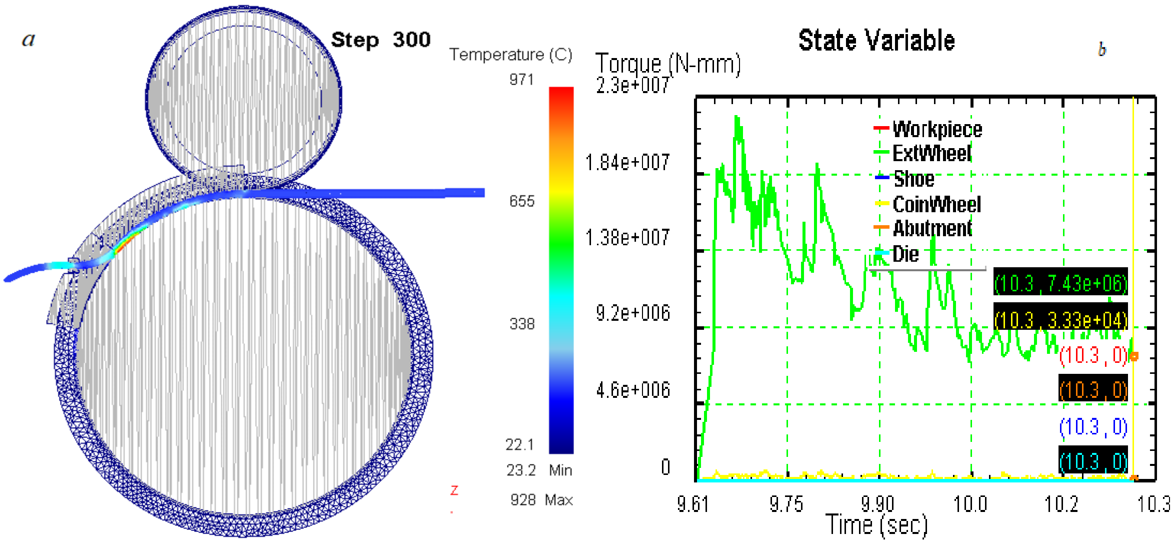

Figure 4. 29 (a) Temperature distribution and (b) Total torque required for deformation of 12.5 mm CP-Titanium grade 2 under 12 rpm extrusion wheel velocity and 200 ^{0}C feedstock temperature.

Figure 4.29 above depicts, the temperature distribution and total torque required for deformation of work material at 12 rpm and 200 ^{0}C preheating temperature. As its displayed the temperature appears 928 ^{0}C in the deformation regions due to physical shearing of work material and total torque required decreases as process time increases during the process.

Case study 8. Simulation run at 12 rpm extrusion wheel velocity and 400 ^{0}C preheating temperature.

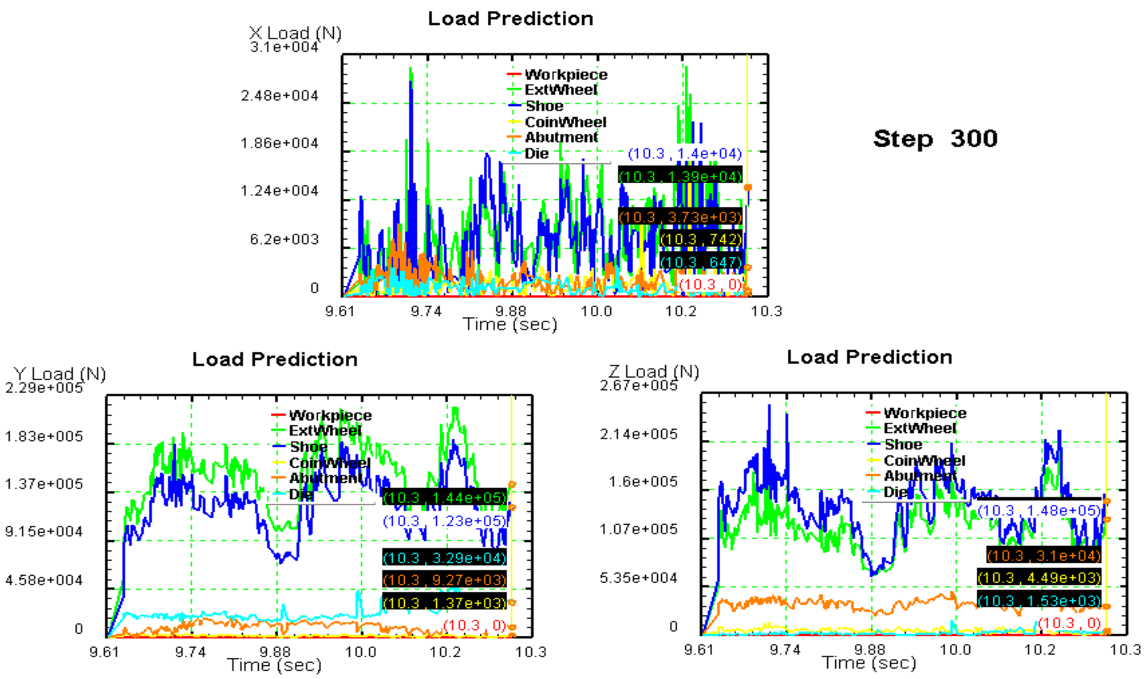

Figure 4. 30 The total load required for deformation of the 12.5 mm CP-Titanium grade 2 under 12 rpm extrusion wheel velocity and 400 ^{0}C feedstock temperature.

Figure 4.30 demonstrates the total load required for deformation at 12 rpm and 200 ^{0}C. total load (x-load, y-load and z- load). At this condition the highest load applied in the x – axis direction is on extrusion wheel and shoe surface which is 1.39 x 10^4 and 1.4 x 10^3 respectively, in the y- axis direction is on extrusion wheel and shoe surface which is 1.44 x 10^5 and 1.23 x 10^5 respectively, in z- axis direction is on extrusion wheel and shoe surface which is 1.42 x 10^5 and 1.48 x 10^5 respectively. So, from all machine parts the highest load applied is on the shoe material from z-axis direction which is 1.48 x 10^5 N.

Figure 4.31 shown below illustrates the damage distribution and effective-strain distribution of 12.5 mm CP-Titanium grade 2 simulation results at 12 rpm extrusion wheel velocity and 400 ^{0}C feedstock temperature. As the simulation results displayes the effective strain distribution scored during the process is 17.5 mm/mm and the damage distribution value is 3.07. Figure 4.32 shown below depicts the effective-stress distribution and total velocity distribution of 12.5 mm CP-Titanium grade 2 simulation results at 12 rpm extrusion wheel velocity and 400 ^{0}C feedstock temperature. As the simulation results displayes the effective stress distribution scored during the process is 647 MPa and the total velocity distribution value is 232 mm/sec.

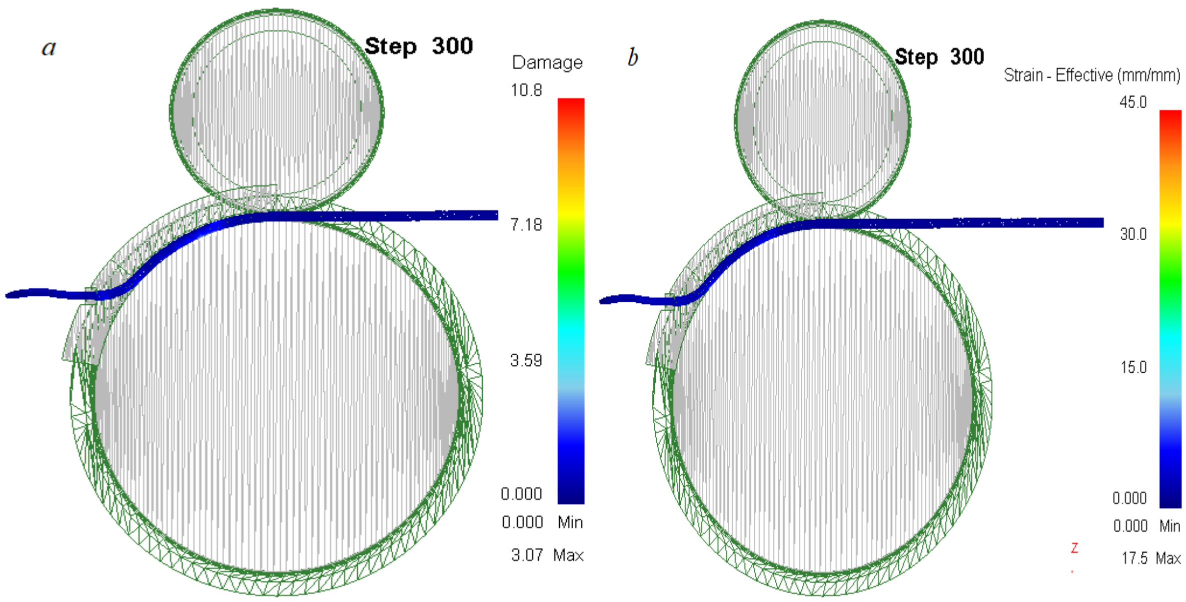

Figure 4. 31 (a) Damage distrubution and (b) Effective-strain distribution of 12.5 mm CP-Titanium grade 2 under 12 rpm (extrusion wheel velocity) and 400 ^{0}C (feedstock temperature).

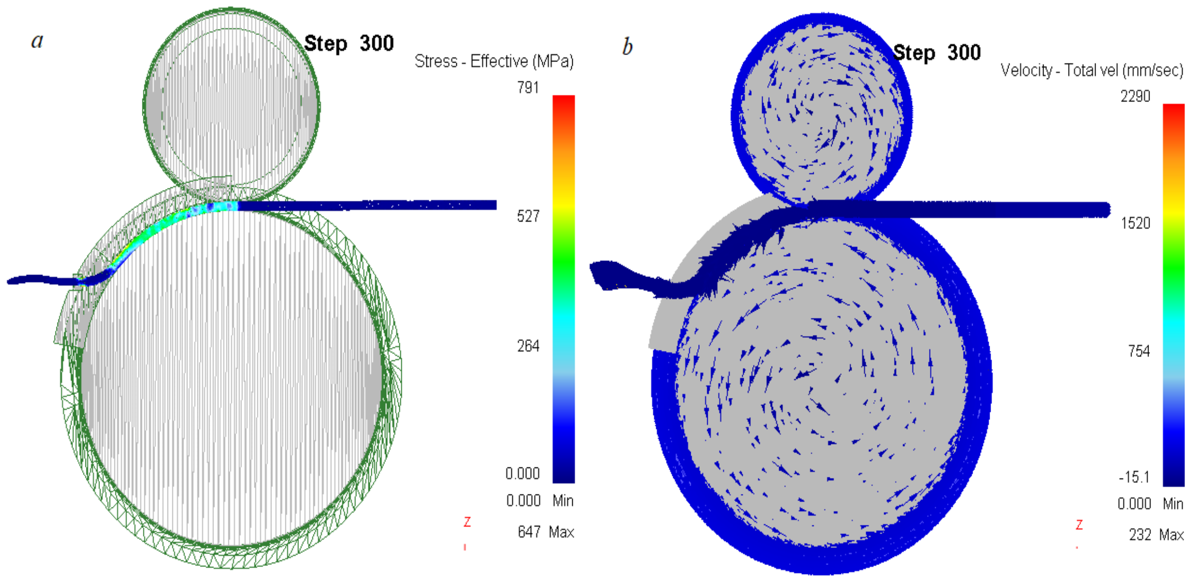

Figure 4. 32 (a) Effective-stress distribution and (b) Total velocity distribution of 12.5 mm CP-Titanium grade 2 under 12 rpm extrusion wheel velocity and 400 ^{0}C(feedstock temperature.

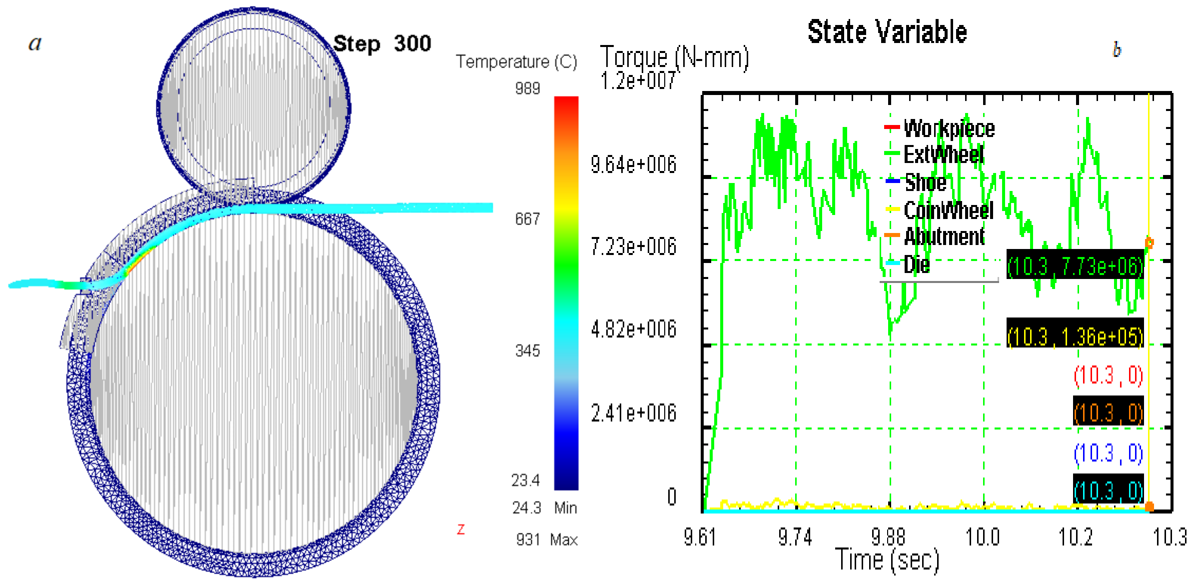

Figure 4. 33 (a) Temperature distribution and (b) Total torque required for deformation of 12.5 mm CP-Titanium grade 2 under 12 rpm extrusion wheel velocity and 400 ^{0}C feedstock te mperature.

Figure 4.33 above depicts, the temperature distribution and total torque required for deformation of work material at 12 rpm and 400 ^{0}C preheating temperature. As its displayed the temperature appears 931 ^{0}C in the deformation regions due to physical shearing of work material and total torque required has been scored maximum during the process by extrusion wheel material.

Case study 9. Simulation run at 12 rpm extrusion wheel velocity and 600 ^{0}C preheating temperature.

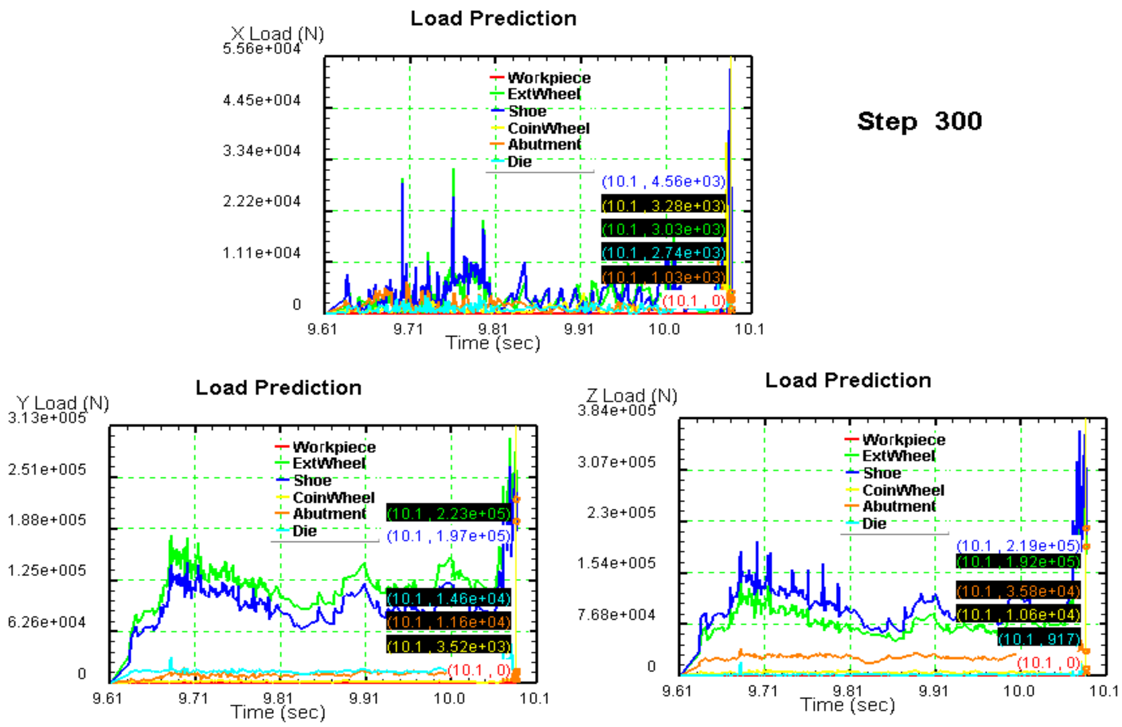

Figure 4. 34 The total load required for deformation of the 12.5 mm CP-Titanium grade 2 under 12 rpm (extrusion wheel velocity) and 600 ^{0}C (feedstock temperature).

Figure 4.34 demonstrates the total load required for deformation at 12 rpm and 600 ^{0}C. total load (x-load, y-load and z- load). At this condition the highest load applied in the x – axis direction is on abutment and shoe surface which is 3.28 x $10^{3}$and 4.56 x 10^{3} respectively, in the y- axis direction is on extrusion wheel and shoe surface which is 2.23 x 10^{5} and 1.97 x 10^{5} respectively, in z- axis direction is on extrusion wheel and shoe surface which is 1.92 x 10^{5} and 2.19 x 10^{5} respectively. So, from all machine parts the highest load applied is on the extrusion wheel material from y-axis direction which is 2.23 x 10^{5} N.

Figure 4.35 shown below, illustrates the damage distribution and effective-strain distribution of 12.5 mm CP-Titanium grade 2 simulation results at 12 rpm extrusion wheel velocity and 600 ^{0}C feedstock temperature. As the simulation results displayes the effective strain distribution scored during the process is 7.44 mm/mm and the damage distribution value is 2.68.

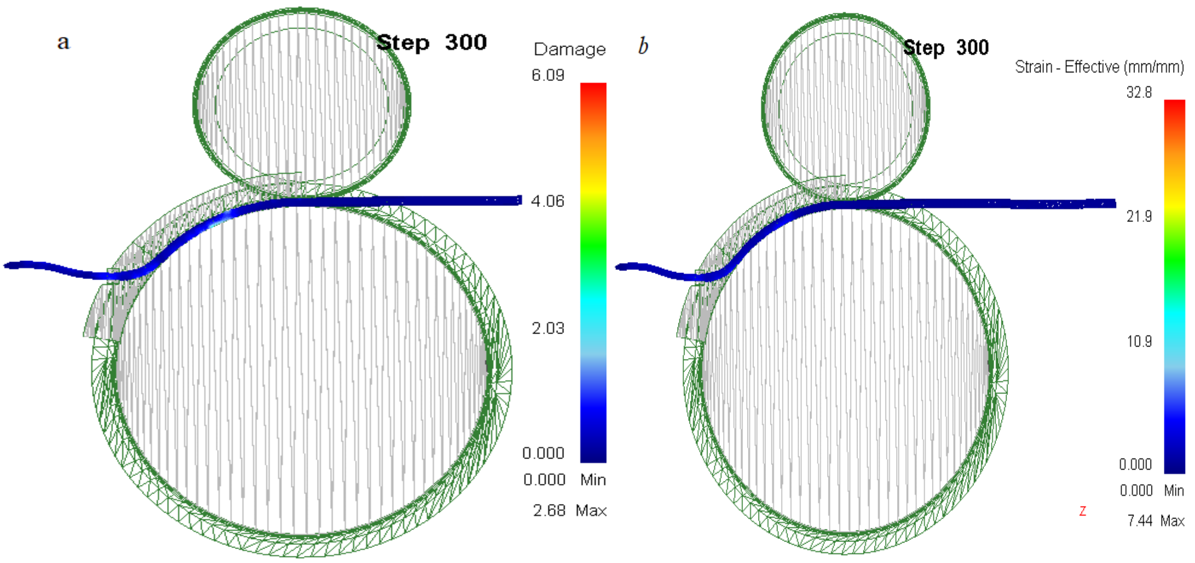

Figure 4. 35 (a) Damage distrubution and (b) Effective-strain distribution of 12.5 mm CP-Titanium grade 2 under 12 rpm extrusion wheel velocity and 600 ^{0}C feedstock temperature.

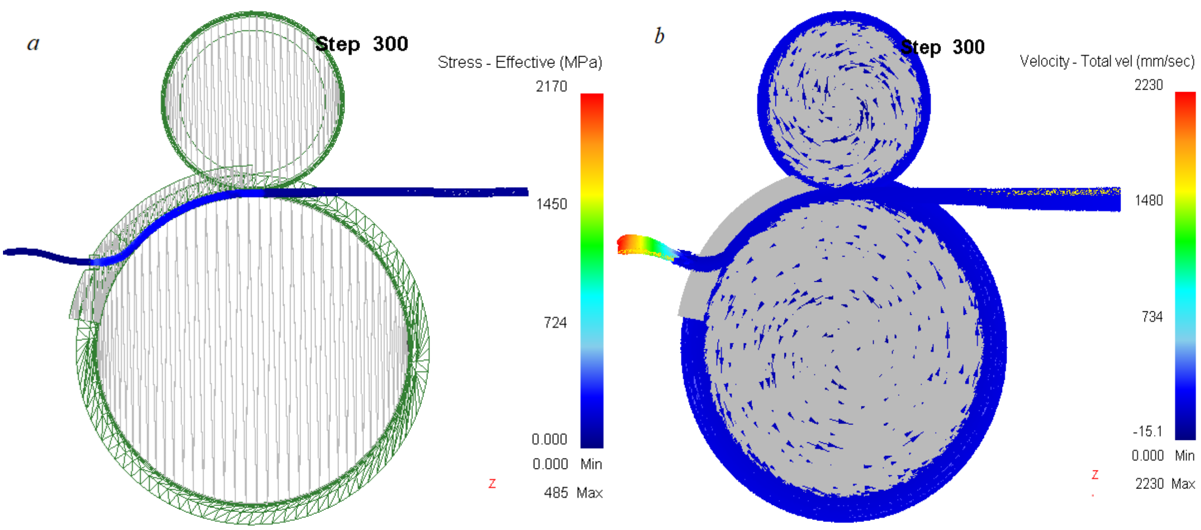

Figure 4. 36 (a) Effective-stress distribution and (b) Total velocity distribution of 12.5 mm CP-Titanium grade 2 under 12 rpm extrusion wheel velocity and 600 ^{0}C feedstock temperature.

Figure 4.36 above depicts, the effective-stress distribution and total velocity distribution of 12.5 mm CP-Titanium grade 2 simulation results at 12 rpm extrusion wheel velocity and 600 ^{0}C feedstock temperature. As the simulation results displayes the effective stress distribution scored during the process is 485 MPa and the total velocity distribution value is 2230 mm/sec. Figure 4.37 below depicts, the temperature distribution and total torque required for deformation of work material at 12 rpm and 600 ^{0}C preheating temperature. As its displayed the temperature appears 914 ^{0}C in the deformation regions due to physical shearing of work material and total torque required has been scored maximum as the process time increases during the process.

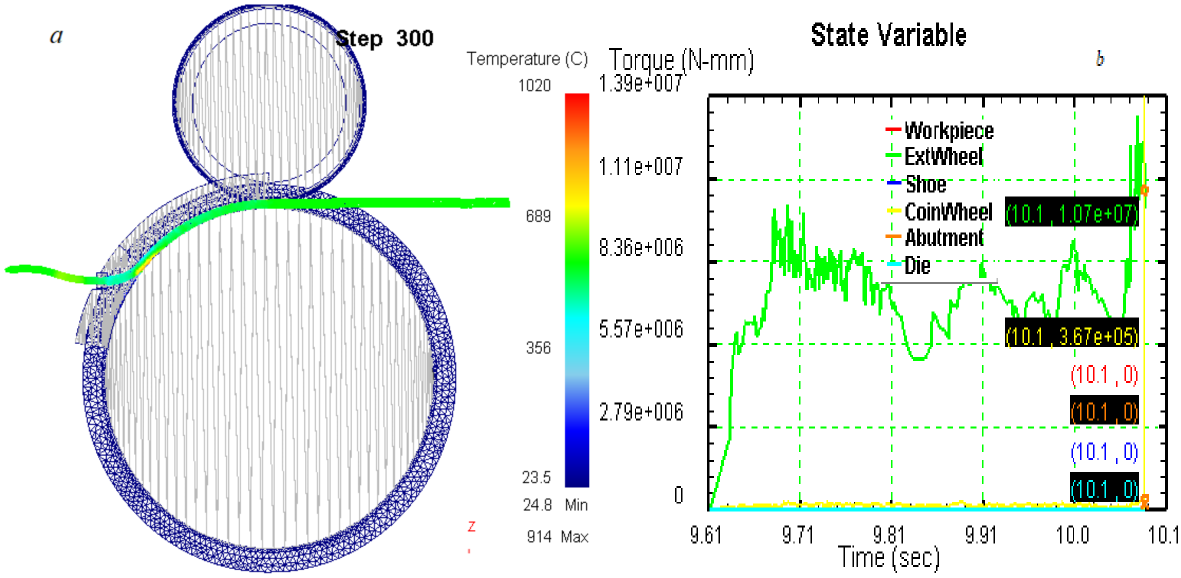

Figure 4. 37 (a) Temperature distribution and (b) Total torque required for deformation of 12.5 mm CP-Titanium grade 2 under 12 rpm extrusion wheel velocity and 600 ^{0}C feedstock temperature.

4.5 Summary on Numerical simulation results

After conducting the numerical simulation of CP-Titanium grade 2 material in continuous forming process by using DEFORM-3D plat-form , the following results are obtained.

1. During continuous forming process, by increasing the preheating temperature of feedstock material at the same extrusion wheel velocity the effective stress of a material can be decreased. As the effective stress of a material decreased the total load required for deformation also decreased.
2. During continuous forming process, power consumptions of conform machine decreased by decreasing the extrusion wheel velocity (rpm) and vice versa.
3. During continuous forming process, the maximum temperature present during the process decrases as the preheating temperature of the material increases at the same extrusion wheel velocity.

Table 4. 4 Numerical simulation results of CP- Titanium grade 2 material through DEFORM-3D.

Run Order	Extrusion wheel Velocity (RPM)	Feedstock Temperature (^{0}C)	Effective stress (MPa)	Maximum temperature (^{0}C)	Total load (kN)	Torque (kN-m)	Effective Strain (mm/mm)	Damage value	Power required (KW)
1	4	200	1020	864	5.81	21.4	20.3	3.05	117.86
2	4	400	746	746	3.93	15.6	7.97	3.05	52.56
3	4	600	575	597	2.90	13	7.97	2.41	25.31
4	8	200	981	921	5.81	21.9	12.9	2.82	230.88
5	8	400	763	966	3.31	13.7	23.8	3.02	99.7
6	8	600	479	833	3.28	11.3	5.05	2.74	52.7
7	12	200	935	928	6.84	23	26.3	3.21	339.95
8	12	400	647	931	3.53	12	17.5	3.07	155.39
9	12	600	485	914	4.98	13.9	7.44	2.68	78.23

4.6 Analysis of effective-stress

Effective-stress is analysed by using taguchi method. To understand the effective-stress of the cp-titanium grade 2 material, two factors (extrusion wheel velocity and feedstock temperature) are considered during continuous forming process to know there effects on the effective-stress of the materials. Table 4.4 above explains about the effects of both factors on the effective-stress of the sample materials during continuous forming process. As table 4.5 illustrates Feedstock temperature has more effect than extrusion wheel velocity because feedstock temperature has more delta value than extrusion wheel velocity and also, feedstock temperature is ranked as number one regarding on the effect of effective-stress.

Table 4. 5 Response Table for Signal to Noise Ratios

Level	Extrusion Wheel Velocity (RPM)	Feedstock Temperature (^{0}C)
1	-57.61	-59.81
2	-57.03	-57.11
3	-56.45	-54.17
Delta	1.16	5.64
Rank	**2**	**1**

Smaller is better

Table 4.6 below demonstrate the response table for effective-stress. In this table effect of extrusion wheel velocity and feedstock temperature on the response of effective-stress has been presented. As its enlightened the feedstock temperature score the highest delta value and ranked as the first effect on the response of effective-stress, secondly the extrusion wheel velocity scores the lower delta value and ranked as the second effect on the response of effective-stress.

Table 4. 6 Response Table for Means

Level	Extrusion Wheel Velocity (RPM)	Feedstock Temperature (^{0}C)
1	780.3	978.7
2	741.0	718.7
3	689.0	513.0
Delta	91.3	465.0
Rank	**2**	**1**

4.6.1 Analysis of main effects plot for effective- stress

The below Figure 4.38 illustrates about the main effect plot for effective stress. As its displayed on the figure the result indicates that the feedstock temperature has the largest effect on the mean of effective-stress. Extrusion wheel velocity has less effect than feedstock tempertature on the mean of effective stress result.

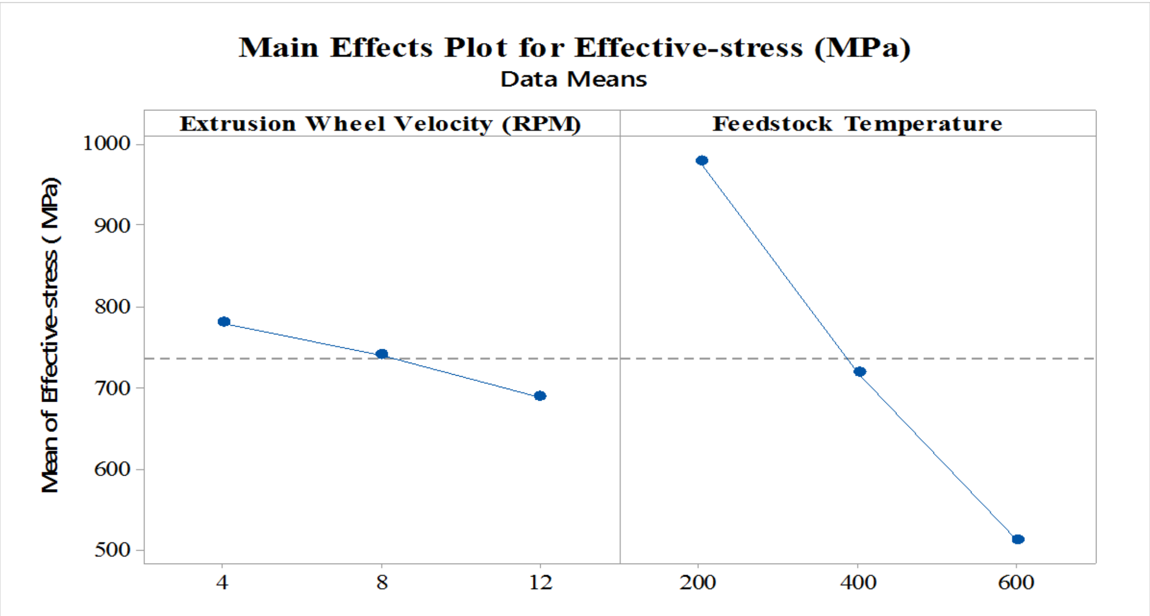

Figure 4. 38 Main effects plot for Effective-stress

4.6.2 Analysis of interaction plot for effective-stress

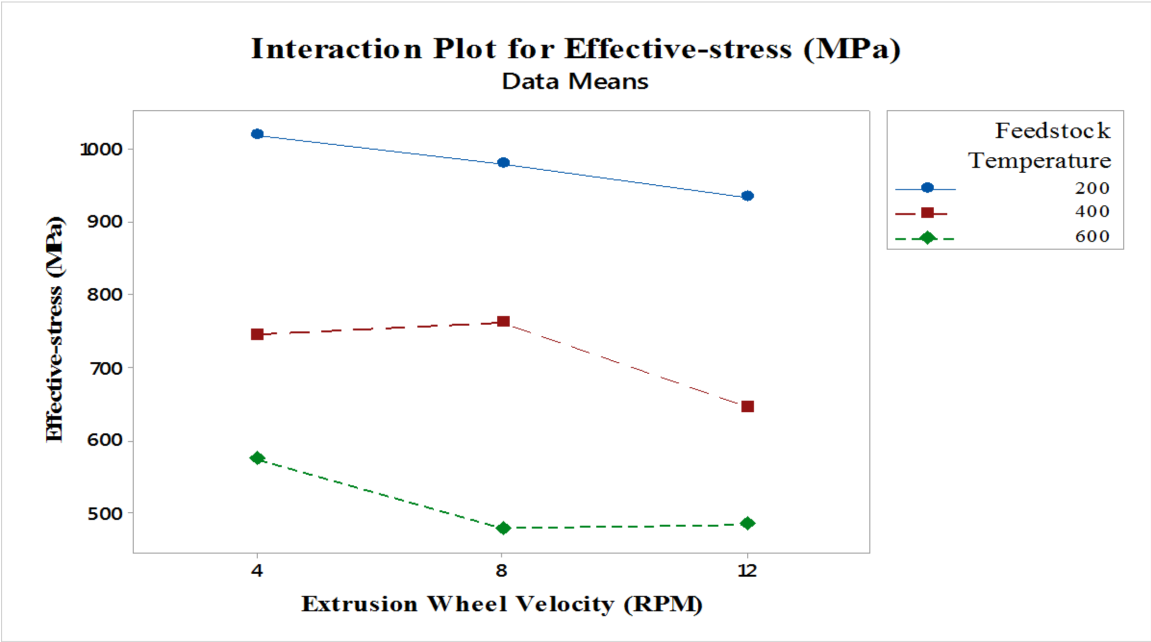

Figure 4. 39 Interaction plot for Effective-stress

Figure 4.39 demonstrates about the interaction plot of mean of effective-stress. In this interaction plot the lines are not parallel. Hence, the interaction effect indicates that the relationship between Extrusion wheel velocity and feedstock temperature on the value of mean effective stress has a significant effect. In this, the interaction between extrusion wheel velocity at 8 rpm and 600 ^{0}C feedstock temperature scores the lower mean of effective stress.

4.6.3 Analysis of main effect plot for signal to noise ratios

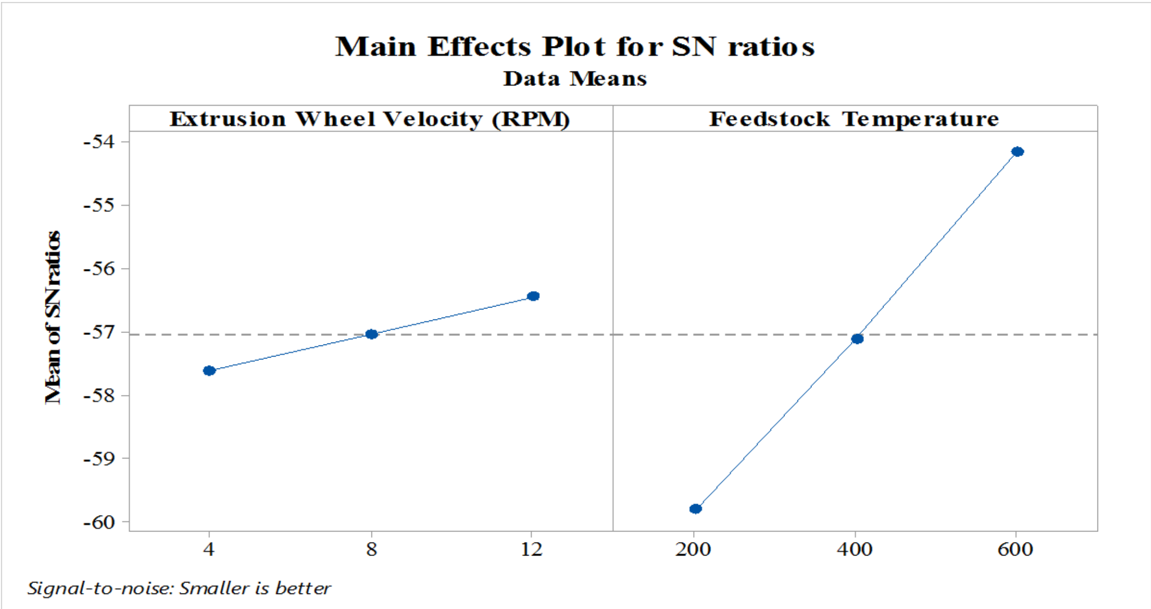

Figure 4. 40 Main effects plot for SN ratios

Figure 4.40 shown above illustrates about the main effect plot for signal-to-noise ratios of effective stress. As displayed in the figure the result indicates that the feedstock temperature has the largest effect on the signal-to-noise ratio. Extrusion wheel velocity has less effect than feedstock tempertature on effective sress result.

4.6.4 Analysis of interaction plot for signal to noise ratios

Figure 4.41 explains about the interaction plot for signal noise ratios of effective stress. As illustrated in the figure the extrusion wheel velocity at 8 rpm and 600 ^{0}C feedstock temperature has a higher signal-to-noise ratio than the combination of other extrusion wheel velocity and feedstock temperature.

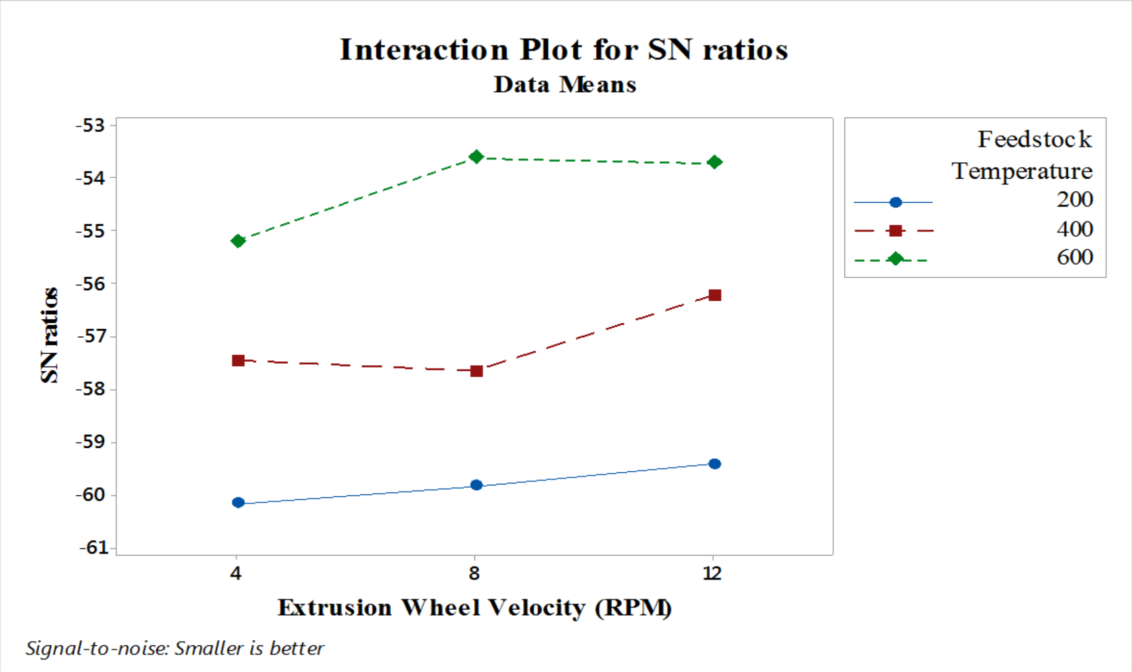

Figure 4. 41 Interaction plot for SN ratios

4.7 Analysis of power consumptions

Power consumption is analysed by using taguchi method. To understand the power consumption of the conform machine, two factors (extrusion wheel velocity and feedstock temperature) are considered to know there role on the power consumption.

Table 4.7 below explain about the effects of both factors (extrusion wheel velocity and feedstock temperature) on the consumption of power during continuous forming process. So, as table 4.7 illustrates Feedstock temperature has more effect than extrusion wheel velocity because feedstock temperature has more delta value than extrusion wheel velocity and also, feedstock temperature is ranked as number one regarding on the effect of power consumptions.

Table 4. 7 Response Table for Signal to Noise Ratios

Level	Extrusion Wheel Velocity (RPM)	Feedstock Temperature (^{0}C)
1	-34.64	-46.44
2	-40.56	-39.41
3	-44.11	-33.46
Delta	9.47	12.98
Rank	**2**	**1**

Smaller is better

As displayed below, Table 4.8 clarifies the response table for power consumption. In this table effect of extrusion wheel velocity and feedstock temperature on the response of power consumption has been highlighted. As demonstrated the feedstock temperature score the highest delta value and ranked as the first effect on the response of power consumption, secondly the extrusion wheel velocity scores the lower delta value and ranked as the second effect on the response of power consumption.

Table 4. 8 Response Table for Means

Level	Extrusion Wheel Velocity (RPM)	Feedstock Temperature (^{0}C)
1	65.24	229.56
2	127.76	102.55
3	191.19	52.08
Delta	125.95	177.48
Rank	**2**	**1**

4.7.1 Analysis of main effect plot for power consumptions

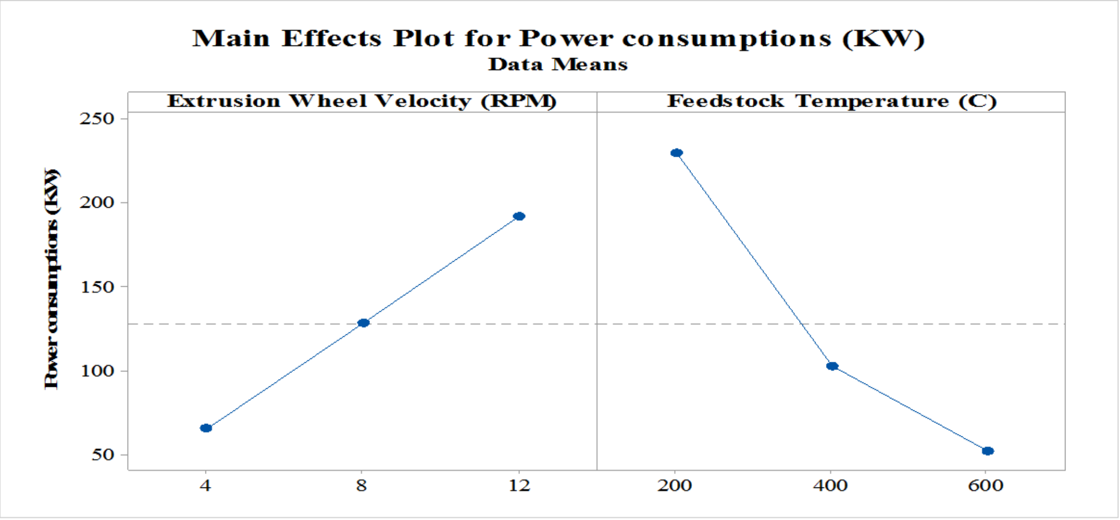

Figure 4. 42 Main effects plot for power consumption

Figure 4.42 shown above describes main effects plot for power consumption. As displayed in the figure the result indicates that the feedstock temperature has the largest effect on the power consumption and also extrusion wheel velocity has also a significant effect but, less than feedstock temperature on the result of power consumption.

4.7.2 Analysis of interaction plot for power consumption

Figure 4.43 demonstrates the interaction plot of mean of power consumption. In this interaction plot the lines are not parallel. Hence, the interaction effect indicates that the relationship between extrusion wheel velocity and feedstock temperature has a significant effect on the value of mean effective stress. In this result, the interaction between extrusion wheel velocity at 4 rpm and 600 ^{0}C feedstock temperature scores the lower mean of power consumption.

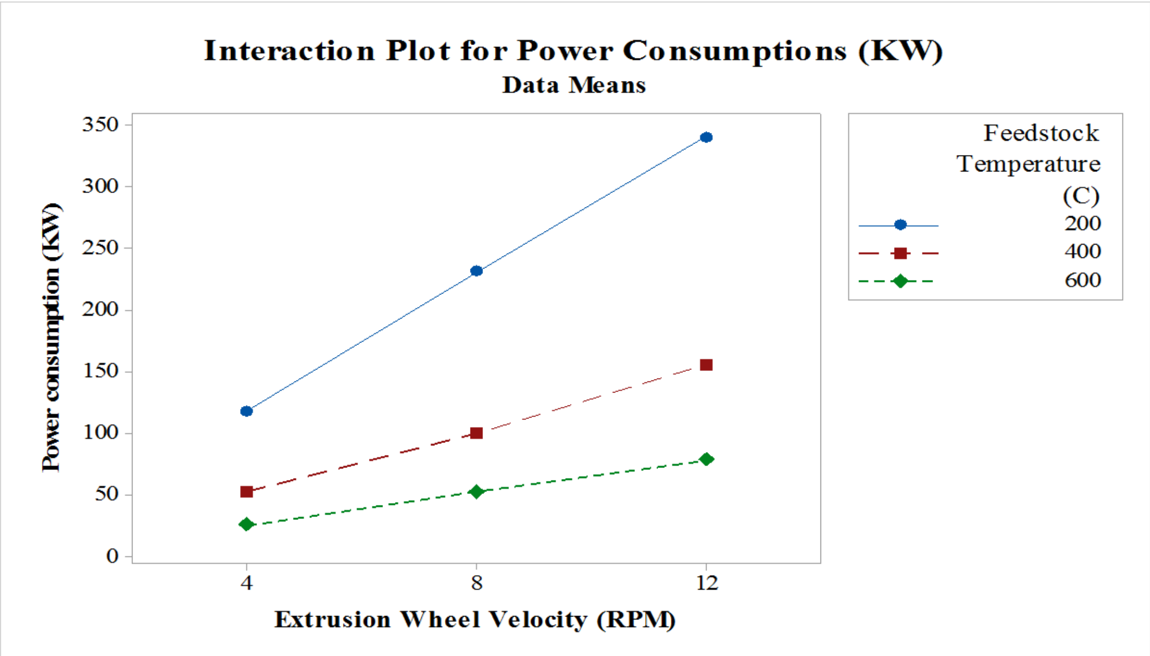

Figure 4. 43 Interaction plot for power consumption

4.7.3 Analysis of main effect plot for signal to noise ratios

Figure 4.44 reflects the main effect plot for signal-to-noise ratios. As its displayed in the figure the results indicate that the feedstock temperature has the largest effect on the power consumption and also, Extrusion wheel velocity has also a significant effect but, little less than feedstock temperature in the result of power consumption.

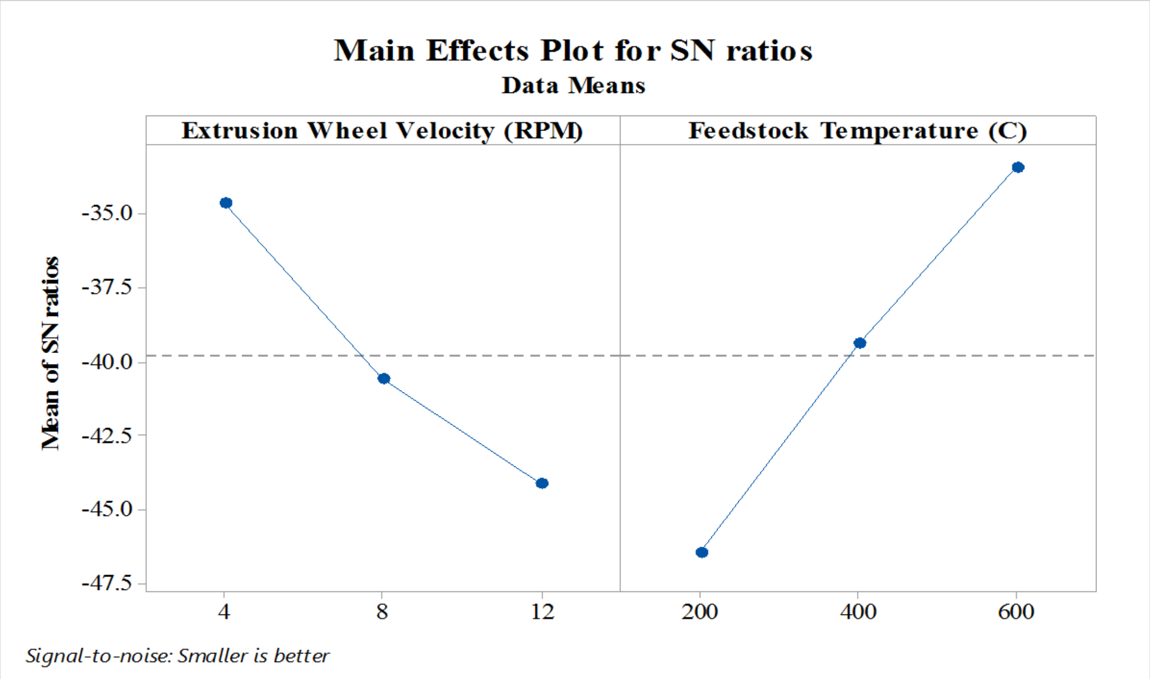

Figure 4. 44 Main effects plot for SN ratios

4.7.4 Analysis of interaction plot for signal to noise ratio

Figure 4.45 Elucidates about the interaction plot for signal noise ratios of power consumption. As illustrated in the figure the extrusion wheel velocity at 4 rpm and 600 ^{0}C feedstock temperature has a higher signal-to-noise ratio than the combination of other extrusion wheel velocity and feedstock temperature. Hence, the optimum working condition is 4 rpm and 600 ^{0}C.

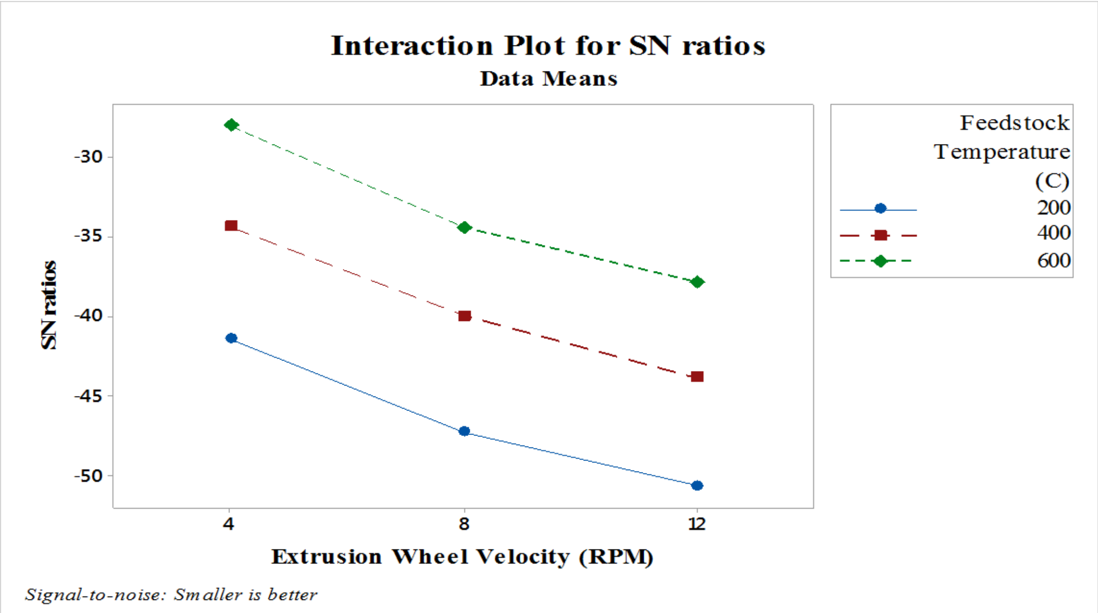

Figure 4. 45 Interaction plot for SN ratios

4.8 Analysis of Variance

As illustrated in Table 4.9, the feedstock temperature creates the prime impact on the total sum of squares through 94.96% as the percentage contribution followed by the effect of extrusion wheel velocity of percentage contribution 3.65%. It can be observed that the interaction effect of extrusion wheel velocity and feedstock temperature creates minimum impact having percentage contribution as 0.02 %.

Table 4. 9 Test result of ANOVA for effective stresses of CP- Titanium grade 2 feedstock material.

Source	DF	Seq SS	Adj SS	Adj MS	F-Value	P-Value	Contribution
Model	5	335632	335632	67126	99.81	0.002	99.40%
Linear	2	332959	332959	166479	247.53	0.000	98.61%
Extrusion wheel velocity (RPM)	1	12331	12331	12331	18.33	0.023	3.65%
Feedstock Temperature (C)	1	320628	320628	320628	476.73	0.000	94.96%
Square	2	2592	2592	1296	1.93	0.290	0.77%
Extrusion wheel velocity (RPM) * Extrusion wheel velocity (RPM)	1	968	968	968	1.44	0.316	0.29%
Feedstock Temperature (C)* Feedstock Temperature (C)	1	1624	1624	1624	2.42	0.218	0.48%
2-Way Interaction	1	81	81	81	0.12	0.751	0.02%
Extrusion wheel velocity (RPM) * Feedstock Temperature (C)	1	81	81	81	0.12	0.751	0.02%
Error	3	2018	2018	673			0.60%
Total	8	337650					100.00%

DF: degree of freedom; Adj SS: adjusted sums of squares; Adj MS: adjusted mean

Figure 4.46 illustrates, the contour plot of effective-stress vs extrusion wheel velocity and feedstock temperature. The 3-dimensional surface depicts on a two-dimensional plane and it graphs with two predictors X-Y (extrusion wheel velocity, feedstock temperature respectively) on the x-y axis and a response variable Z (effective-stress) as contour plot. It is observed that the highest value of effective stresses occurs at high level of wheel velocity and low value of feedstock temperature whereas the lowest value of effective stresses occurs at high value of extrusion wheel velocity and feedstock temperature.

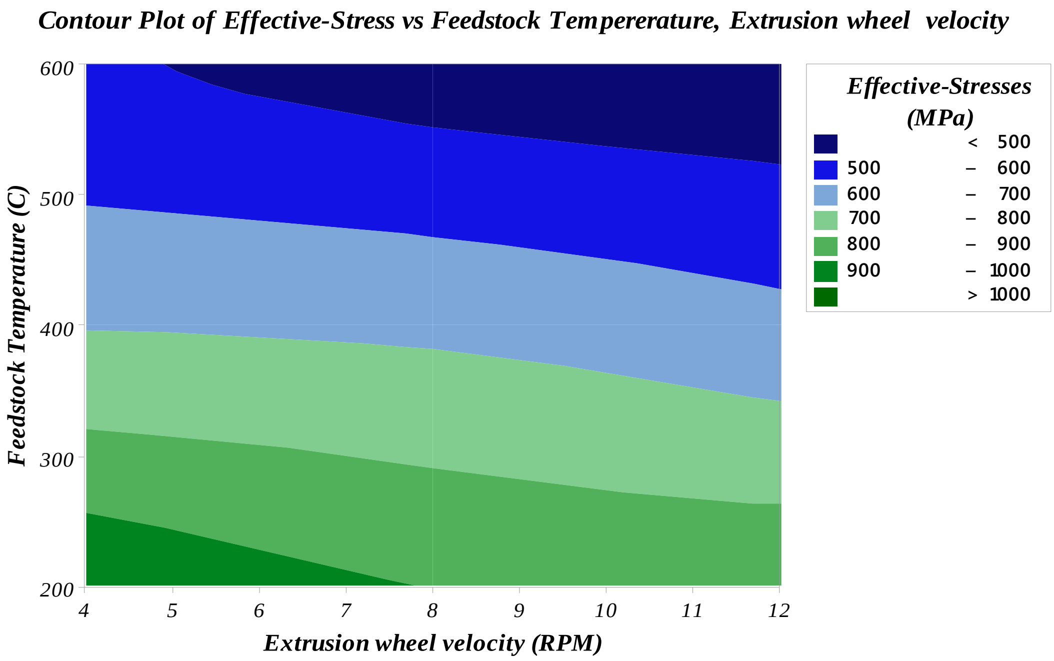

Figure 4. 46 Contour plot of effective-stress vs wheel velocity and feedstock temperature.

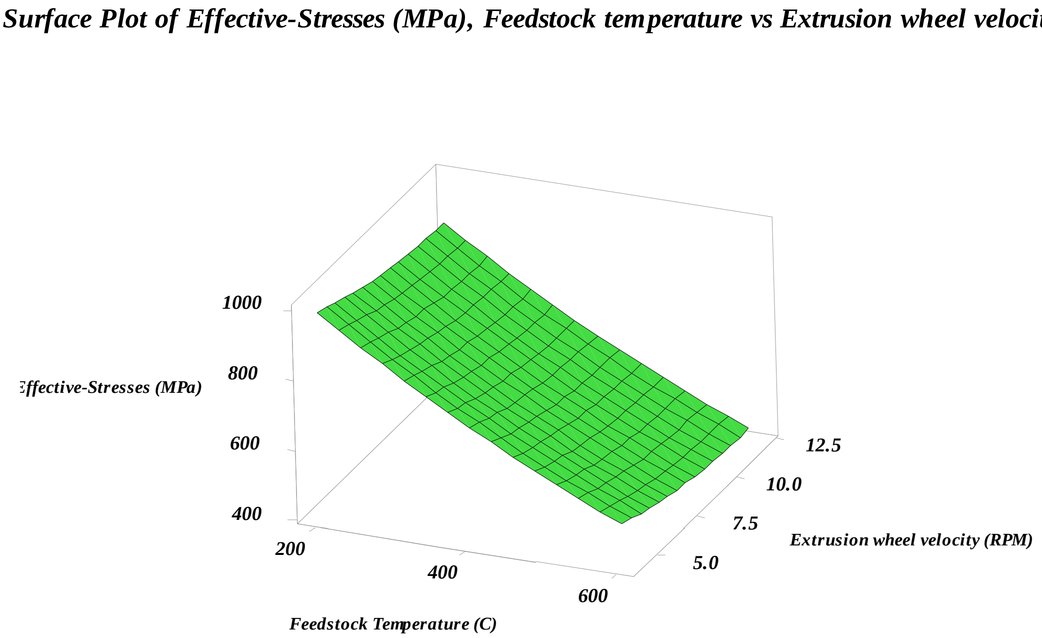

Figure 4. 47 Surface plot of effective stress vs feedstock temperature and wheel velocity

Figure 4.47 demonstrates Surface plot of effective stress vs feedstock temperature and wheel velocity and it shows the effective stress of cp titanium grade 2 decreases as both feedstock temperature and extrusion wheel velocity increases.

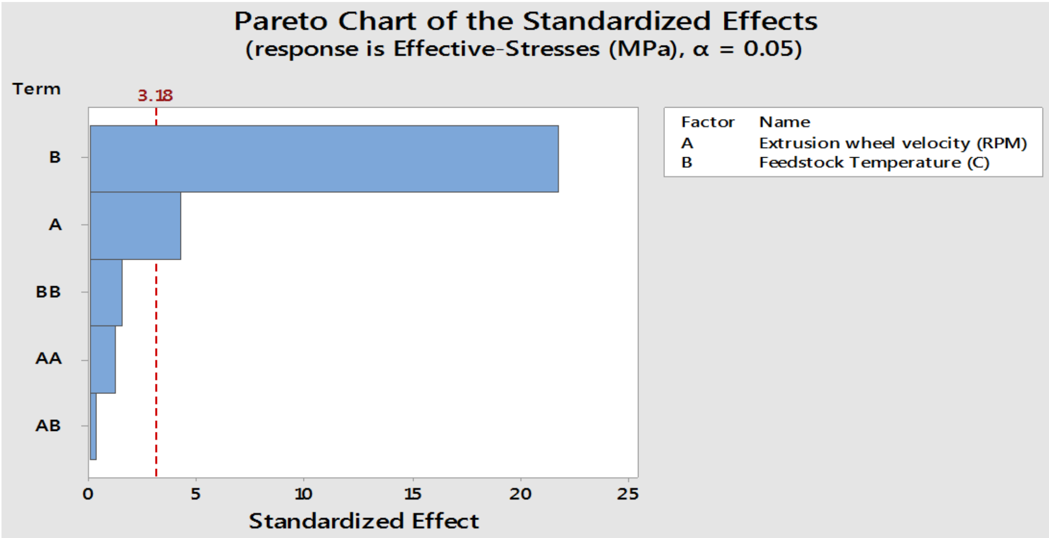

Figure 4. 48 Pareto chart of the standardized effects

Figure 4.48 explains the effects of each factor and the interaction of factors between them on the effective stress of CP-Titanium grade 2. Hence, as demostrated in the above pareto chart the standardized effects of the feedstock temperature score the highest effect on the effective stress , extrusion wheel velocity score the second highest effect is the effective stress, thirdly the combination of feedstock temperature scores the third level effect on the effective stress, followed by the combination of extrusion wheel velocity as a fouth level effect on the effective stress and finally, the combination of both factors (feedstock temperature and extrusion wheel velocity) score the least effect on the effective stress of CP-Titanium grade 2 material during continuous forming process.

4.9 Experimental Analysis

Commercial Continuous Extrusion setup is used to carry out continuous deformation experiments for CP titanium grade 2 feedstock materials. Hence, the results obtained have to be validated for correctness of the theory (simulations) and practice (experiments). In the continuous extrusion set up, extrusion ratio, extrusion wheel velocity and locking pressure by intensifier can be set and calculated for the best condition of extrusion of the CP titanium grade 2 feedstock materials so that a defect free part is produced. An experimental validation results are found in a good agreement with a results of Numerical simulation. Defects that may occur due to the set ups are internal cracking, piping and surface cracking due to high temperature and high extrusion speed. These probable defects are considered for analyzing the scope of the setup fabricated.

The commercial continuous extrusion setup TBJ350 (Figure 4.49) having specification (Table 4.10) has been used for deformation process of feedstock material.

Table 4. 10 Specification of Commercial Setup

S. No.	Parameters	Values	Applications
1	Bed Length	5 meters	Setup is applicable for extrusion of non-ferrous round rods, square rods, tubes and bus bars with wide range of extrusion ratio.
2	Weight	5 ton	
3	Motor Power	200 kW	
4	Extrusion wheel Diameter	350 mm	
5	Feedstock Diameter	12.5 mm	

Figure 4. 49 Commercial Continuous Extrusion setup 1[Internet Resource 2]

4.9.1 Experimental plans

There are two main factors to be studied with respect to their interdependencies while products are formed and therefore plan of the experiments need to be designed in such a way that if one parameter is changed, the effect of other parameters remains constant. The parameters varied are given below: Changing the Extrusion Wheel Velocity, Extrusion Ratio and Feedstock Temperature.

Table 4. 11 Experimental plans

Exp. No	Preheating Temperature (^{0}C)	Extrusion Wheel Velocity (RPM)	Extrusion Ratios (D_0^2/D_f^2)
1			1.56
2	1000	4	2.44
3			4.34

The main aim of the experiment is to extrude the feedstock material. Figure 4.50 shows CP-Titanium grade 2 Titanium feedstock material before deformation and figure 4.51 to figure 4.53 depicts CP-Titanium grade 2 Titanium feedstock material after deformation.

Figure 4. 50 CP-Titanium grade 2 feedstock material before deformation

Figure 4. 51 Extruded product of CP-Titanium grade 2 feedstock material at a diameter of; (a) 10 mm, (b) 8 mm, and (c) 6 mm.

Table 4. 12 Experimental Results for CP titanium grade 2 feedstock material

Sample No.	Shape	Preheating Temperature (^{0}C)	Extruded rod diameter (mm)	Extrusion Ratio	RPM	Total Power (kW)
1	Circular Rod	1000	6	4.34	4	3.62
2			8	2.44	4	3.81
3			10	1.56	4	4.22

Table 4. 13 Validation of power consumption for deformation of CP-Titanium grade 2 material

Parameters		Simulation Power Result (kW)	Experimental Power Result (kW)	% Error (Between Simulation & Experiment)
Feedstock Diameter =12.5mm, Preheating Temperature = 1000 ^{0}C Extrusion Wheel Velocity = 4 RPM	Extrusion ratio=4.34	3.48	3.62	3.9
	Extrusion ratio=2.44	3.71	3.81	2.4
	Extrusion ratio=1.56	4.05	4.22	4.3

Table 4.12 above depicts the experimental results of total power required for deformation of cp-titanium grade 2 material through continuous forming machine (TBJ 350) set up at constant preheating temperature and extrusion wheel velocity through different extrusion ratios. The result revealed that as extrusion ratio increases the power consumption of the machine also increases. Table 4.13 shows the error percentage power consumption between simulation and experimental analysis of power consumption during the process, and the error percentages are kept under 5%.

4.10 Material testing and characterizations

In this material characterization section several types of tests have been conducted to understand the deformation behaviour of CP-Titanium grade 2 material after continous forming process. Those analysis are mechanical (*hardness test, tensile test*), and metallurgical (*microstructure*) analysis.

4.10.1 Mechanical Analysis

4.10.1.1 Hardness test

Hardness test has been conducted to know the resistance of CP-Titanium Grade-2 feedstock material to plastic deformation which induced by applied force, by using Vickers hardness test methods which consists a diamond indenter in the form of right pyramids with a square base and an angle of 136 degrees between opposite faces subjected to a load of 10 kgf and the full load is applied for average time of 10 to 15 seconds. As illustrated in the table 4.14 below, surface hardness of CP-Titanium grade 2 and deformed product of CP-Titanium grade 2 materials have been examined each three times and then average values of Vickers Hardness was taken to understand the change that have been made after the processes.

Table 4. 14 Vickers hardness test results of deformed material specimens.

Hardness Test Results					
Material types	Extrusion ratio	Test 1	Test 2	Test 3	Average VH values
Prepared specimens (Deformed products)	1.56	199.8	192.4	189.6	193.9VH10
	2.44	238.6	241.5	244.6	241.6VH10
	4.34	233.7	238.6	256.2	242.8VH10

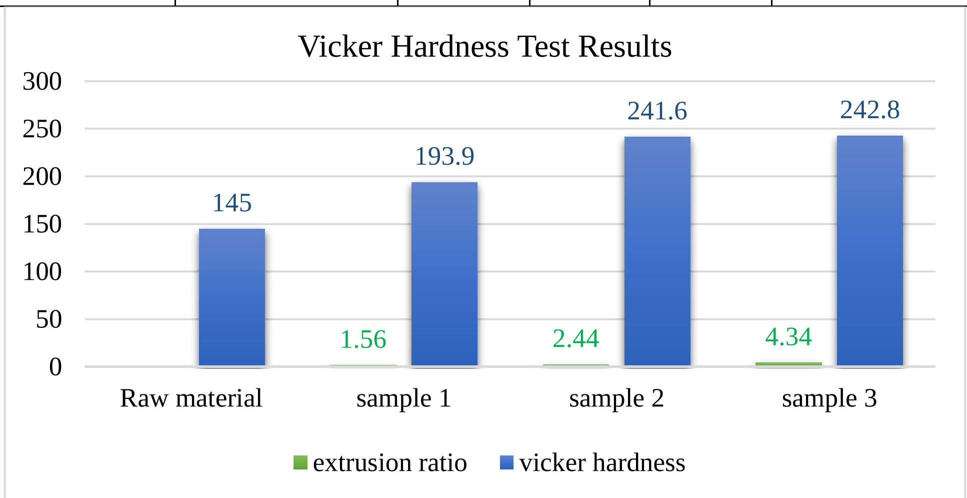

Figure 4. 52 The graphical illustration of vickers hardness test results of raw material and deformed productes.

As shown in figure 4.52, vickers hardness test result clarifies that as the extrusion ratio of deformed product increases from 1.56 to 2.44, and 2.44 to 4.34 the surface hardness of the product has been increased when as compared with a raw feedstock material and when the hardness improvent expresed in terms of percentage for (10 mm, 8 mm and 6 mm rod) of extruded products are 33.72 % , 66.62% and 67.45 % respectively.

4.10.1.2 Tensile Test Analysis

Tensile testing has been performed to find how strong a material is and also how much it can be stretched before its failure. This test technique is used to determine yield strength,ultimate tensile strength, ductility and so on. Table 4.15 displays, the Tensile testing results of raw material and deformed product commercialy pure titanium grade 2 material. As the table depicts tensile testing results of (10 mm, 8 mm and 6 mm deformed products displayed at what applied force and elongation failure occurs.

Table 4. 15 Tensile test results of commercialy pure titanium grade 2 material

Tensile test results of CP-Ti Gr-2 material					
10 mm product		8 mm product		6 mm product	
L (mm)	F(KN)	L (mm)	F (KN)	L (mm)	F (KN)
0	0	0	0	0	0
0.174	0.3	-0.0021	0.102368	-0.00221	0.110512
0.6604	5.98	0	0	0	0
0.9456	9.72	-0.0005	0.025592	-0.000555	0.027628
1.2258	13.21	0.0376	0.038388	0.04061316	0.041442
1.5308	15.96	0.4429	0.243124	0.47824068	0.262466
1.8516	17.92	0.8826	1.932196	0.95288972	2.085914
2.1834	19.33	1.2642	5.24636	1.3648232	5.66374
2.5326	20.37	1.666	9.46904	1.7985828	10.22236
2.8888	21.06	2.064	13.909252	2.22764564	15.01582
3.2468	21.66	2.4739	17.696868	2.670799	19.105
3.6178	22.11	2.9359	20.192088	3.16948	21.7985
3.9912	22.44	3.89	21.740404	4.19973	23.48
4.3664	22.68	4.4131	22.469776	4.76417	24.2574
4.7428	22.86	4.803	25.361672	5.18522	27.3794
5.13	23	5.2085	28.125608	5.622851	30.3632

5.8558	23.21	5.6523	29.609944	6.101921	31.967
6.2638	23.31	6.1114	30.32652	6.597566	32.7392
6.6524	23.38	6.587	30.863952	7.11089	33.3194
7.041	23.45	7.0652	31.260628	7.62726	33.748
7.43	23.5	7.5581	31.567732	8.15938	34.079
7.819	23.55	8.039	31.823652	8.67878	34.355
8.2182	23.59	8.5339	32.041184	9.21284	34.5903
8.6178	23.61	9.04191	32.233124	9.76125	34.7975
8.9974	23.63	9.5374	32.412268	10.29613	34.991
9.3972	23.64	10.0333	32.56582	10.83156	35.157
9.8072	23.64	10.9754	32.809	11.84855	35.4191
10.21	23.63	11.5107	32.911	12.42653	35.5297
10.608	23.6	12.0208	33.001	12.9772	35.626
11.009	23.55	12.5186	33.065	13.5145	35.6954
11.752	23.37	13.0294	33.116	14.0659673	35.751
12.195	23.21	13.5405	33.1544	14.6177	35.7921
12.620	22.96	14.03	33.18002	15.1559	35.8197
13.059	22.55	14.5508	33.18002	15.7085	35.8197
13.502	21.89	15.0754	33.18002	16.275	35.8197
13.964	20.8	15.588	33.14164	16.83	35.7783
14.430	19.47	16.101	33.09045	17.382	35.7230
15.345	17.71	16.6146	33.001	17.9364	35.6263
16.919	15.52	17.1167	32.8473	18.478	35.4605
17.832	13.67	17.6201	32.6298	19.022	35.2257
18.547	11.96	18.661	31.7725	20.14551	34.300
19.521	9.54	19.2813	30.826	20.815	33.278
19.956	6.32	19.8878	29.29	21.46998	31.62
20.231	4.21	20.5151	27.358	22.147	29.534
20.856	3.81	21.4497	24.773	23.156	26.7439
21.512	2.03	22.793	8.1511	24.606	8.79952
21.857	0.1	23.269	0.3455	25.1202	0.37298

21.989	0.12	23.306	0.4351	25.1597	0.4697
22.056	0.13	23.331	0.461	25.187	0.497

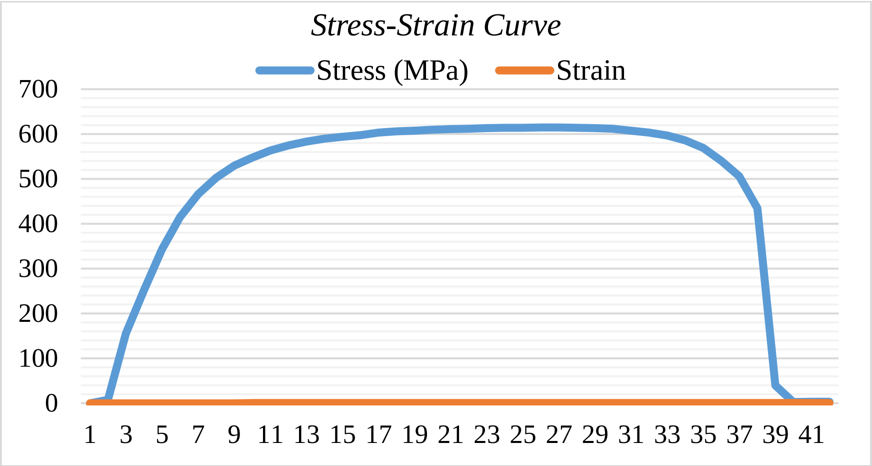

Figure 4. 53 Stress-Strain curve of 10 mm deformed product of CP-Titanium grade 2 material

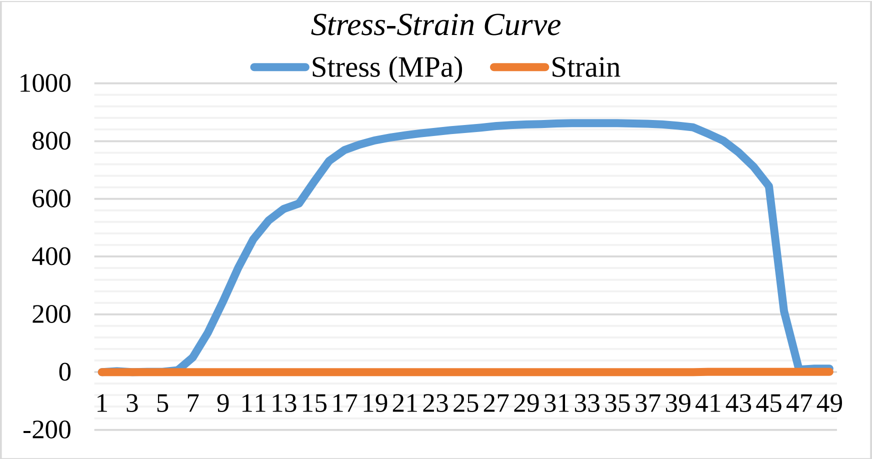

Figure 4. 54 Stress-Strain curve of 8 mm deformed product of CP-Titanium grade 2 material

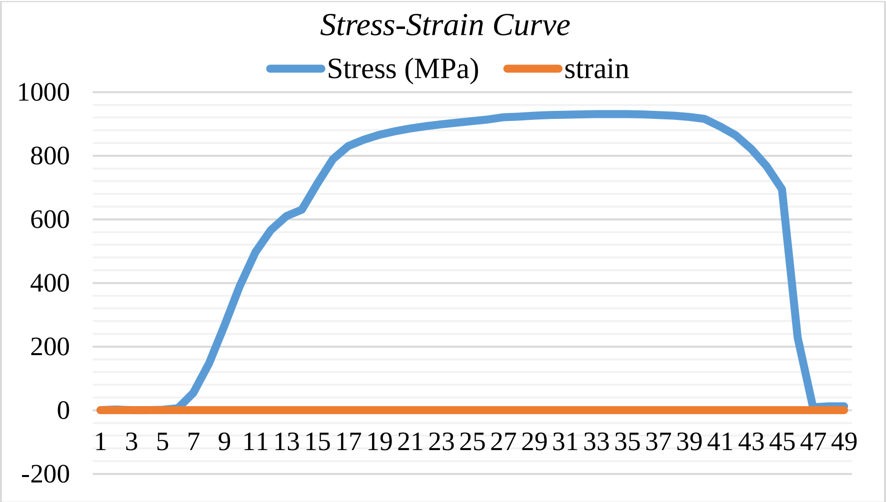

Figure 4. 55 Stress-Strain curve of 6 mm deformed product of CP-Titanium grade 2 material

Figure 4.53 to Figure 4.55 display the Stress-Strain curve of CP-Titanium grade 2 of deformed products. As demonstrated the tensile strength of 10 mm deformed product scored as 614.34 MPa at maximum strain of 0.183, The tensile strength of 8 mm deformed product scores 862.26 MPa at maximum strain of 0.259 and The tensile strength 6 mm deformed product scored as 930.86 MPa at maximum strain of 0.279. Hence, the tensile strength test of the CP-Titanium grade 2 material before and after continuous deformation has been summarised as follows:

1. The ultimate tensile strength of 10 mm, 8 mm and 6 mm of deformed product CP-Titanium grade 2 material increased by 40.98 %, 71.51 %, 83.14 % respectively when compared to a raw material of CP-Titanium grade 2.
2. The ultimate elongation of 10 mm, 8 mm and 6 mm of deformed product CP-Titanium grade 2 material increased by 10.28 %, 16.66 %, 25.94 % respectively when compared to a raw material of CP-Titanium grade 2.

4.10.2 Microstructural Analysis

Microstructure of 12.5 mm diameter of raw material and 10 mm diameter of deformed specimens are shown below in Fig. 4.56 (a) and (b) respectively. As illustrated below in figure 4.56 (a) the surface of 12.5 mm diameter of raw material highly attacked by corrosion due to etching chemical (HNO_3) during etching process µ.

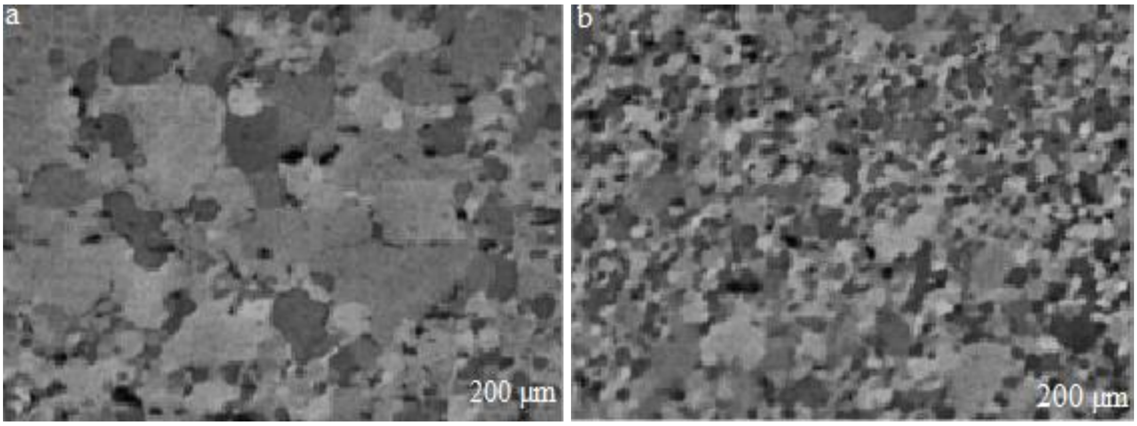

Figure 4. 56 Microstructural analysis of CP- Titanium grade 2 feedstock material; a) 12.5 mm diameter (raw material), and b) 10 mm diameter deformed product.

Large α phase and discrete β phase are broken under upsetting force. The upset deformation on two sides happens asynchronously. Figure 4.57 (b) depicts that the grains are extremely small after deformation.

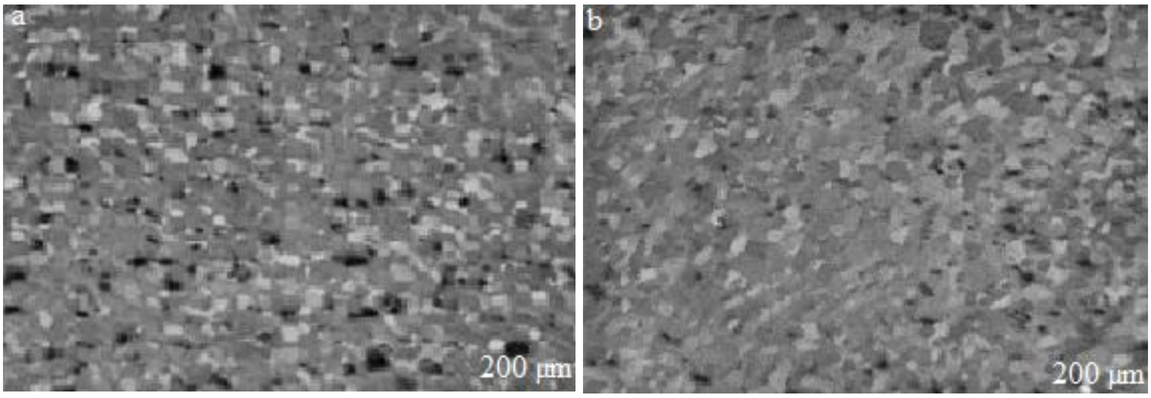

Figure 4. 57 Microstructural analysis of CP- Titanium grade 2 deformed specimens a) 8 mm diameter of deformed specimens.and b) 6 mm diameter of deformed specimens.

As illustrated above figure 4.56 to figure 4.57, when the microstructure of 10 mm, 8 mm and 6 mm of deformed product is compared with the microstructure of 12.5 mm raw material, the microstructures of the extruded products are obviously refined and evenly distributed in the deformed products, which is beneficial for improving the Hardness and tensile strength of the product. And also, it was observed a trend towards a more homogeneous microstructure as the extrusion ratio increases.

Table 4. 16 Comparison of Theoretical, Numerical and Experimental Analysis of Required Power (KW) for deformation CP- Titanium grade 2 material.

Run Order	Extrusion wheel Velocity (RPM)	Feedstock Temperature (^{0}C)	Theoretical Analysis Results (KW)	Numerical Analysis Results (KW)	Experimental Analysis Results (KW)	% Error Between theoretical and numerical analysis	% Error Between numerical and experimental analysis
1	4	200	108.83	117.86	127.99	8.29	8.5
2	4	400	47.96	52.56	55.50	9.59	5.59
3	4	600	24.38	25.31	26.18	3.81	3.44
4	8	200	217.61	230.88	251.28	6.09	8.84
5	8	400	95.9	99.7	107.26	3.96	7.58
6	8	600	48.88	52.7	56.47	7.82	7.15
7	12	200	326.4	339.95	372.25	4.15	9.5
8	12	400	143.88	155.39	161.45	7.99	3.89
9	12	600	73.28	78.23	84.16	6.75	7.58

The Theoretica analysis, Numerical simulation and Exprimental analysis of power consumption results for deformation of CP- Titanium grade 2 material have been illustrated on the above table 4.16 and have been found to be in fully agreement, thereby maintaining the error up to 10 %.

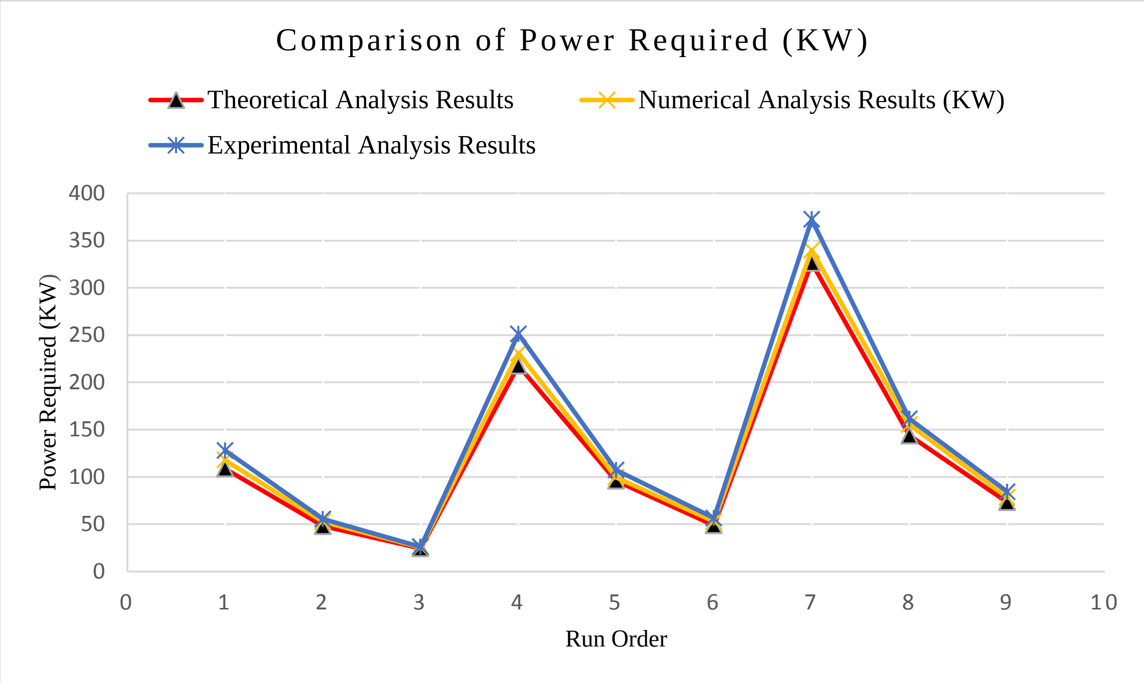

Figure 4. 58 Comparison of power required for deformation process

4.11 Analysis of Grey Relation of Effective-Stress and Power Consumption

Grey relation analysis is implemented to decide the optimum process parameter of this study to get the optimum effective-stress and power consumption during continuous forming process. As shown below in table 4.17 and table 4.18, signal to noise ratios of effective stress and power consumption, Normilized signal to noise values of effective stress and power consumption, quality loss of effective stress and power consumption, grey relational coefficient of effective stress and power consumption and grey relational grade are displayed to determine the optimum factors of the process to get less effective stress and power consumption.

Table 4. 17 S/N ratios and Normalized S/N ratios

Ex.no	Effective stress (MPa)	Power consumption (KW)	S/N ratios		Normalized S/N ratios	
			Effective-Stress	Power Consumption	Effective-Stress	Power Consumption
1	1020	117.86	-60.17	-41.43	1.000	0.79
2	746	52.56	-57.46	-34.41	0.586	0.55
3	575	25.31	-55.19	-28.15	0.242	0.33
4	981	230.88	-59.83	-47.27	0.948	1.00

5	763	99.70	-57.65	-39.97	0.616	0.74
6	479	52.70	-53.61	-34.44	0.000	0.55
7	935	339.95	-59.42	-25.31	0.885	0.22
8	647	155.39	-56.22	-21.91	0.398	0.10
9	485	78.23	-53.72	-18.94	0.016	0.00

Table 4. 18 Grey Relational coefficient and grey relational grade

Ex. no	Normalized S/N ratios		Quality loss		Grey Relational coefficient		Grey grade
	Effective-Stress	Power Consumption	$\Delta_{Effective\text{-}Stress}$	$\Delta_{Power\ Consumption}$	$GC_{Effective\text{-}Stress}$	$GC_{Power\ Consumption}$	
1	1.000	0.79	0.000	0.21	1.000	0.826	0.913
2	0.586	0.55	0.414	0.45	0.707	0.687	0.697
3	0.242	0.33	0.758	0.67	0.569	0.598	0.584
4	0.948	1.00	0.052	0.00	0.951	1.000	**0.976**
5	0.616	0.74	0.384	0.26	0.723	0.794	0.759
6	0.000	0.55	1.000	0.45	0.500	0.688	0.594
7	0.885	0.22	0.115	0.78	0.897	0.560	0.729
8	0.398	0.10	0.602	0.90	0.624	0.530	0.577
9	0.016	0.00	0.984	1.0	0.504	0.500	0.502

Table 4. 19 Mean of MRPI values and ranking of factors effect.

Factors		Extrusion Wheel Velocity (A)	Feedstock Temperature (B)
levels	1	0.7312	**0.8723***
	2	**0.776***	0.6775
	3	0.6025	0.5598
Rank		2	1

Table 4.19 displays the Multi Response Performance Index (MRPI) of extrusion wheel velocity and feedstock temperature on effective stress and power consumption during continuous forming process. From table 4.18 the highest number of Grey Relational Grade indicates the optimum factors combination of factors and the optimum combination has been found at experiment number 4 (8 rpm and 200 ^{0}C) and also, table 4.19 demonstrates the highest score of extrusion wheel velocity factor that has been found at level 2 and the highest score of feedstock temperature found at level 1 hence, the optimum values of both effective stress and power consumption found at $\mathbf{A_2}$ and $\mathbf{B_1}$ levels (8 rpm and 200 ^{0}C).

4.12 Special Case Study

This special case study paper unique with thesis paper by Feedstock material, Experimental plan and design technique and optimization process. It has been done parallel with thesis paper and already published online by Elsevier on Materials Todays: Proceedings journal, since **March 14, 2021** with Digital Object Identifier (DOI): https://doi.org/10.1016/j.matpr.2021.02.289.

This Special case study paper titled as ***Analysis of effective stresses for titanium alloys in continuous forming process***. The investigation of effective stresses of Titanium Grade 5 feedstock material during the continuous forming process has been carried out. The numerical simulation has been carried out through a finite element tool DEFORM-3D. The experimental plan and design have been carried out by using Response Surface Methodology (RSM) on MINTAB platform by considering extrusion wheel velocity and feedstock temperature as main extrusion parameters. Effective-stresses of Ti-6Al-4 V alloy have been investigated to understand the deformation behavior for further more applicability of feedstock material in the modern industrial sector

4.12.1 Simulation results and analysis

Table 4.20 depicts the effective-stresses of 6 mm product diameter Ti-6Al-4V alloy feedstock material with variation of two different factors.

Table 4. 20 Effective-stresses result of with Experimental plan and design table.

Run Order	Extrusion Wheel Velocity (RPM)	Feedstock Temperature (^{0}C)	Effective-stresses (MPa)
1	4	50	1330
2	8	425	1210
3	12	300	1150
4	16	175	1440
5	8	175	1270
6	8	175	1270
7	4	300	1230
8	8	75	1250
9	8	175	1270
10	0	175	*
11	8	175	1270
12	12	50	2000

13	8	175	1270

4.12.1.1 Effective-stress distribution.

The illustration of effective stresses for titanium grade 5 feedstock material under various extrusion wheel velocity and feedstock temperature have been shown in Figs. 4.59 - 4.61. It is analyzed from Fig. 4.62 (a) that the effective stresses are high in the biting - deformation region and then gradually decreased towards the material flow direction. As the feedstock temperature increases, the effective stress decreases. Also, it can be inferred that the increase of extrusion wheel velocity and feedstock temperature will decrease the shear strength of feedstock material during the continuous extrusion process. Therefore, the deformation of feedstock material is eased. Furthermore, the deformation and wear of extrusion shoe which is one of the most important elements is minimized, thereby the life period of shoe material and other tooling of the machine can be enhanced.

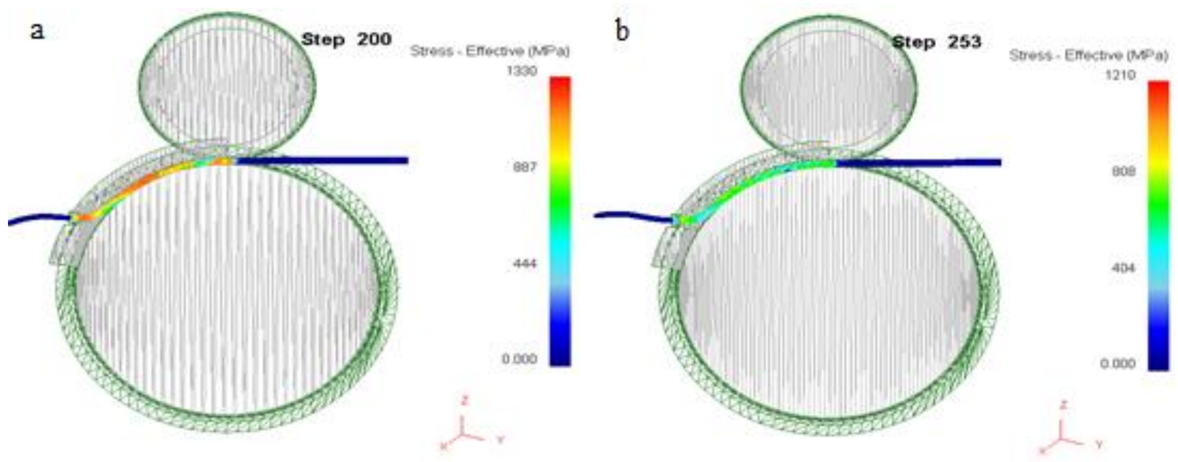

Figure 4. 59 Effective – stress distribution of Ti-6Al-4V alloy under different extrusion wheel velocity and feedstock temperature: (a) 4 rpm and 50 ^{0}C ; (b) 8rpm and 425^{0}C.

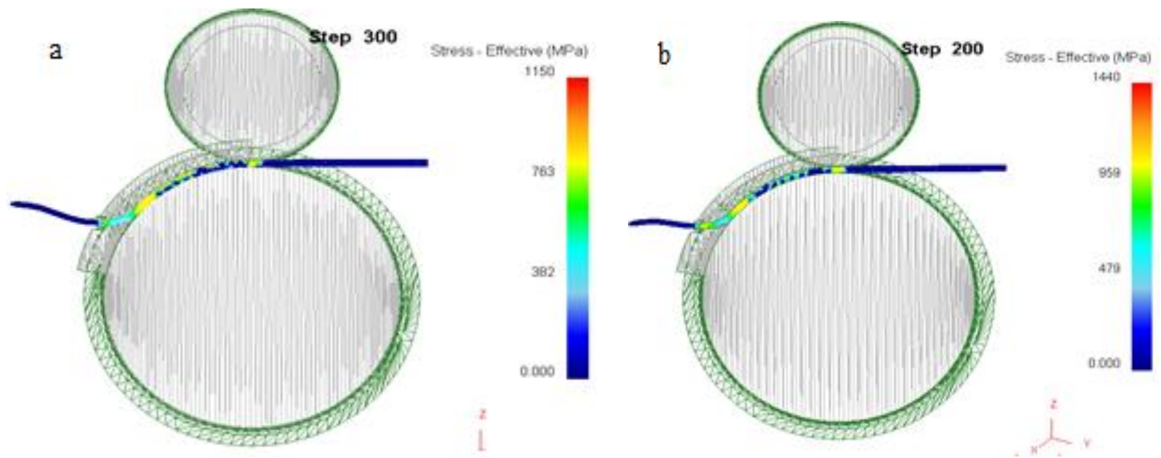

Figure 4. 60 Effective – stress distribution of Ti-6Al-4V alloy under different extrusion wheel velocity and feedstock temperature: (a) 12 rpm and 300 ^{0}C ; (b) 16 rpm and 175^{0}C.

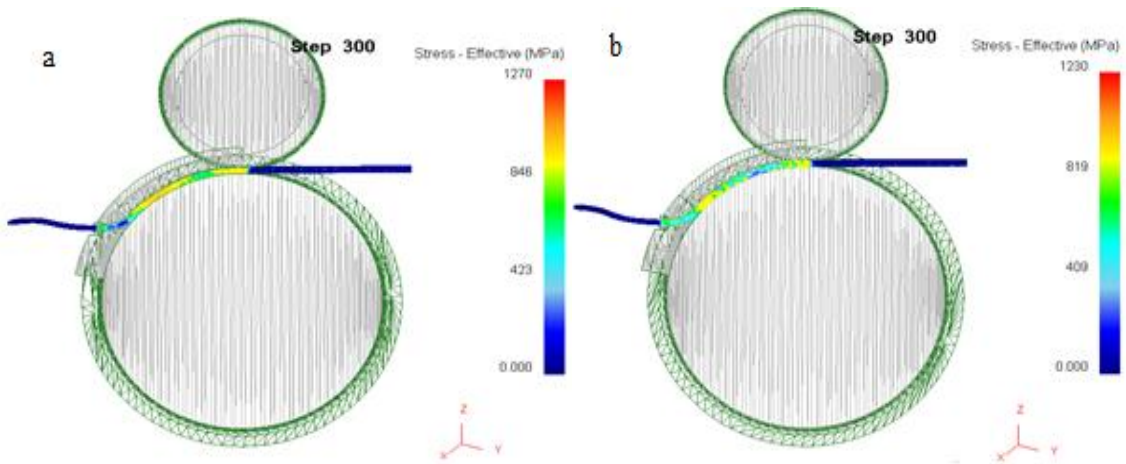

Figure 4. 531 Effective stress distribution of Ti-6Al-4V alloy under different extrusion wheel velocity and feedstock temperature: (a) 8 rpm and 175 ^{0}C; (b) 4 rpm and 300^{0}C.

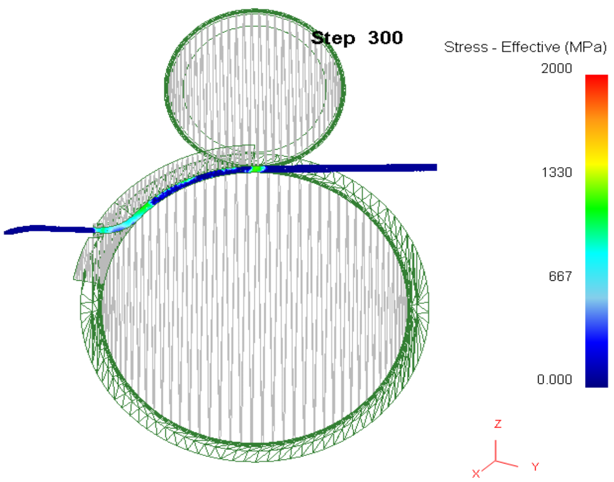

Figure 4. 62 Effective stress distribution of Ti-6Al-4V alloy under different extrusion wheel velocity and feedstock temperature (12 rpm and 50 ^{0}C).

As illustrated in table 4.21, the feedstock temperature creates the prime impact on the total sum of squares through 44.6% as the percentage contribution followed by the interaction effect of extrusion wheel velocity and feedstock temperature of percentage contribution 24.5%. It can be observed that the extrusion wheel velocity creates minimum impact having percentage contribution as 6.89 %.

Table 4. 21 Test result of ANOVA for effective-stresses of Ti-6Al-4V alloy feedstock material.

Source	DF	Adj SS	Adj MS	F-Value	P-Value
Model	5	426137	85227	3.47	0.081
Linear	2	278916	139458	5.68	0.041
Extrusion Wheel Velocity	1	39501	39501	1.61	0.252
Feedstock Temperature	1	255618	255618	10.42	0.018

Square	2	142167	71084	2.90	0.132
Extrusion Wheel Velocity*Extrusion Wheel Velocity	1	33414	33414	1.36	0.288
Feedstock Temperature*Feedstock Temperature	1	108432	108432	4.42	0.080
2-Way Interaction	1	140625	140625	5.73	0.054
Extrusion Wheel Velocity*Feedstock Temperature	1	140625	140625	5.73	0.054
Error	6	147229	24538		
Lack-of-Fit	2	147229	73615	*	*
Pure Error	4	0	0		
Total	11	573367			

DF: degree of freedom; Adj SS: adjusted sums of squares; Adj MS: adjusted mean

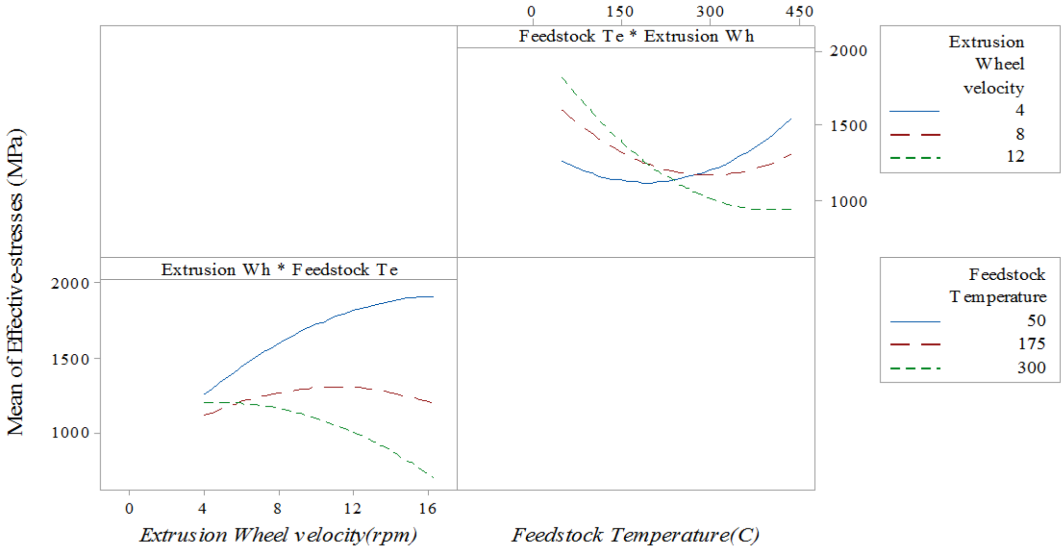

Figure 4. 63 Interaction plot of effective –stress with extrusion wheel velocity and feedstock temperature.

The effective-stress of titanium feedstock material have shown significant results under different extrusion wheel velocity and feedstock temperature which can be seen from Fig. 4.63. The effective stress increases, when the extrusion wheel velocity increases to 50^0C feedstock temperature. The effective-stress shows a slight increment then gradually decrease after 12 rpm at 175^0C.The effective-stress of Ti-6Al-4V alloy decreases as extrusion wheel velocity increases, when the feedstock temperature reaches 300^0C. The effective-stresses decrease when feedstock temperature increases to 12 rpm, slight decrease as feedstock temperature increases to 300^0C then after gradually increases at 8 rpm.Very low decrement in effective stresses are observed as the feedstock temperature increases to 150^0C then after gradually increases at 4rpm.

Figure 4.64, depicts the standardized effects of both factors (extrusion wheel velocity and feedstock temperature) on effective-stresses of titanium alloy feedstock material. As shown in

Fig. 4.64, factor B (feedstock temperature) has high effect on effective-stress at the first level. Secondly,interaction effect AB (feedstock temperature and extrusion wheel velocity) have remarkable effects on effective-stresses of feedstock material.

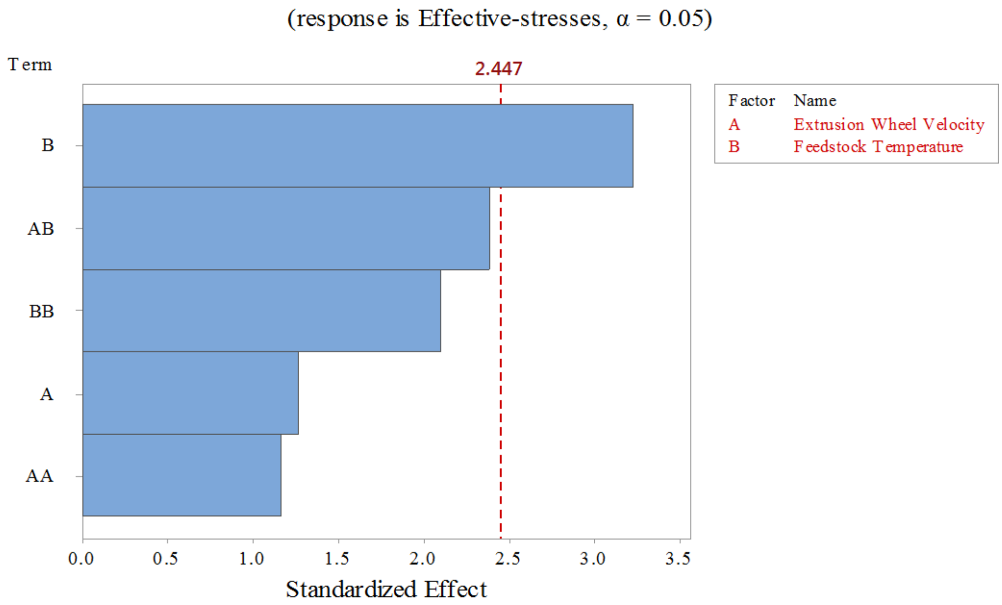

Figure 4. 64 Pareto chart of standardized effects.

Figure 4.65 illustrates the contour plot of effective-stress vs wheel velocity and feedstock temperature. The 3-dimensional surface depicts on a two-dimensional plane and it graphs with two predictors X-Y (extrusion wheel velocity, feedstock temperature respectively) on the x-y axis and a response variable Z (effective-stress) as contour plot.

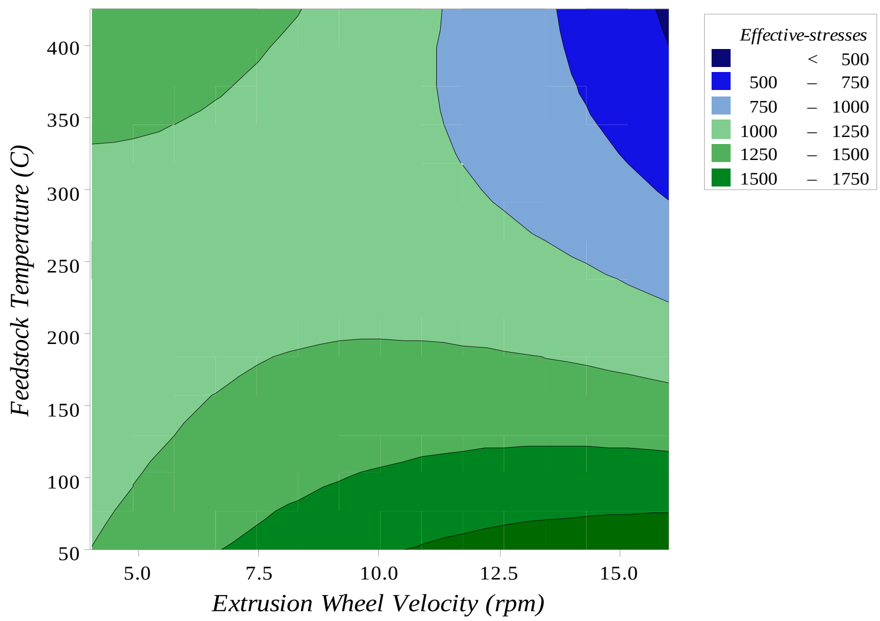

Figure 4. 54 Contour plot of effective-stress vs wheel velocity and feedstock temperature.

From Fig. 4.66, it is observed that the highest value of effective stresses occurs at high level of wheel velocity and low value of feedstock temperature whereas the lowest value of effective stresses occurs at high value of extrusion wheel velocity and feedstock temperature.

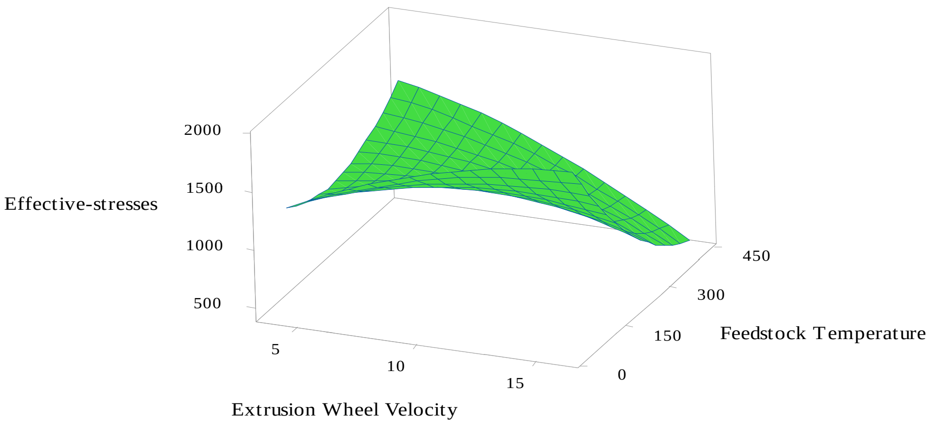

Figure 4. 55 Surface plot of effective stress vs feedstock temperature and wheel velocity.

4.12.1.2 Optimization of effective-stresses.

In this study optimization analysis of input parameter has been carried out using Response Surface Methodology (RSM) optimization technique. The optimum values of Extrusion wheel velocity and feedstock temperature during continuous forming process for target value (σ = 500 MPa) are 16 RPM and 398.5 ^{0}C respectively, as illustrated below in figure 4.69.For the analysis of response surface design, mathematical modelling of Ti-6Al-4V alloy can be expressed is shown below in equation (4.1) through modelling of target value ($\sigma < \sigma_y$) much below the yield stress of feedstock material in order to keep the shoe and other CONFORM machine components safe.

$$\sigma_y = 1005 + 88.9A - 0.84B - 0.372A*B + 0.33A^2 + 0.00628\,B^2 \qquad (4.1)$$

where A and B are extrusion wheel velocity and feedstock temperature respectively. Equation 4.1 illustrates that interaction between two factors (A and B) on the effective-stresses of feedstock material during continuous forming process in order to minimize the yield stress of shoe material to make sure the forming process and its tooling's are safe. As illustrated in the model, both factors have their own impact on yield stress value of feedstock material but comparatively factor A has larger impact than the factor B on yield stress value of feedstock material. The optimized values of effective stresses for titanium feedstock material at the target value of 500 MPa has been shown in table 4.17. The optimization plot of effective stress for parametric combination of feedstock temperature and extrusion wheel velocity is shown in Fig. 4.67.

Table 4. 22 Optimum value of effective stresses at optimal combinations of Wheel velocity and feedstock temperature

Solution	Wheel Velocity (RPM)	Feedstock Temperature (^{0}C)	Effective-Stress (MPa) Fit	Composite Desirability
1	16	398.485	503.238	0.997841

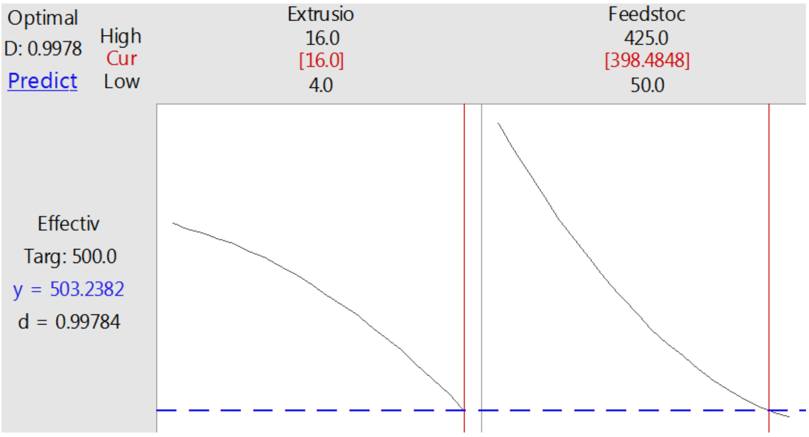

Figure 4. 56 Optimization Plot for effective stress with respect to Extrusion wheel velocity and Feedstock temperature.

The confirmatory numerical experiment has been carried out as illustrated below in Fig. 4.68, to validate the optimal combination of process parameters. The minimum value of effective stress has been found at optimal values of extrusion wheel velocity (16 RPM) and feedstock temperature (398.48 ^{0}C). As depicted in Fig.4.68 below, the confirmatory test result of effective stress has been found to be 527 MPa showing much less deviation from the value obtained through RSM with an error of 4.8%.

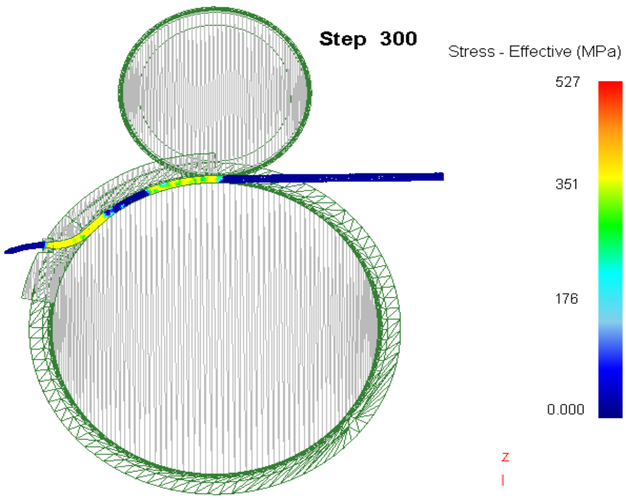

Figure 4.68 Effective stresses distribution of Ti-6Al-4V alloys of confirmatory test result at optimum values of extrusion wheel velocity and feedstock temperature (16 rpm and 398.48 ^{0}C) respectively.

CHAPTER FIVE

CONCLUSIONS AND RECOMMENDATIONS

5.1 Summary

In the present study, investigation of deformation behaviour for CP Titanium grade 2 feedstock materials through continuous forming process has been carried out. In the study theoretical analysis, numerical simulation and experimental Validation have been carried out. Theoretical analysis has been analyzed using Fields-Backofen equation and upper bound technique. Numerical simulation has been carried out using DEFORM-3D platform. The deformation experimental analysis of CP-Titanium grade 2 feedstock materials has been conducted through continuous Extrusion (TBJ350) Machine set up in Banira Industrial Estate, Jalan Complex, Jungalpur, Howrah, India. Parameter Optimization process has been carried out through Minitab platform. And Finally, for material characterization process, Hardness and microstructural test has been done in Materials Science and Engineering lab at Adama science and technology University and Tensile testing has been carried out in basic work shop at Adama science and technology University.

5.2 Conclusions

After successful completion of deformation behaviour investigation for CP-Titanium grade 2 feedstock materials through continuous forming process, the main results are summarized as followings.

1. During continuous forming process, by increasing the preheating temperature of feedstock material at the same extrusion wheel velocity the effective stress of a material can be decreased. As the effective stress of a material decreased the total load required for deformation also decreased.
2. During continuous forming process, power consumptions of Conform machine decreased by decreasing the extrusion wheel velocity (rpm) and vice versa.
3. During continuous forming process, the maximum temperature present during the process decreases as the preheating temperature of the material increases at the same extrusion wheel velocity.
4. It has been observed from experimental validation, the total extrusion powers as 4.22 kW (extrusion ratio 4.34), 3.81 kW (extrusion ratio 2.44) and 3.62 kW (extrusion ratio 1.56) at extrusion wheel velocity of 4 RPM whereas simulation powers are 4.05 kW (extrusion ratio 4.34), 3.71 kW (extrusion ratio 2.44) and 3.48

kW (extrusion ratio 1.56) at extrusion wheel velocity of 4 RPM. Therefore, it is concluded that power required by the simulation process is greater than analytical process.

5. Vickers hardness test result clarifies that as the extrusion ratio of deformed product increases from 1.56 to 2.44, and 2.44 to 4.34 the surface hardness of the product has been increased by 33.72 %, 66.62% and 67.45 % respectively when compared with raw material of CP-Titanium grade 2.
6. The ultimate tensile strength of 10 mm, 8 mm and 6 mm of deformed product CP-Titanium grade 2 material increased by 40.98 %, 71.51 %, 83.14 % respectively when compared with raw material of CP-Titanium grade 2.
7. The ultimate elongation of 10 mm, 8 mm and 6 mm of deformed product CP-Titanium grade 2 material increased by 10.28 %, 16.66 %, 25.94 % respectively when compared with raw material of CP-Titanium grade 2.
8. According to the Multi Response Performance Index (MRPI) of effective stress and power consumption during continuous forming process, the optimum values have been found at 8 rpm extrusion wheel velocity and 200 ^{0}C feedstock temperature).
9. From special case study, it was found that effective stresses were high in the biting region as well as in the deformation zone and then gradually decreased towards the material flow direction. As the feedstock temperature was increased, the effective stresses were found to be decreased. It was observed that as the extrusion wheel velocity and feedstock temperature increased, the shear strength of the feedstock material was found to be decreased during the continuous extrusion process of titanium feedstock material and also, the deformation of feedstock material was very much eased at high extrusion wheel velocity and feedstock temperature. Moreover, the wear of extrusion shoe material was reduced, thereby enhancing the life period of extrusion shoe as well as other tooling's of the of the machine used in the process.

The result reported in this study is highly helpful for metal forming researchers and industries in the area of Continuous Forming process of non-ferrous alloys especially titanium feedstock materials.

5.3 Scope for future Work

The following are recommended as a scope for future works:

1. The process can be explored in detail for other process parameters like friction condition, die temperature, extrusion ratio etc.
2. The design and development of setup can be done for titanium feedstock with pre and post extrusion lines.
3. Arrangement for the extrusion of tubes and multi void tubes can be made.

“This research project is funded by Adama Science and Technology University under the grant number ASTU/SM-R/138/19, Adama, Ethiopia.”

APPENDIX A

SPECIAL CASE STUDY PAPER PUBLICATION

ARTICLE IN PRESS

Materials Today: Proceedings xxx (xxxx) xxx

ELSEVIER

Contents lists available at ScienceDirect

Materials Today: Proceedings

journal homepage: www.elsevier.com/locate/matpr

materialstoday: PROCEEDINGS

Analysis of effective stresses for titanium alloys in continuous forming process

Mulualem Hailu Besha [a], Devendra Kumar Sinha [b], C. Venkatesh [b], Satyam Shivam Gautam [c,*]

[a] *Manufacturing Engineering, School of Mechanical and Industrial Engineering, Dire Dawa University, Dire Dawa 1362, Ethiopia*
[b] *Mechanical Design and Manufacturing Engineering, School of Mechanical, Chemical and Materials Engineering, Adama Science and Technology University, Adama 1888, Ethiopia*
[c] *Department of Mechanical Engineering, North Eastern Regional Institute of Science and Technology, Itanagar, India*

ARTICLE INFO

Article history:
Available online xxxx

Keywords:
Continuous extrusion
Ti-4Al-6V alloy
Feedstock temperature
DEFORM-3D
Extrusion wheel velocity

ABSTRACT

In this study, the investigation of effective stresses of Titanium Grade 5 feedstock material during the continuous forming process has been carried out. The numerical simulation has been carried out through a finite element tool DEFORM-3D. The experimental plan and design have been carried out by using Response Surface Methodology (RSM) on MINTAB platform by considering extrusion wheel velocity and feedstock temperature as main extrusion parameters. Effective-stresses of Ti-6Al-4 V alloy have been investigated to understand the deformation behavior for further more applicability of feedstock material in the modern industrial sector and to keep the shoe and other components of the CONFORM machine safe. It has been found that the effective-stress of feedstock material is high in the biting - deformation region and then gradually decreases towards the flowing direction of the material. It has been observed that as the feedstock temperature increases, the value of effective stresses which occur in other region decreases to some extent. So, the result concludes that increasing extrusion wheel velocity and feedstock temperature of alloy will reduce the shear strength of feedstock material during the continuous forming process. Therefore, the load requirement for deformation can be reduced. Moreover, the wear of extrusion shoe which is one of the most important elements can also be minimized thereby enhancing the life of extrusion shoe material.

Selection and peer-review under responsibility of the scientific committee of the International Conference on Advancement in Materials, Manufacturing and Energy Engineering (ICAMME-2021).

Please cite this article as: M. Hailu Besha, D. Kumar Sinha, C. Venkatesh et al., Analysis of effective stresses for titanium alloys in continuous forming process, Materials Today: Proceedings, https://doi.org/10.1016/j.matpr.2021.02.289

APPENDIX B

VICKERS HARDNESS TEST RESULTS

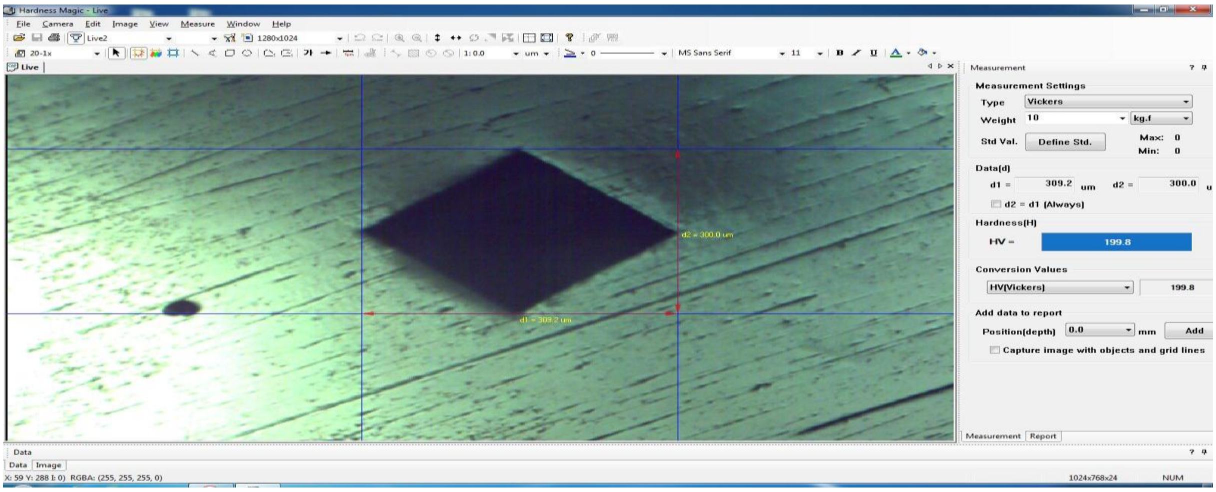

Test one of product with Diameter 10 mm

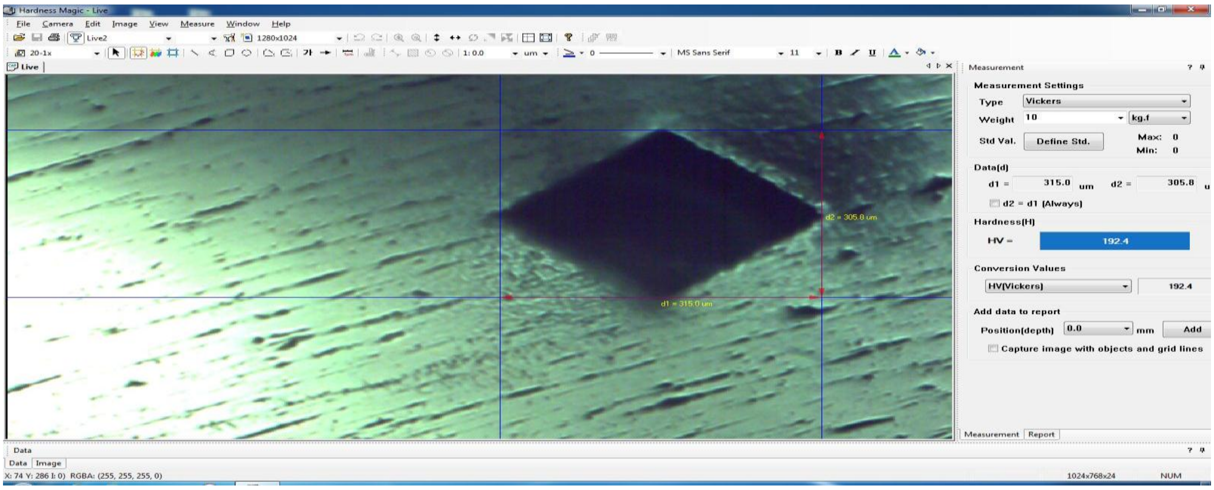

Test two of product with Diameter 10 mm

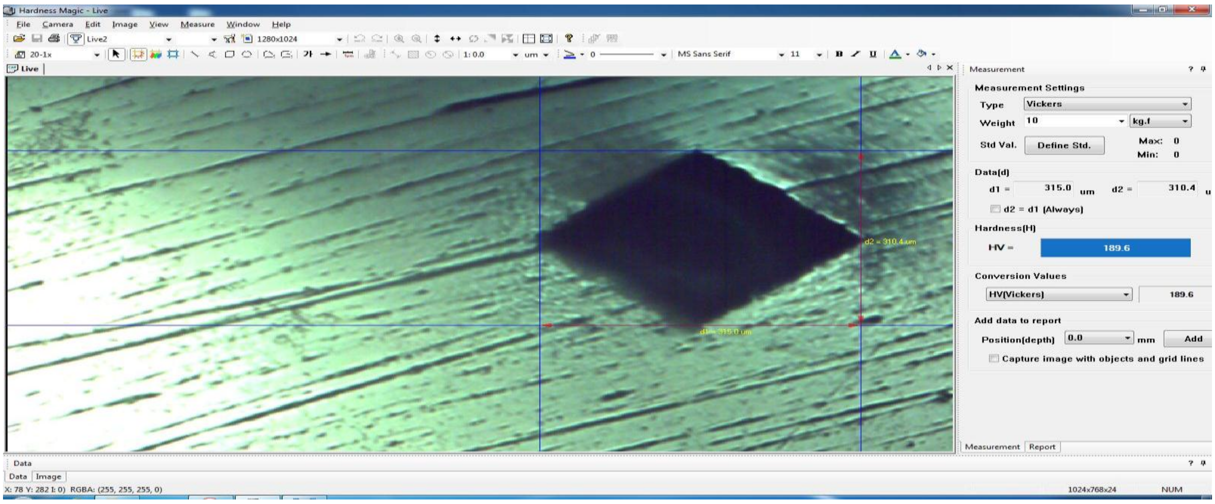

Test three of product with Diameter 10 mm

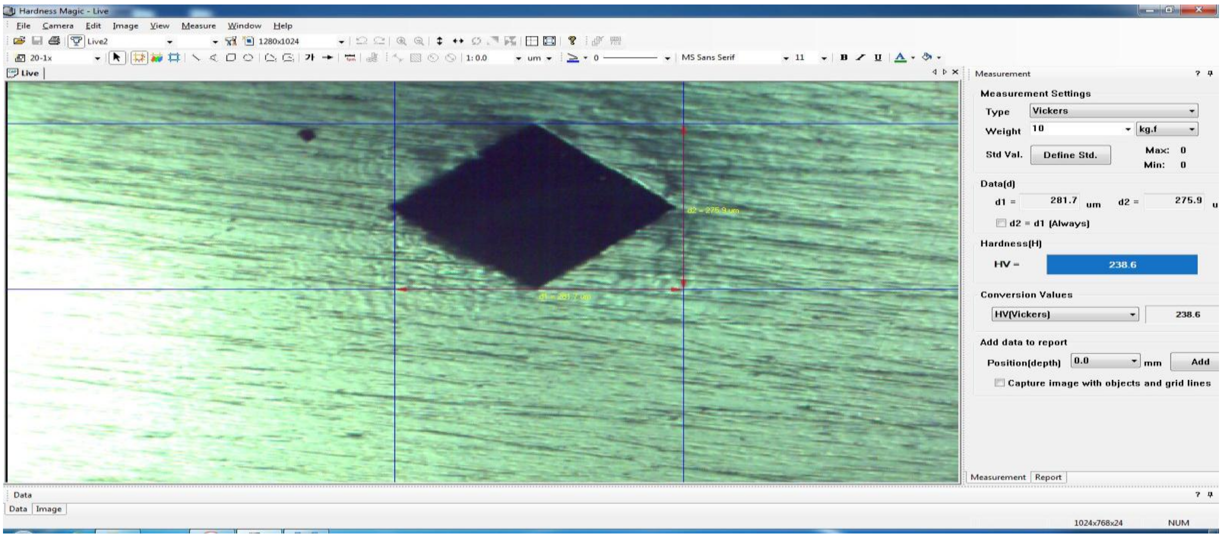

Test one of product with Diameter 8 mm

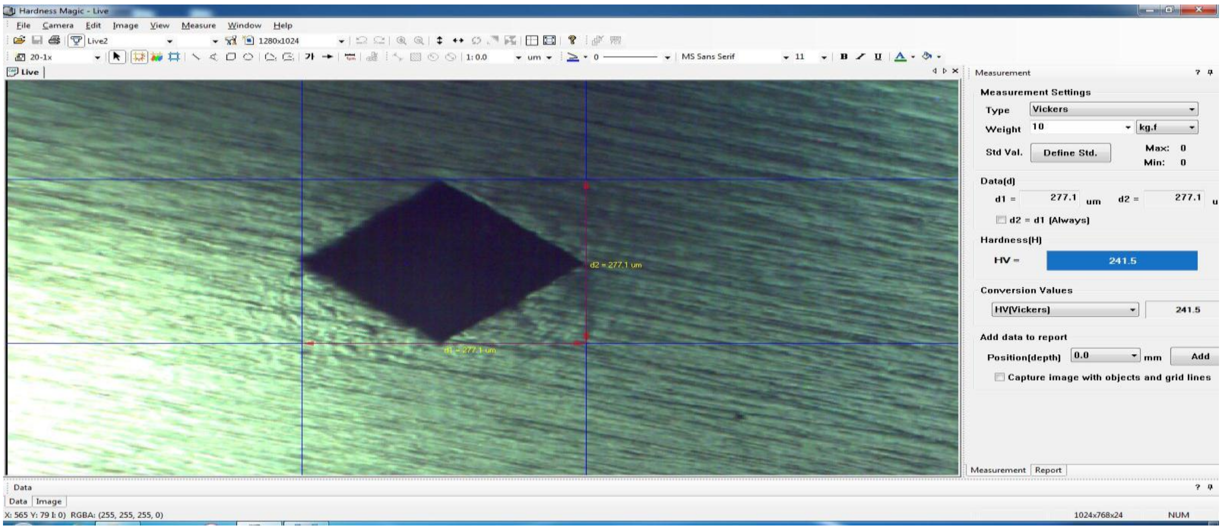

Test two of product with Diameter 8 mm

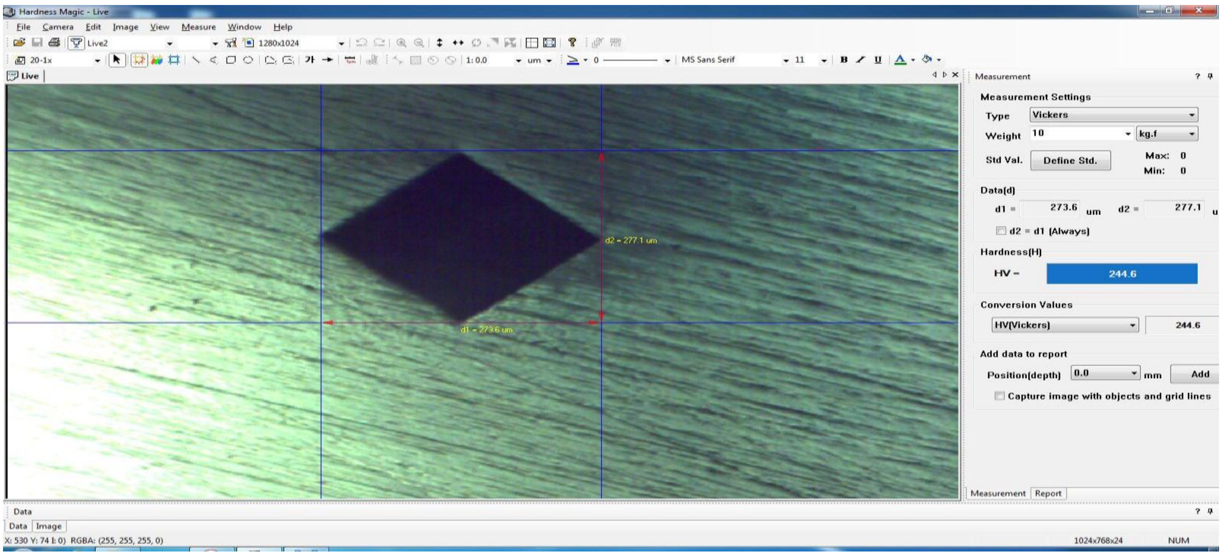

Test one of product with Diameter 8 mm

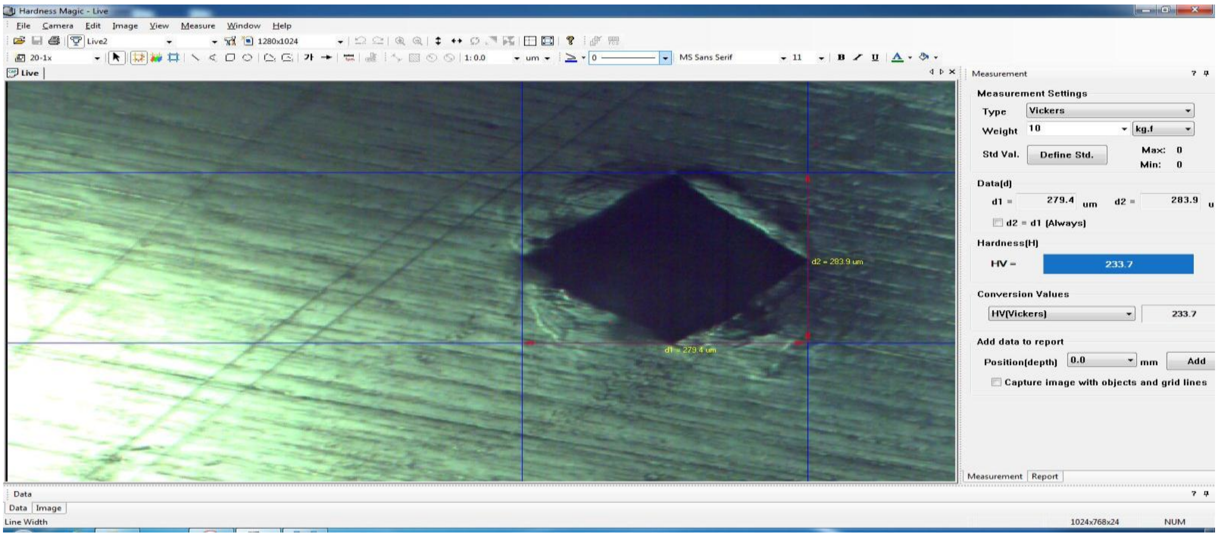

Test one of product with Diameter 6 mm

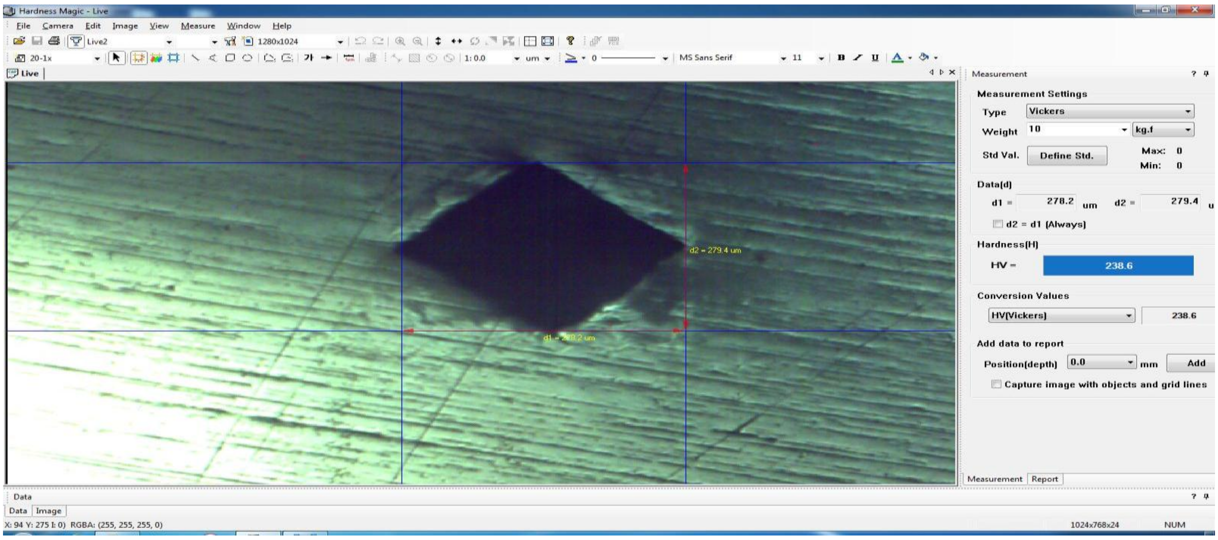

Test two of product with Diameter 6 mm

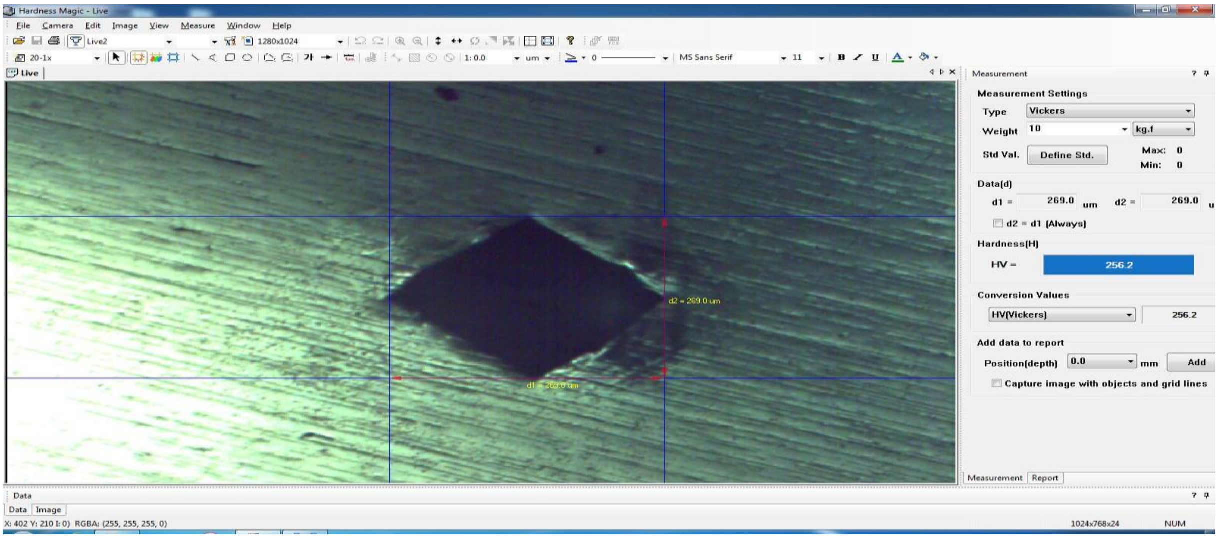

Test three of product with Diameter 6 mm

APPENDIX C

SAMPLE PREPARATION FOR TENSILE TEST USING CONVENTIONAL MACHINE (LATHE MACHINE) ***at ASTU machine shop***

Deformed product and Raw material before prepared for tensile test

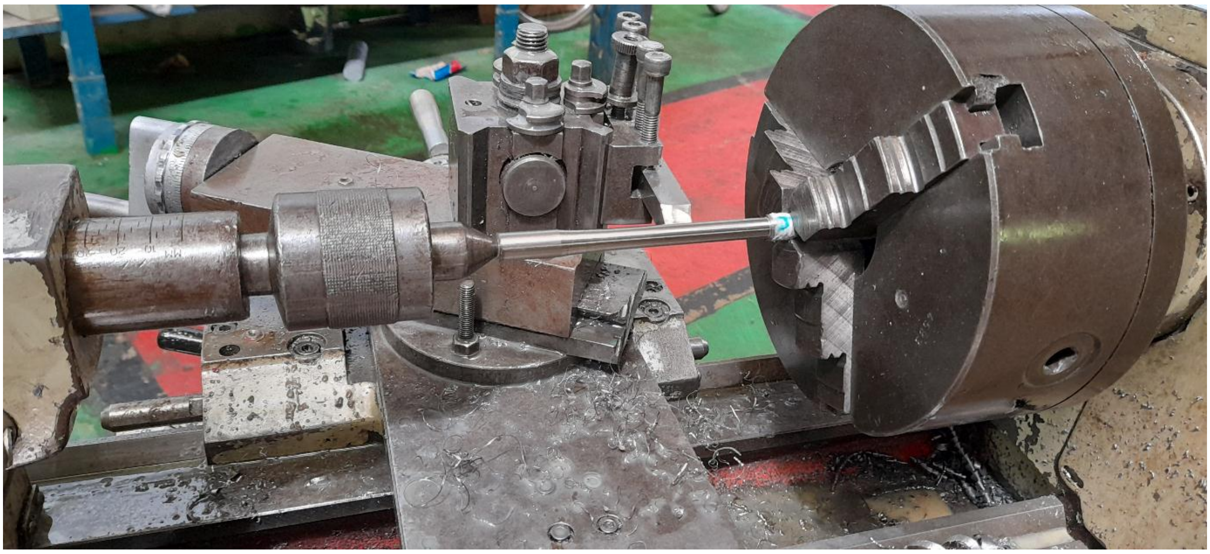

Turning process of deformed product of CP-titanium grade 2 on lathe machine at ASTU machine shop

Prepared specimens of CP-titanium grade 2 rods for tensile test according to ASTM B348/ B348M-19.

APPENDIX D

TENSILE TEST EQUEPIMENTS and DISPLAYED RESULTS

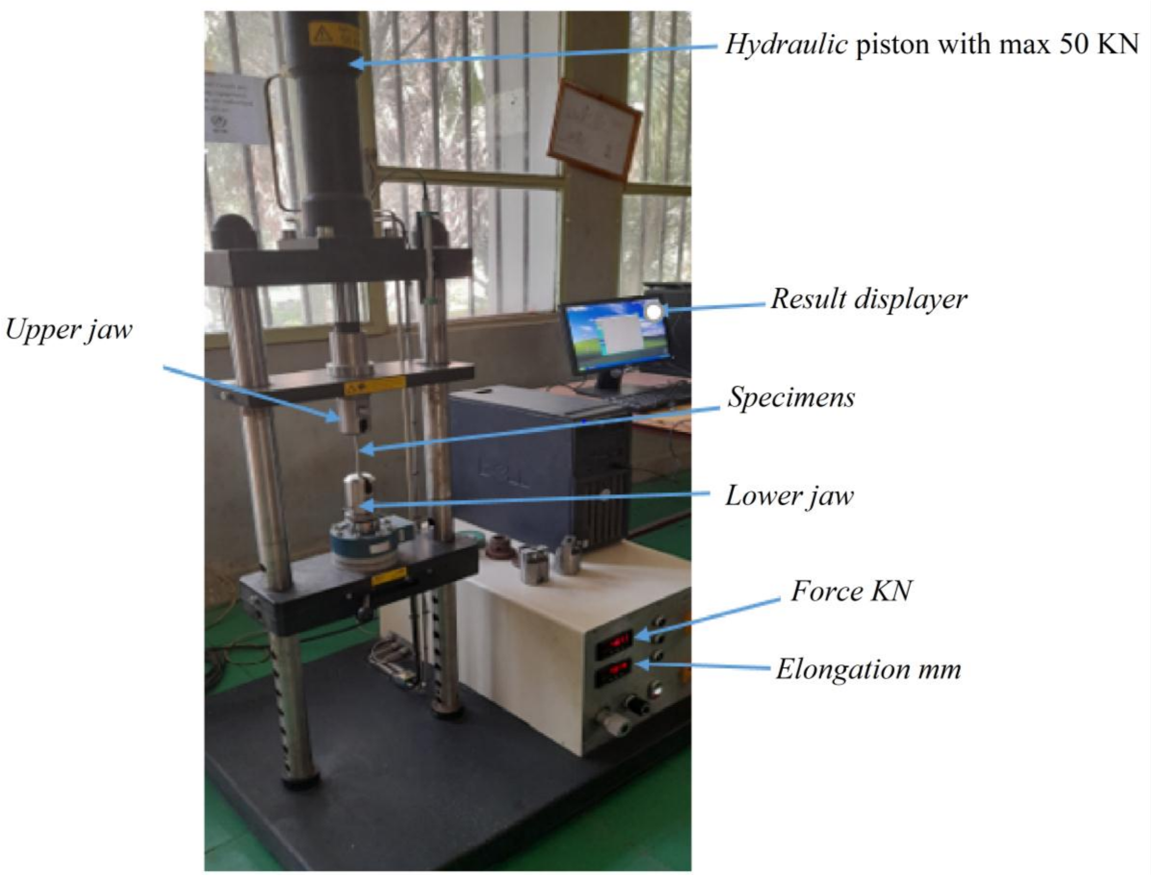

Tensile test machine at ASTU

Tensile testing of 12.5 mm CP-Titanium grade 2 after failure

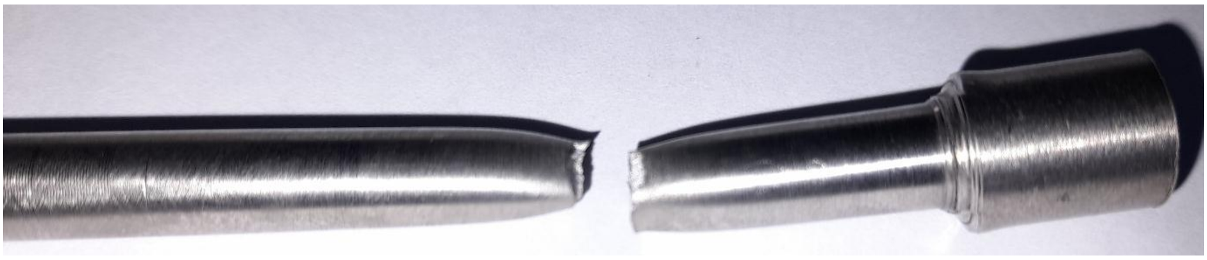

Tensile testing of 10 mm CP-Titanium grade 2 after failure

Tensile testing of 8 mm CP-Titanium grade 2 after failure

Tensile testing of 6 mm CP-Titanium grade 2 after failure

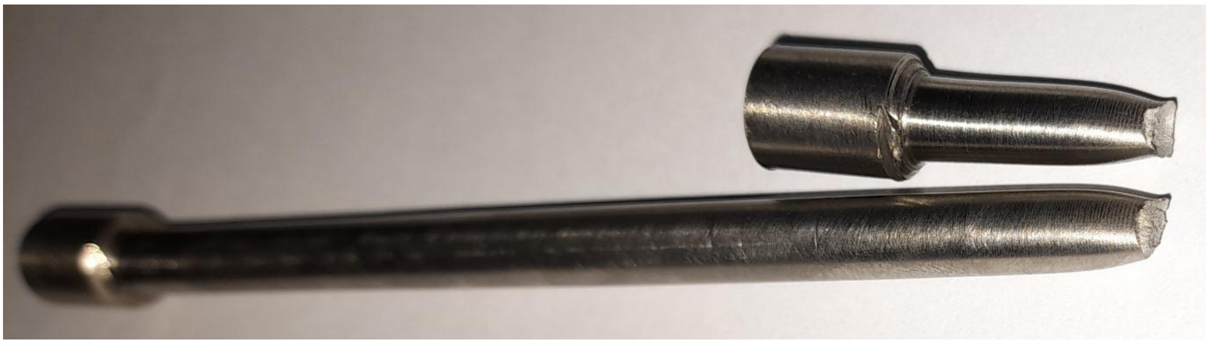

Tensile testing of 10 mm CP-Titanium grade 2 after failure

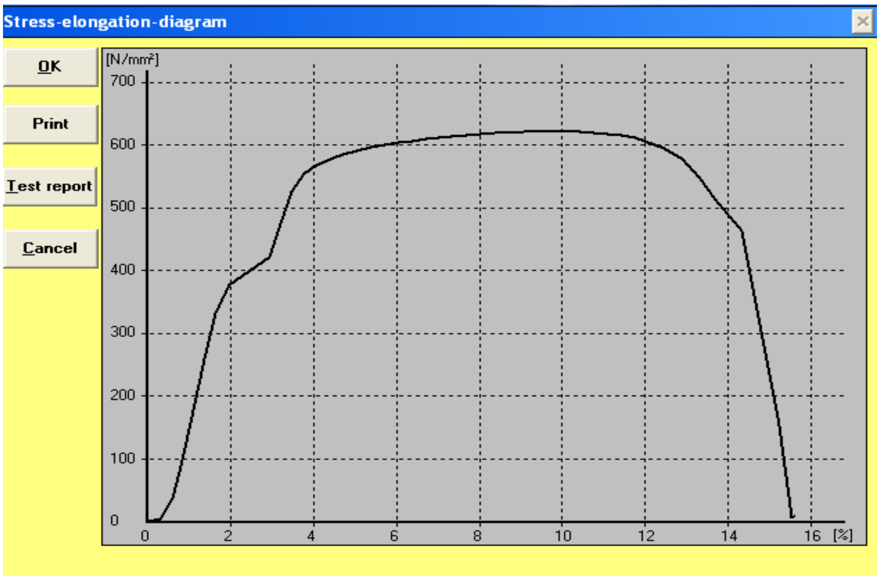

Stress-elongation diagram of 6 mm deformed product of CP-Titanium grade 2

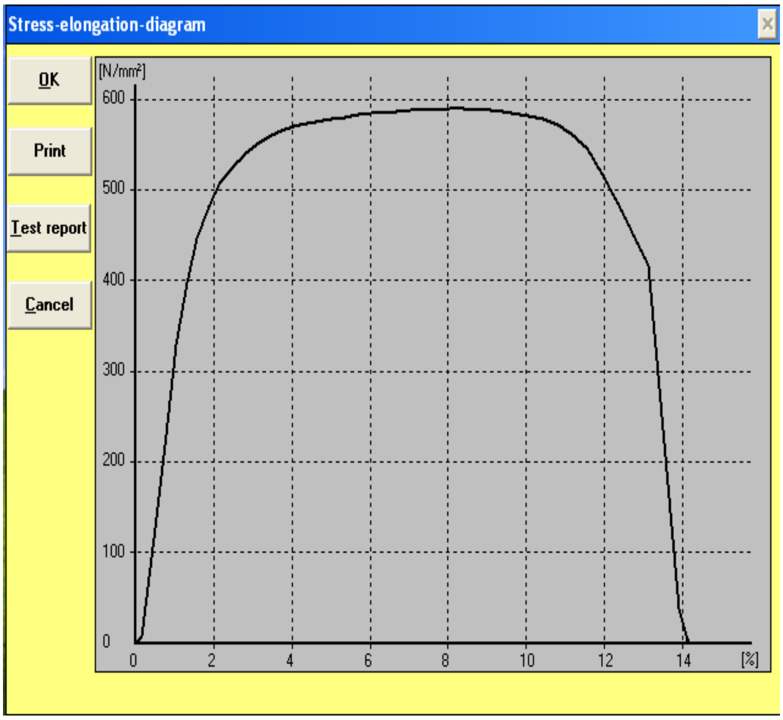

Stress-elongation diagram of 8 mm deformed product of CP Titanium grade 2

References

[1] B. M. Thomas, F. Derguti & M. Jackson, “Continuous extrusion of a commercially pure titanium powder via the Conform process,” Materials Science and Technology, 33:7(2017) 899-903.

[2] Bauser.M, Sauer.G, Siegert.K, Extrusion, 2nd edition.: ASM International, 2006; pp.59-126.

[3] Bing Li, Zikai Lin, Cheng Peng, Xue Wang, Jingfeng Zhang, Characteristics of microstructure evolution of two-phase H62 brass alloy during continuous extrusion, Procedia Eng. 207 (2017) 1123–1128.

[4] Bing Li, Qi Wei, Jiu-yang Pei, Ying Zhao, “Flow characteristics of brass rod during continuous extrusion,” Procedia Engineering 81 (2014) 647 – 651.

[5] Bing Li, Zikai Lin, Cheng Peng, Xue Wang, Jingfeng Zhang, “Characteristics of microstructure evolution of two-phase H62 brass alloy during continuous extrusion,” Procedia Engineering 207 (2017) 1123–1128.

[6] Boyer R, Welsch G, Collings EW. Materials properties handbook: titanium alloys. Materials Park (OH): ASM International; 1994.

[7] C. Etherington, Conform-A New concept for the continuous extrusion forming of metals, ASME Trans. of J. Eng.Ind. 96B (3) (1974) 893-900.

[8] Chen FK, Chiu KH. Stamping formability of pure titanium sheets. J Mater Process Technol 2005; 170:181–6.

[9] Chun YB, Yu SH, Semiatin SL, Hwang SK. Effect of deformation twinning on microstructure and texture evolution during cold rolling of CP-titanium. Mater. Sci. Eng. A 2005; 398:209–19.

[10] D. Green, the continuous extrusion-forming of wire sections, J. Inst. Metals 100(8) (1972) 295−300.

[11] Fu-rong CAO, Jing-lin WEN, Hua DING, Zhao-dong WANG, Ying-long LI, Ren-guo GUAN, Hui HOU, “Force analysis and experimental study of pure aluminum and Al−5%Ti−1%B alloy continuous expansion extrusion forming process,” Trans. Nonferrous Met. Soc. China 23(2013) 201−207.

[12] Gilbert R, Shannon CR. ASM handbook: heat treating, vol. 4. ASM International; 1991. p. 913–23.

[13] GUAN Ren-guo, ZHAO Zhan-yong, CHAO Run-ze, LIAN Chao, WEN Jing-lin, “Simulation of temperature field and metal flow during continuous semisolid

extending extrusion process of 6201 alloy tube,” Trans. Nonferrous Met. Soc. China 22(2012) 1182-1189.

[14] Henry S. Valberg, Applied Metal Forming: Including FEM Analysis, 1st edition.: Cambridge University Press, 2010; pp. 219-241.

[15] Huang W, Zan X, Nie X, Gong M, Wang Y, Xia Y. Experimental study on the dynamic tensile behavior of a poly-crystal pure titanium at elevated temperatures. Mater. Sci. Eng. A 2007; 443:33–41.

[16] J.R. Cho, and H.S. Jeong, “Parametric investigation on the curling phenomenon in CONFORM process by three-dimensional finite element analysis,” Journal of Materials Processing Technology 110 (2001) 53-60.

[17] Jiamin Hua, Jie Tenga, Xiankun Jia, Dingfa Fua, Wengang Zhanga, Hui Zhang, “Enhanced mechanical properties of an Al-Mg-Si alloy by repetitive continuous extrusion forming process and subsequent aging treatment,” Materials Science & Engineering A 695 (2017) 35–44.

[18] L.C. Tsao H.Y. Wu, J.C. Leong, C.J. Fang. Flow stress behavior of commercial pure titanium sheet during warm tensile deformation. Materials and Design 34 (2012) 179–184.

[19] Lonardelli L, Gey N, Wenk HR, Humbert M, Voge SC, Lutterotti L. In situ observation of texture evolution during α-□ and □- α phase transformations in titanium alloys investigated by neutron diffraction. Acta Mater 2007; 55:5718–27.

[20] Monika Mitka, Maciej Gawlik, Mariusz Bigaj, Wojciech Szymanski, Wojciech Z. Misiolek, Continuous rotary extrusion of AZ81 magnesium alloy, Procedia Manuf. 15 (2018) 257–263.

[21] Mulualem Hailu Besha, Devendra kumar Sinha, C. Venkatesh, Satyma Gautam Shivam, “Analysis of Effective stress of Titanium alloy in Continuous forming process” material todays proceeding (2021).

[22] Nijenthan Rajendran, Monika Mitka, Marzena Lech-Grega, Wojciech Z. Misiolek, Effect of tool geometry on the velocity and strain rate fields in continuous rotary extrusion of magnesium AZ91 alloy, Procedia Manuf. 15 (2018) 264–271.

[23] Peng Penga, Ji Shea, Aitao Tanga, Jianyue Zhang, Shibo Zhoua, Xiao Xiong, Fusheng Pana, “Novel continuous forging extrusion in a one-step extrusion process for bulk ultrafine magnesium alloy,” Materials Science & Engineering A 764 (2019) 138-144.

[24] Sheng BI, Xin-bing YUN, Jiu-yang PEI, Ying ZHAO, Zhi-yong YAN, Xu ZHANG, "Microstructure evolution of Al−Sr master alloy during continuous extrusion," Trans. Nonferrous Met. Soc. China 27(2017) 305−311.

[25] Shiro Kobayashi, Soo-Ik Oh, Taylan Altan, Metal Forming and the Finite- Element Method, Oxford University Press, Inc., New York 10016,1989.

[26] Sinha, D. K. and Kumar, S., Kumar, A., and Yadav, A, Mathematical modeling to predict mechanical properties of copper (C101) feedstock in continuous extrusion, IOP Conf. Series: Mater. Sci. Eng. 404 (2018) 012052.

[27] Sinha, D. K. and Kumar, S., Kumar, A., and Yadav, A. Optimization of process parameters in continuous extrusion of aluminum alloy, International Conference on Computational and Characterization Techniques in Engineering and Science (CCTES), 2018.

[28] T. Katajarinne, T. Manninen, P. Ramsayc, "Numerical simulation of flash formation in continuous rotary extrusion of copper," Journal of Materials Processing Technology 177 (2006) 604–607.

[29] T. Manninen, T. Katajarinne, P. Ramsayc, "Analysis of flash formation in continuous rotary extrusion of copper," Journal of Materials Processing Technology 177 (2006) 600–603.

[30] Tung-Sheng Yang, Finite Element Analysis of Square Cup Deep Drawing of Pure Titanium Metal Sheet at elevated Temperatures, Advanced Design and Manufacture to Gain a Competitive Edge, (2008) 33-42.

[31] Woei-Shyan Lee and Chi-Feng Lin, "Plastic deformation and fracture behaviour of Ti–6Al–4V alloy loaded with high strain rate under various temperatures," Materials Science and Engineering A241 (1998) 48–59.

[32] WU Peng-yue, XIE Shui-sheng, LI Hua-qing, YAN Ming, HUANG Guo-jie, CHENG Lei, "Effect of extrusion wheel angular velocity on continuous extrusion forming process of copper concave bus bar," Trans. Nonferrous Met. SOC. China 17(2007) 280-286.

[33] Xin bing YUN, Fan WAN, Sheng BI, Bing LI, "Effect of Billet Preheating Temperature on Continuous extrusion forming of Al-Sr alloys," Procedia Engineering 207 (2017) 395–400.

[34] Xinbing YUN, Fan WAN, Sheng BI, Bing LI, Effect of Billet Preheating Temperature on Continuous extrusion forming of Al-Sr alloy, Procedia Eng. 207(2017) 395–400.

[35] Xinbing YUN, Fan WAN, Sheng BI, Bing LI, "Effect of Billet Preheating Temperature on Continuous extrusion forming of Al-Sr alloys," Procedia Engineering 207 (2017) 395–400.

[36] Xin-bing YUN, Wei YOU, Ying ZHAO, Bing LI, Zhi-xin FAN, "Continuous extrusion and rolling forming velocity of copper strip," Trans. Nonferrous Met. Soc. China 23(2013) 1108_1113.

[37] Y.H. Kim, J.R. Cho, H.S. Jeog, K.S. Kim, S.S. Yoon, A study on optimal design for CONFORM process, J. Mater. Process. Technol, 80–81 (1998) 671–675.

[38] Y.H. Kim, J.R, Cho, K.S. Kim, H.S. Jeong, S.S. Yoon, "A study of the application of upper bound method to the CONFORM process," Journal of Materials Processing Technology 97 (2000) 153-157.

[39] Yassin Mustafa Ahmed, Khairul Salleh Mohamed Sahari, Mahadzir. Ishak, Basim Ali Khidhir, "Titanium and its Alloy", International Journal of Science and Research (IJSR) · October 2014.

[40] Ying Zhaoa, Baoyun Song, Jiuyang Pei, Chunbo Jia, Bing Li, Guo Linlin, "Effect of deformation speed on the microstructure and mechanical properties of AA6063 during continuous extrusion process," Journal of Materials Processing Technology 213 (2013) 1855– 1863.

[41] Ying Zhaoa, Baoyun Song, Zhiyong Yan, Xu Zhang, Jiuyang Pei, "Microstructure and mechanical properties of extrusion welds in continuous extrusion of AA6063 aluminum alloy with double billets," Journal of Materials Processing Technology 235 (2016) 149–157.

[42] Yuan Yuan, Zhou Li, Zhu Xiao, Ziqian Zhao, Ziqi Yang, "Microstructure evolution and properties of Cu-Cr alloy during continuous extrusion process," Journal of Alloys and Compounds 703 (2017) 454-460.

[43] ZHAO Ying, SONG Bao-yun, YUN Xin-bing, PEI Jiu-yang, JIA Chun-bo, YAN Zhi-yong, "Effect of process parameters on sheath forming of continuous extrusion sheathing of aluminum," Trans. Nonferrous Met. Soc. China 22(2012) 3073−3080.